

Discontinuous Finite Element Transport Solutions in Thick Diffusive Problems

Marvin L. Adams*

Texas A&M University, Department of Nuclear Engineering
College Station, Texas 77843-3133

Received April 4, 2000

Accepted October 23, 2000

Abstract—The performance of discontinuous finite element methods (DFEMs) on problems that contain optically thick diffusive regions is analyzed and tested. The asymptotic analysis is quite general; it holds for an entire family of DFEMs in slab, XY, and XYZ geometries on arbitrarily connected polygonal or polyhedral spatial grids. The main contribution of the work is a theory that predicts and explains how DFEMs behave when applied to thick diffusive regions. It is well known that in the interior of such a region, the exact transport solution satisfies (to leading order) a diffusion equation, with boundary conditions that are known. Thus, in the interiors of such regions, the ideal discretized transport solution would satisfy (to leading order) an accurate discretization of the same diffusion equation and boundary conditions. The theory predicts that one class of DFEMs, which we call “zero-resolution” methods, fails dramatically in thick diffusive regions, yielding solutions that are completely meaningless. Another class—full-resolution methods—has leading-order solutions that satisfy discretizations of the correct diffusion equation. Full-resolution DFEMs are classified according to several categories of performance: continuity, robustness, accuracy, and boundary condition. Certain kinds of lumping, some of which are believed to be new, improve DFEM behavior in the continuity, robustness, and boundary-condition categories. Theoretical results are illustrated using different variations of linear and bilinear DFEMs on several test problems in XY geometry. In every case, numerical results agree precisely with the predictions of the asymptotic theory.

I. INTRODUCTION

In this paper, we analyze and test the behavior of a family of transport spatial discretizations, namely, discontinuous finite element methods (DFEMs) that are algebraically linear, for problems that are optically thick and diffusive. Regions that are extremely optically thick and diffusive often appear in radiative-transfer problems of practical interest. Computational limitations force the use of spatial grids whose cells are often quite thick compared to a mean-free-path (mfp), especially in low-energy groups. Thus, the radiative-transfer community is very interested in the performance of numerical transport methods in regions whose cells are optically thick and diffusive.

An obvious question is why the community does not simply solve the diffusion equation in thick diffusive regions. There are several reasons. First, a typical radiative-transfer problem has a wide range of material properties. In a given energy group, some spatial regions may be quite thick and others quite thin. Further, in a given spatial region, the material may be quite thick and diffusive to photons in some energy groups but thin to photons in other groups. Second, if part of the problem is to be solved with diffusion theory and part with transport, then the problem must be so divided. If the division is made such that diffusion theory is applied to regions that are not very thick and diffusive, then errors will result. If, on the other hand, the division leaves some relatively thick and diffusive regions for the transport equation, then the transport solution cannot be trusted unless it is known to behave well in the thick diffusive limit. This is certainly

*E-mail: mladams@tamu.edu

not a complete discussion of the question; it is intended only to help motivate what follows.

Our work follows from that of many researchers; we give only a partial list of that work here. Although asymptotic diffusion-limit analyses have been performed for decades in radiative-transfer work, ours descends most directly from the seminal work of Larsen, Morel, and Miller.¹ These authors first performed diffusion-limit analyses of a few different spatial discretizations in slab geometry, assuming steady-state problems with a single energy group. Larsen and Morel followed² with an extended analysis that included unresolved boundary layers; their setting was also slab geometry and steady-state problems with a single energy group. Adams and co-workers extended this analysis to families of methods and multidimensional geometries in several publications, including a conference paper that reports an early version of the present work.³⁻⁶ Larsen⁷ reviewed these and other steady-state one-group results in a 1992 review paper. Morel, Wareing, and Smith⁸ extended the analysis in a different direction, analyzing a method with time and energy discretization in addition to spatial and angular; the spatial discretization method was the lumped linear DFEM in slab geometry. Adams and Nowak⁹ performed a similar analysis with time and energy included, with strong emphasis on unresolved boundary layers and initial layers. The work cited here is only a sample and is not intended to be a complete survey of the field; however, it contains the main threads that lead to the present work. In this work, we apply the asymptotic diffusion-limit analysis to a family of DFEMs in a very general geometric setting, considering steady-state problems with a single energy group.

Our asymptotic analysis is quite general; it holds for the entire family of algebraically linear DFEMs in slab, XY, and XYZ geometries on arbitrarily connected polygonal or polyhedral spatial grids. To our knowledge, this type of analysis has not been previously reported for this family of DFEMs. (The exception is our conference paper that was a preliminary report of the present work.³) Our first main result is that this extremely general analysis yields sharp results, that relate specific solution behaviors to specific properties of DFEM weight and basis functions. Without such results, it is difficult to learn general truths, and the process of creating improved methods can be very tedious. Our theory allows us to quickly determine how any proposed DFEM will behave in thick diffusive regions. It also guides us to develop modifications, which we introduce here, that improve DFEM behavior in such regions. Similarly, it should enable other researchers to develop DFEMs with improved diffusion-limit performance.

Our second main result is a sort of diffusion-limit "taxonomy" of DFEMs—a system of classification according to several categories of performance in thick diffusive regions. The classification categories that we have chosen are *resolution*, *continuity*, *robustness*, *accuracy*,

and *boundary-condition*. *Resolution* measures how many degrees of freedom in the leading-order solution are devoted to satisfying a discretization of the correct diffusion equation. We find that some DFEMs devote *no* leading-order degrees of freedom to approximating anything physically meaningful. Such *zero-resolution* methods fail dramatically in thick diffusive regions, yielding absurd solutions. In contrast, *full-resolution* DFEMs employ one leading-order degree of freedom per spatial-grid vertex (or edge or face) to satisfy discretizations of the correct diffusion equation. We show that the resolution of a given method is determined completely by its weight functions, and we describe two simple properties of the weight function that guarantee full resolution.

The *continuity* category simply describes whether or not the leading-order DFEM solution is continuous in the interior of a thick diffusive region. DFEM solutions are in general discontinuous at cell surfaces; such discontinuities can help the methods capture sharp variations in transport solutions in many problems. In the interior of a thick diffusive region, however, the exact leading-order solution is smooth; thus, one would expect that a good discrete solution would be continuous to leading order. We show that standard DFEMs do not usually produce continuous leading-order solutions in thick diffusive regions. We introduce *lumping* of the DFEM surface matrix and show that this causes the leading-order solution to be continuous. (While mass-matrix lumping is a common finite-element technique, we believe that surface-matrix lumping is new, having been introduced in our conference papers.^{3,10})

We also attempt to describe the *accuracy* and *robustness* of DFEMs in thick diffusive regions. These categories are not precise; nevertheless, they convey useful information. We say that a method is highly *robust* if its solution is nonnegative and free from unphysical oscillations even on spatial grids that do not resolve the leading-order solution. We say that a method is highly *accurate* if its leading-order solution is highly accurate on high-quality spatial grids that finely resolve variations in the exact leading-order solution in the interior of diffusive regions. (In an optically thick diffusive region, the spatial grid can be extremely coarse compared to an mfp ($1/\sigma$) but fine compared to a diffusion length ($1/\sqrt{3\sigma\sigma_a}$), and the leading-order solution tends to vary on the scale of the diffusion length.) We introduce lumping techniques that add robustness to standard DFEMs. (We believe that these lumping techniques are new, having been introduced in our conference papers.^{3,10})

The *boundary-condition* category describes how DFEMs behave in the presence of boundary layers that are not resolved by the spatial grid. The width of a boundary layer is on the order of an mfp; thus, the spatial grid in a thick diffusive region will not usually resolve boundary layers unless special care is taken. The theory presented here is intended to help code developers decide whether such special care is necessary. As we have

mentioned, it is well known that in the interior of a thick diffusive region, the exact leading-order solution satisfies a diffusion equation. The boundary conditions satisfied by this leading-order solution are also known; they are Dirichlet conditions that are weighted angular integrals of the angular intensity incident upon the region. Our analysis finds the boundary conditions satisfied by the leading-order interior DFEM solution. We compare these against the exact conditions and thereby assess each DFEM's boundary-condition behavior. We find that if incident intensities are not isotropic, unresolved boundary layers can give rise to terms that have the effect of artificial sources in the discretized diffusion equations satisfied by the leading-order solutions of full-resolution DFEMs. These terms distort the leading-order interior solution. We show that our lumping techniques improve the boundary-condition behavior of DFEMs but that they do not eliminate all defects.

We have mentioned that this paper introduces new lumping techniques to modify finite element methods. The modifications are similar to the mass-matrix lumping that is common in finite element theory; however, here the modifications are made to every submatrix, not just to the mass matrix. This sort of generalized lumping was introduced in our conference papers,^{3,10} and lumped methods have been studied since then.¹¹ (Adams recognized that the fully lumped bilinear DFEM equations on rectangles in XY geometry could be viewed as simple particle-balance equations on "corner" subcells; as a result, a new family of "corner-balance" methods was developed.¹¹⁻¹⁴) In general, lumping tends to add robustness but reduce fine-mesh accuracy.

The principal purpose of this paper is to present the theory that we have developed concerning the behavior of DFEMs in thick diffusive regions. The setting is so general (entire family of methods, one to three spatial dimensions, and arbitrary spatial grids) that it is impractical to include numerical results that test all of the theoretical predictions. Instead, we try to illustrate the main predictions in the relatively simple setting of rectangular grids in XY geometry. We find that the linear and bilinear DFEMs are excellent vehicles for our illustrations because they have many variants for which the theory predicts substantially different behavior. Thus, while the numerical results shown here do illustrate many of our theoretical predictions and do agree precisely with those predictions, they are too limited in scope to be taken as verification of the theory.

As a final introductory remark, we note that in the interior of thick diffusive regions, many DFEMs behave (to leading order) exactly like balance-based characteristics methods, as reported in a recent paper.⁶ For example, the standard bilinear characteristics method gives the same leading-order solution as the standard bilinear DFEM (BLD) method.

The remainder of this paper is organized as follows. In Sec. II, we describe the spatial grids and DFEMs

that we study here. In Sec. III, we review results from an asymptotic analysis of the exact transport solution in thick diffusive regions, apply this analysis to DFEMs, and discuss the results in some detail. In Sec. IV, we provide numerical results from diffusive test problems in XY geometry, which illustrate (and in every case agree fully with) the predictions of the analysis. In Sec. V, we offer a summary and some concluding remarks.

II. DISCONTINUOUS FINITE ELEMENT METHODS

The main application that drives our interest in optically thick and diffusive problems is that of radiative transfer. The complete time- and energy-dependent problem is discussed elsewhere.^{8,9,15} For our purposes here, it is sufficient to consider the following steady-state problem with a single energy group and with a discrete ordinates treatment of the direction variable:

$$\mathbf{\Omega} \cdot \nabla \Psi + \sigma(\mathbf{r}) \Psi(\mathbf{r}, \mathbf{\Omega}) = \frac{1}{4\pi} Q_{tot}(\mathbf{r}) , \quad \mathbf{r} \in \mathbb{V} , \quad (1)$$

$$Q_{tot}(\mathbf{r}) = [\sigma(\mathbf{r}) - \sigma_a(\mathbf{r})] \Phi(\mathbf{r}) + q_{ext}(\mathbf{r}) , \quad (2a)$$

$$\Phi(\mathbf{r}) \equiv \sum_{m=1}^M \Delta_m \Psi(\mathbf{r}, \mathbf{\Omega}_m) , \quad (2b)$$

$$\Psi(\mathbf{r}, \mathbf{\Omega}) = \psi_{inc}(\mathbf{r}, \mathbf{\Omega}) , \quad \mathbf{r} \in \partial\mathbb{V} , \quad \mathbf{n}(\mathbf{r}) \cdot \mathbf{\Omega} < 0 , \quad (3)$$

where

$\{\Delta_m, \mathbf{\Omega}_m\}$ = discrete ordinates quadrature weights and directions

\mathbb{V} = problem domain

\mathbf{n} = outward unit normal on the boundary $\partial\mathbb{V}$.

We shall refer to the solution Ψ as the *angular intensity*, and its integral Φ as the *scalar intensity*. We shall refer to σ as the total cross section and σ_a as the absorption cross section. (These are generally called opacities in the radiative-transfer literature.) The value Q_{tot} is the total source; q_{ext} is the fixed source, which does not depend on Φ .

We divide the problem domain \mathbb{V} into nonoverlapping cells \mathbb{V}_k , $k = 1 \dots K$, where each cell is a polyhedron. We define

L_k = number of faces of k 'th cell ,

$\partial\mathbb{V}_{kl}$ = l 'th face of k 'th cell

$\Rightarrow \partial\mathbb{V}_k = \cup \{\partial\mathbb{V}_{kl}, l = 1, \dots, L_k\} .$

We do not assume that cell faces are planar; however, we define an averaged outward unit normal on each face:

$$\mathbf{n}_{kl} \equiv \int_{\partial\mathbb{V}_{kl}} d^2\mathbf{r}\mathbf{n}(\mathbf{r}) / \int_{\partial\mathbb{V}_{kl}} d^2r . \quad (4)$$

II.A. Without Lumping

We now define the family of DFEMs that we study in this work. We begin our derivation of the DFEM family by choosing a set of *weight functions* for each spatial cell:

$$w_{ki}(\mathbf{r}) = i\text{'th weight function in cell } k , \quad i = 1 \dots J_k ;$$

$$w_{ki}(\mathbf{r}) = 0 \quad \text{for } \mathbf{r} \notin \text{cell } k . \quad (5)$$

We have defined J_k to be the number of weight functions in cell k , and we have noted that each of cell k 's weight functions is zero outside of cell k . A weight function may be nonzero as it approaches the boundary from inside its cell, in which case it goes discontinuously from nonzero inside the cell to zero outside it. For example, a weight function could be unity inside its cell and zero outside.

Once the weight functions w_{ki} are chosen for all $i = 1 \dots J_k$ and all $k = 1 \dots K$, we multiply the transport equation by w_{ki} and integrate over the volume of cell k :

$$\int_{\mathbb{V}_k} d^3r w_{ki}(\mathbf{r}) [\mathbf{\Omega} \cdot \nabla \Psi + \sigma(\mathbf{r}) \Psi(\mathbf{r}, \mathbf{\Omega})]$$

$$= \int_{\mathbb{V}_k} d^3r w_{ki}(\mathbf{r}) \frac{Q_{tot}(\mathbf{r})}{4\pi} ,$$

$$i = 1 \dots J_k , \quad k = 1 \dots K . \quad (6)$$

We use Green's theorem on the leakage term (and drop arguments of functions for brevity's sake):

$$\int_{\partial\mathbb{V}_k} d^2r w_{ki} \mathbf{n} \cdot \mathbf{\Omega} \Psi + \int_{\mathbb{V}_k} d^3r [-\Psi \mathbf{\Omega} \cdot \nabla w_{ki} + w_{ki} \sigma \Psi]$$

$$= \int_{\mathbb{V}_k} d^3r w_{ki} \frac{Q_{tot}}{4\pi} . \quad (7)$$

Equation (7) is often called the ki 'th spatial moment of the transport equation.

The next step in the derivation of a DFEM is the selection of *basis functions*. The DFEM approximate solution will be a linear combination of these functions. There must be J_k basis functions for cell k . We have

$$\Psi(\mathbf{r}, \mathbf{\Omega}) \approx \psi(\mathbf{r}, \mathbf{\Omega}) \equiv \sum_{j=1}^{J_k} \psi_{kj}(\mathbf{\Omega}) b_{kj}(\mathbf{r}) , \quad \mathbf{r} \in \mathbb{V}_k .$$

$$(8)$$

Each basis function in cell k is zero outside of cell k , and as is the case with weight functions, a basis function may be discontinuous at cell surfaces.

We now insert the DFEM approximation ψ into the cell-interior terms of the weighted-integral transport equation (7):

$$\int_{\partial\mathbb{V}_k} d^2r w_{ki} \mathbf{n} \cdot \mathbf{\Omega} \Psi$$

$$+ \sum_{j=1}^{J_k} \psi_{kj} \int_{\mathbb{V}_k} d^3r [-b_{kj} \mathbf{\Omega} \cdot \nabla w_{ki} + w_{ki} \sigma b_{kj}]$$

$$= \int_{\mathbb{V}_k} d^3r w_{ki} \frac{Q_{tot}}{4\pi} . \quad (9)$$

There now arises the question of how to treat the cell-surface terms, where the approximate function ψ is in general discontinuous. The DFEMs that we consider use the *upstream* value on each surface:

$$\Psi(\mathbf{r}_{kl}, \mathbf{\Omega}) \approx \psi(\mathbf{r}_{kl}, \mathbf{\Omega}) \equiv \begin{cases} \psi(\mathbf{r}_{kl}^-, \mathbf{\Omega}) & \mathbf{n}_{kl} \cdot \mathbf{\Omega} > 0 \\ \psi(\mathbf{r}_{kl}^+, \mathbf{\Omega}) & \mathbf{n}_{kl} \cdot \mathbf{\Omega} < 0 \end{cases} ,$$

$$\mathbf{r} \in \partial\mathbb{V}_{kl} . \quad (10)$$

where \mathbf{r}_{kl}^+ is just outside the l 'th surface of cell k and \mathbf{r}_{kl}^- is just inside. [This definition ensures that the surface value is determined by the cell from which the particles flow.] At the point \mathbf{r}_{kl}^- , the expansion of Eq. (8) is used for ψ , for this point is inside cell k . If the point \mathbf{r}_{kl}^+ is in a neighboring cell, then the value of ψ is taken from the neighboring cell's basis-function expansion. If the point \mathbf{r}_{kl}^+ is adjacent to the boundary of the problem domain, then the value of ψ is taken from the boundary condition, Eq. (3). Note that even if a cell face is not planar, we identify one side of it to be "upstream" for the entire face, using the face-averaged outward normal to make this determination. Wareing et al.¹⁶ have determined this to be an effective treatment for three-dimensional problems with arbitrary grids. We remark that this treatment provides a simple way to treat cells with all manner of curved surfaces, including for example circular arcs in two-dimensional problems. This is an interesting subject for future investigations.

The resulting DFEM can now be written as a $J_k \times J_k$ matrix equation for each cell k , with the cells coupled by Eq. (10):

$$\mathbf{\Omega} \cdot [\underline{\mathbf{L}}_k^{surf} \underline{\psi}_k^{surf} + \underline{\mathbf{L}}_k \underline{\psi}_k] + \underline{\mathbf{T}}_k \underline{\psi}_k$$

$$= \frac{1}{4\pi} [\underline{\mathbf{T}}_k - \underline{\mathbf{A}}_k] \underline{\phi}_k + \frac{1}{4\pi} q_k , \quad (11)$$

where

$$\underline{\psi}_k(\mathbf{\Omega}) = [\psi_{k,1}(\mathbf{\Omega}), \psi_{k,2}(\mathbf{\Omega}), \dots, \psi_{k,J_k}(\mathbf{\Omega})]^t \quad (12)$$

$$\underline{\phi}_k = [\phi_{k,1}, \phi_{k,2}, \dots, \phi_{k,J_k}]^t, \quad (13)$$

$$\phi_{kj}(r) \equiv \sum_{m=1}^M \Delta_m \psi_{kj}(\mathbf{\Omega}_m)$$

$$\underline{q}_k = [q_{k,1}, q_{k,2}, \dots, q_{k,J_k}]^t, \quad (14)$$

$$q_{ki} \equiv \int_{\mathbb{V}_k} d^3r w_{ki}(\mathbf{r}) q_{ext}(\mathbf{r})$$

$$[\underline{\mathbf{L}}_k^{surf} \underline{\psi}_k^{surf}]_i \equiv \sum_{l=1}^{L_k} \mathbf{n}_{kl} \int_{\partial \mathbb{V}_{kl}} d^2r w_{ki}(\mathbf{r}) \psi(\mathbf{r}_{kl}, \mathbf{\Omega}) \quad (15)$$

$$[\underline{\mathbf{L}}_k]_{ij} = - \int_{\mathbb{V}_k} d^3r b_{kj}(\mathbf{r}) \nabla w_{ki}(\mathbf{r}) \quad (16)$$

$$[\underline{\mathbf{T}}_k]_{ij} \equiv \int_{\mathbb{V}_k} d^3r w_{ki}(\mathbf{r}) \sigma(\mathbf{r}) b_{kj}(\mathbf{r}), \quad (17a)$$

$$[\underline{\mathbf{A}}_k]_{ij} \equiv \int_{\mathbb{V}_k} d^3r w_{ki}(\mathbf{r}) \sigma_a(\mathbf{r}) b_{kj}(\mathbf{r}). \quad (17b)$$

Equation (11), definitions (12) through (17), and definition (10) define the very general family of DFEMs that we study in this work. Note that if the cross sections σ and σ_a are constant in cell k , which we assume in this paper, then

$$\underline{\mathbf{T}}_k = \sigma_k \underline{\mathbf{M}} \quad \text{and} \quad \underline{\mathbf{A}}_k = \sigma_{a,k} \underline{\mathbf{M}}, \quad (18)$$

where

$$[\underline{\mathbf{M}}_k]_{ij} \equiv \int_{\mathbb{V}_k} d^3r w_{ki}(\mathbf{r}) b_{kj}(\mathbf{r}). \quad (19)$$

We shall refer to $\underline{\mathbf{M}}_k$ as the *mass matrix* for cell k .

II.A.1. Specific Discontinuous Finite Element Method: Bilinear on Rectangles

We recognize that the preceding description is somewhat abstract and mathematical. To make this more concrete (and to set the stage for later numerical results), we now describe a specific DFEM, namely, the BLD method for rectangular cells in XY geometry.^{17,18} Figure 1 illustrates the location of various points associated with cell k ; our notation follows from this figure.

The BLD method uses the following weight and basis functions:

$$w_{k1} = b_{k1} = \frac{x_R - x}{\Delta x_k} \frac{y_T - y}{\Delta y_k}, \quad (20)$$

$$w_{k2} = b_{k2} = \frac{x - x_L}{\Delta x_k} \frac{y_T - y}{\Delta y_k}, \quad (21)$$

$$w_{k3} = b_{k3} = \frac{x - x_L}{\Delta x_k} \frac{y - y_B}{\Delta y_k}, \quad (22)$$

and

$$w_{k4} = b_{k4} = \frac{x_R - x}{\Delta x_k} \frac{y - y_B}{\Delta y_k}. \quad (23)$$

We remark that these weight and basis functions are *cardinal* functions: Each is unity at its own support point and zero at all other support points. BLD is an example of a Galerkin method, which means that its weight and basis functions are the same.

If we define $\mu = \Omega_x$ and $\eta = \Omega_y$, then Eq. (11) for the BLD method is as follows:

$$\begin{aligned} & \frac{\mu \Delta y}{6} \begin{bmatrix} -2\psi_{1L} - \psi_{4L} \\ 2\psi_{2R} + \psi_{3R} \\ \psi_{2R} + 2\psi_{3R} \\ -\psi_{1L} - 2\psi_{4L} \end{bmatrix} + \frac{\mu \Delta y}{12} \begin{bmatrix} 2 & 2 & 1 & 1 \\ -2 & -2 & -1 & -1 \\ -1 & -1 & -2 & -2 \\ 1 & 1 & 2 & 2 \end{bmatrix} \begin{bmatrix} \psi_1 \\ \psi_2 \\ \psi_3 \\ \psi_4 \end{bmatrix} + \frac{\eta \Delta x}{6} \begin{bmatrix} -2\psi_{1B} - \psi_{2B} \\ -\psi_{1B} - 2\psi_{2B} \\ 2\psi_{3T} + \psi_{4T} \\ \psi_{3T} + 2\psi_{4T} \end{bmatrix} \\ & + \frac{\eta \Delta x}{12} \begin{bmatrix} 2 & 1 & 1 & 2 \\ 1 & 2 & 2 & 1 \\ -1 & -2 & -2 & -1 \\ -2 & -1 & -1 & -2 \end{bmatrix} \begin{bmatrix} \psi_1 \\ \psi_2 \\ \psi_3 \\ \psi_4 \end{bmatrix} + \frac{\sigma \Delta x \Delta y}{36} \begin{bmatrix} 4 & 2 & 1 & 2 \\ 2 & 4 & 2 & 1 \\ 1 & 2 & 4 & 2 \\ 2 & 1 & 2 & 4 \end{bmatrix} \begin{bmatrix} \psi_1 \\ \psi_2 \\ \psi_3 \\ \psi_4 \end{bmatrix} \\ & = \frac{(\sigma - \sigma_a) \Delta x \Delta y}{(4\pi) 36} \begin{bmatrix} 4 & 2 & 1 & 2 \\ 2 & 4 & 2 & 4 \\ 1 & 2 & 4 & 2 \\ 2 & 1 & 2 & 4 \end{bmatrix} \begin{bmatrix} \phi_1 \\ \phi_2 \\ \phi_3 \\ \phi_4 \end{bmatrix} + \frac{\Delta x \Delta y}{(4\pi) 36} \begin{bmatrix} 4 & 2 & 1 & 2 \\ 2 & 4 & 2 & 4 \\ 1 & 2 & 4 & 2 \\ 2 & 1 & 2 & 4 \end{bmatrix} \begin{bmatrix} q_1 \\ q_2 \\ q_3 \\ q_4 \end{bmatrix}, \quad (24) \end{aligned}$$

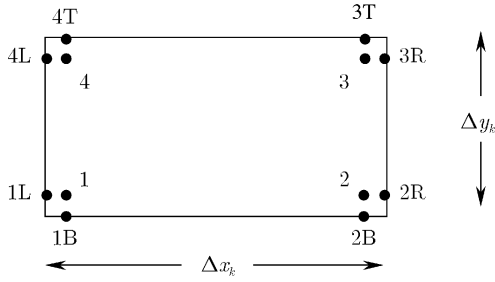


Fig. 1. Location of points in rectangular cell.

where we have omitted the subscript k and the argument Ω . We have also assumed that the extraneous source q_{ext} can be expanded in terms of the bilinear basis functions $\{b_{ki}\}$, which leads to the last term in the equation.

We remark that there are many ways to write a given DFEM such as BLD. For example, instead of the unknowns $\{\psi_1, \psi_2, \psi_3, \psi_4\}$ we could define the alternative unknowns

$$\begin{aligned} \psi^a &\equiv \frac{\psi_1 + \psi_2 + \psi_3 + \psi_4}{4}, & \psi^x &\equiv \frac{\psi_2 + \psi_3 - \psi_1 - \psi_4}{4}, \\ \psi^y &\equiv \frac{\psi_3 + \psi_4 - \psi_1 - \psi_2}{4}, & \psi^{xy} &\equiv \frac{\psi_1 + \psi_3 - \psi_2 - \psi_4}{4}, \end{aligned} \quad (25)$$

$$\begin{aligned} \psi_R &\equiv \frac{\psi_{2R} + \psi_{3R}}{2}, & \psi_R^y &\equiv \frac{\psi_{3R} - \psi_{2R}}{2}, \\ \psi_B &\equiv \frac{\psi_{1B} + \psi_{2B}}{2}, & \psi_T^x &\equiv \frac{\psi_{3T} - \psi_{4T}}{2}, \text{ etc.} \end{aligned} \quad (26)$$

We use similar definitions for other quantities. We then take linear combinations of Eqs. (11) to obtain the following completely equivalent system:

$$\begin{aligned} \frac{\mu}{\Delta x} (\psi_R - \psi_L) + \frac{\eta}{\Delta y} (\psi_T - \psi_B) + \sigma \psi^a \\ = \frac{\sigma - \sigma_a}{4\pi} \phi^a + \frac{1}{4\pi} q^a, \end{aligned} \quad (27)$$

$$\begin{aligned} \frac{3\mu}{\Delta x} (\psi_R + \psi_L - 2\psi^a) + \frac{\eta}{\Delta y} (\psi_T^x - \psi_B^x) + \sigma \psi^x \\ = \frac{\sigma - \sigma_a}{4\pi} \phi^x + \frac{1}{4\pi} q^x, \end{aligned} \quad (28)$$

$$\begin{aligned} \frac{\mu}{\Delta x} (\psi_R^y - \psi_L^y) + \frac{3\eta}{\Delta y} (\psi_T + \psi_B - 2\psi^a) + \sigma \psi^y \\ = \frac{\sigma - \sigma_a}{4\pi} \phi^y + \frac{1}{4\pi} q^y, \end{aligned} \quad (29)$$

and

$$\begin{aligned} \frac{3\mu}{\Delta x} (\psi_R^y + \psi_L^y - 2\psi^y) + \frac{3\eta}{\Delta y} (\psi_T^x + \psi_B^x - 2\psi^x) + \sigma \psi^{xy} \\ = \frac{\sigma - \sigma_a}{4\pi} \phi^{xy} + \frac{1}{4\pi} q^{xy}. \end{aligned} \quad (30)$$

(We continue to omit the cell index k and the argument Ω to avoid clutter.)

The unknowns in the BLD system (24) are “point” values—values of ψ at support points. This is always the case when the basis functions are cardinal functions. The unknowns in the equivalent system Eqs. (27) through (30) are “slopes” and averages—the cell-average value (ψ_k^a) and the values ψ_k^x , ψ_k^y , ψ_k^{xy} , which are proportional to the cell-averaged x , y , and xy derivatives of ψ , respectively. Note that the latter system could be obtained directly from Eq. (9) using the following weight and basis functions:

$$w_k^a = b_k^a = 1, \quad w_k^x = b_k^x = 2 \frac{x - x_k}{\Delta x_k},$$

$$w_k^y = b_k^y = 2 \frac{y - y_k}{\Delta y_k}, \quad w_k^{xy} = b_k^{xy} = 4 \frac{x - x_k}{\Delta x_k} \frac{y - y_k}{\Delta y_k}. \quad (31)$$

[We have defined (x_k, y_k) to be the coordinates of the center of cell k .] These functions yield Eqs. (27) through (30); the functions of Eqs. (20) through (23) yield Eqs. (24).

The systems (24) and (27)–(30) are completely equivalent—the DFEM solution $\psi(x, y)$ is identical regardless of which form is used. This illustrates an important point: The *function spaces* spanned by the weight and basis functions, not the particular form of those functions, define a particular DFEM. Using different weight or basis functions that span the same space can change the form of the equations but not the solution and thus not the method. For example, the functions $\{1, x\}$ span the same space as the functions $\{6 - x, x - 5\}$. The functions shown in Eqs. (31) span the same space as those in Eqs. (20)–(23). [That is, any function that is a linear combination of the functions in Eqs. (31) is also a linear combination of the functions in Eqs. (20)–(23) and vice versa.] Thus, the two sets of functions produce the same DFEM, which we call BLD.

II.A.2. Specific Discontinuous Finite Element Method: Linear on Rectangles

The linear DFEM (LD) on rectangles uses weight and basis functions in each cell that span the same space as the functions $\{1, x, y\}$. Note that there is no bilinear (xy) term. In slope-and-average form, the LD equations are

$$\begin{aligned} \frac{\mu}{\Delta x} (\psi_R - \psi_L) + \frac{\eta}{\Delta y} (\psi_T - \psi_B) + \sigma \psi^a \\ = \frac{\sigma - \sigma_a}{4\pi} \phi^a + \frac{1}{4\pi} q^a, \end{aligned} \quad (32)$$

$$\begin{aligned} & \frac{3\mu}{\Delta x} (\psi_R + \psi_L - 2\psi^a) + \frac{\eta}{\Delta y} (\psi_T^x - \psi_B^x) + \sigma\psi^x \\ &= \frac{\sigma - \sigma_a}{4\pi} \phi^x + \frac{1}{4\pi} q^x, \end{aligned} \quad (33)$$

and

$$\begin{aligned} & \frac{\mu}{\Delta x} (\psi_R^y - \psi_L^y) + \frac{3\eta}{\Delta y} (\psi_T + \psi_B - 2\psi^a) + \sigma\psi^y \\ &= \frac{\sigma - \sigma_a}{4\pi} \phi^y + \frac{1}{4\pi} q^y. \end{aligned} \quad (34)$$

The LD approximation $\psi(x, y)$ in cell k is

$$\psi(x, y) = \psi_k^a + \psi_k^x \frac{2(x - x_k)}{\Delta x_k} + \psi_k^y \frac{2(y - y_k)}{\Delta y_k}. \quad (35)$$

II.B. Mass-Matrix Lumping

The mass matrix in a transport DFEM is defined for cell k in Eq. (19). To provide a general formulation of mass-matrix lumping, we must assume that the weight and basis functions are cardinal. We shall assume cardinal functions for the remainder of this paper unless otherwise specified. Given this assumption, the lumped mass matrix is

$$[\underline{\underline{\mathbf{M}}}_k^{lump}]_{ij} = \delta_{ij} \sum_{j'=1}^{J_k} [\underline{\underline{\mathbf{M}}}_k]_{i,j'} = \delta_{ij} \int_{\mathbb{V}_k} d^3r w_{ki}(\mathbf{r}). \quad (36)$$

[We have used the fact that the cardinal basis functions sum to unity.] Note that lumping makes the collision term more “local”—in the i ’th row of the mass-lumped version of Eq. (11), the collision term involves the solution only at the i ’th support point, and the source term involves only the source at the i ’th support point.

The mass-lumped BLD equations, in cardinal form, are

$$\begin{aligned} & \frac{\mu\Delta y}{6} \begin{bmatrix} -2\psi_{1L} - \psi_{4L} \\ 2\psi_{2R} + \psi_{3R} \\ \psi_{2R} + 2\psi_{3R} \\ -\psi_{1L} - 2\psi_{4L} \end{bmatrix} + \frac{\mu\Delta y}{12} \begin{bmatrix} 2 & 2 & 1 & 1 \\ -2 & -2 & -1 & -1 \\ -1 & -1 & -2 & -2 \\ 1 & 1 & 2 & 2 \end{bmatrix} \begin{bmatrix} \psi_1 \\ \psi_2 \\ \psi_3 \\ \psi_4 \end{bmatrix} + \frac{\eta\Delta x}{6} \begin{bmatrix} -2\psi_{1B} - \psi_{2B} \\ -\psi_{1B} - 2\psi_{2B} \\ 2\psi_{3T} + \psi_{4T} \\ \psi_{3T} + 2\psi_{4T} \end{bmatrix} \\ & + \frac{\eta\Delta x}{12} \begin{bmatrix} 2 & 1 & 1 & 2 \\ 1 & 2 & 2 & 1 \\ -1 & -2 & -2 & -1 \\ -2 & -1 & -1 & -2 \end{bmatrix} \begin{bmatrix} \psi_1 \\ \psi_2 \\ \psi_3 \\ \psi_4 \end{bmatrix} + \frac{\sigma\Delta x\Delta y}{4} \begin{bmatrix} \psi_1 \\ \psi_2 \\ \psi_3 \\ \psi_4 \end{bmatrix} = \frac{(\sigma - \sigma_a)\Delta x\Delta y}{(4\pi)4} \begin{bmatrix} \phi_1 \\ \phi_2 \\ \phi_3 \\ \phi_4 \end{bmatrix} + \frac{\Delta x\Delta y}{(4\pi)4} \begin{bmatrix} q_1 \\ q_2 \\ q_3 \\ q_4 \end{bmatrix}. \end{aligned} \quad (37)$$

In slope-and-average form the mass-lumped BLD equations are

$$\begin{aligned} & \frac{\mu}{\Delta x} (\psi_R - \psi_L) + \frac{\eta}{\Delta y} (\psi_T - \psi_B) + \sigma\psi^a \\ &= \frac{\sigma - \sigma_a}{4\pi} \phi^a + \frac{1}{4\pi} q^a, \end{aligned} \quad (38)$$

$$\begin{aligned} & \frac{\mu}{\Delta x} (\psi_R + \psi_L - 2\psi^a) + \frac{\eta/3}{\Delta y} (\psi_T^x - \psi_B^x) + \sigma\psi^x \\ &= \frac{\sigma - \sigma_a}{4\pi} \phi^x + \frac{1}{4\pi} q^x, \end{aligned} \quad (39)$$

$$\begin{aligned} & \frac{\mu/3}{\Delta x} (\psi_R^y - \psi_L^y) + \frac{\eta}{\Delta y} (\psi_T + \psi_B - 2\psi^a) + \sigma\psi^y \\ &= \frac{\sigma - \sigma_a}{4\pi} \phi^y + \frac{1}{4\pi} q^y, \end{aligned} \quad (40)$$

and

$$\begin{aligned} & \frac{\mu/3}{\Delta x} (\psi_R^y + \psi_L^y - 2\psi^y) + \frac{\eta/3}{\Delta y} (\psi_T^x + \psi_B^x - 2\psi^x) \\ &+ \sigma\psi^{xy} = \frac{\sigma - \sigma_a}{4\pi} \phi^{xy} + \frac{1}{4\pi} q^{xy}. \end{aligned} \quad (41)$$

[These are simply linear combinations of Eqs. (37).]

We can write the standard and mass-lumped BLD equations simultaneously as follows:

$$\begin{aligned} & \frac{\mu}{\Delta x} (\psi_R - \psi_L) + \frac{\eta}{\Delta y} (\psi_T - \psi_B) + \sigma\psi^a \\ &= \frac{\sigma - \sigma_a}{4\pi} \phi^a + \frac{1}{4\pi} q^a, \end{aligned} \quad (42)$$

$$\begin{aligned} & \frac{\theta_x \mu}{\Delta x} (\psi_R + \psi_L - 2\psi^a) + \frac{\gamma_y \eta}{\Delta y} (\psi_T^x - \psi_B^x) + \sigma\psi^x \\ &= \frac{\sigma - \sigma_a}{4\pi} \phi^x + \frac{1}{4\pi} q^x, \end{aligned} \quad (43)$$

$$\begin{aligned} \frac{\gamma_x \mu}{\Delta x} (\psi_R^y - \psi_L^y) + \frac{\theta_y \eta}{\Delta y} (\psi_T + \psi_B - 2\psi^a) + \sigma \psi^y \\ = \frac{\sigma - \sigma_a}{4\pi} \phi^y + \frac{1}{4\pi} q^y, \end{aligned} \quad (44)$$

and

$$\begin{aligned} \frac{\delta_x \mu}{\Delta x} (\psi_R^y + \psi_L^y - 2\psi^y) + \frac{\delta_y \eta}{\Delta y} (\psi_T^x + \psi_B^x - 2\psi^x) + \sigma \psi^{xy} \\ = \frac{\sigma - \sigma_a}{4\pi} \phi^{xy} + \frac{1}{4\pi} q^{xy}. \end{aligned} \quad (45)$$

Here, we have inserted the parameters θ_u , γ_u , and δ_u , where $u = x$ or y ; these parameters take on the following values:

$$\theta_x = \theta_y = \begin{cases} 3, & \text{standard BLD,} \\ 1, & \text{mass-lumped BLD,} \end{cases} \quad (46)$$

$$\gamma_x = \gamma_y = \begin{cases} 1, & \text{standard BLD,} \\ \frac{1}{3}, & \text{mass-lumped BLD,} \end{cases} \quad (47)$$

and

$$\delta_x = \delta_y = \begin{cases} 3, & \text{standard BLD,} \\ \frac{1}{3}, & \text{mass-lumped BLD.} \end{cases} \quad (48)$$

II.C. Further Localizations (Lumpings)

II.C.1. Surface Lumping

As we shall see later from our asymptotic analysis, DFEMs gain robustness when they are made more “local”. Mass-matrix lumping makes the collision and source terms local, but other terms can benefit from this as well. Consider the surface term in the i ’th equation of a general DFEM for cell k :

$$[\underline{\mathbf{L}}_k^{surf} \underline{\psi}_k^{surf}]_i \equiv \sum_{l=1}^{L_k} \mathbf{n}_{kl} \int_{\partial V_{kl}} d^2 r w_{ki}(\mathbf{r}_{kl}) \psi(\mathbf{r}_{kl}, \mathbf{\Omega}). \quad (49)$$

We assume that our weight and basis functions are in cardinal form. We further assume (for the moment) that the surface quantity $\psi(\mathbf{r}_{kl}, \mathbf{\Omega})$ can be represented as a linear combination of cell k ’s basis functions on any given surface kl . (This is always true if the basis functions have the surface-matching property that we describe later.) Then the general DFEM surface matrix for cell k is

$$[\underline{\mathbf{L}}_k^{surf}]_{ij} = \sum_{l=1}^{L_k} \mathbf{n}_{kl} \int_{\partial V_{kl}} d^2 r w_{ki}(\mathbf{r}) b_{kj}(\mathbf{r}). \quad (50)$$

With this notation in place, we can now define surface lumping for our general DFEM. To our knowledge, this is a new concept for finite element methods (except for our previous conference papers^{3,10}). The lumped surface matrix is

$$\begin{aligned} [\underline{\mathbf{L}}_k^{surf, lump}]_{ij} &= b_{kj}(\mathbf{r}_{ki}) \sum_{l=1}^{L_k} \mathbf{n}_{kl} \int_{\partial V_{kl}} d^2 r w_{ki}(\mathbf{r}) \\ &= \delta_{ij} \sum_{l=1}^{L_k} \mathbf{n}_{kl} \int_{\partial V_{kl}} d^2 r w_{ki}(\mathbf{r}), \end{aligned} \quad (51)$$

where \mathbf{r}_{ki} is the support point for the ki ’th weight and basis function.

For a more concrete illustration, we present the BLD equations with both mass and surface lumping:

$$\begin{aligned} \frac{\mu \Delta y}{2} \begin{bmatrix} -\psi_{1L} \\ \psi_{2R} \\ \psi_{3R} \\ -\psi_{4L} \end{bmatrix} + \frac{\mu \Delta y}{12} \begin{bmatrix} 2 & 2 & 1 & 1 \\ -2 & -2 & -1 & -1 \\ -1 & -1 & -2 & -2 \\ 1 & 1 & 2 & 2 \end{bmatrix} \begin{bmatrix} \psi_1 \\ \psi_2 \\ \psi_3 \\ \psi_4 \end{bmatrix} \\ + \frac{\eta \Delta x}{12} \begin{bmatrix} 2 & 1 & 1 & 2 \\ 1 & 2 & 2 & 1 \\ -1 & -2 & -2 & -1 \\ -2 & -1 & -1 & -2 \end{bmatrix} \begin{bmatrix} \psi_1 \\ \psi_2 \\ \psi_3 \\ \psi_4 \end{bmatrix} + \frac{\eta \Delta x}{2} \begin{bmatrix} -\psi_{1B} \\ -\psi_{2B} \\ \psi_{3T} \\ \psi_{4T} \end{bmatrix} \\ + \frac{\sigma \Delta x \Delta y}{4} \begin{bmatrix} \psi_1 \\ \psi_2 \\ \psi_3 \\ \psi_4 \end{bmatrix} = \frac{(\sigma - \sigma_a) \Delta x \Delta y}{(4\pi)4} \begin{bmatrix} \phi_1 \\ \phi_2 \\ \phi_3 \\ \phi_4 \end{bmatrix} + \frac{\Delta x \Delta y}{(4\pi)4} \begin{bmatrix} q_1 \\ q_2 \\ q_3 \\ q_4 \end{bmatrix}. \end{aligned} \quad (52)$$

II.C.2. Lumping of Within-Cell Gradient Term

As we shall see later from our analysis, lumping of the mass and surface matrices does help DFEMs achieve robustness in optically thick, diffusive problems. However, these measures do not produce completely robust methods; their solutions can still contain unphysical oscillations and negativities in diffusive regions. To further rectify this, we introduce a localization of the only remaining terms in the DFEM—the within-cell portions of the gradient terms. Following the same philosophy as in mass- and surface-matrix lumping, we make the gradient terms as local as possible. Without lumping, the surface and within-cell gradient matrices satisfy the following:

$$\begin{aligned} [\underline{\mathbf{L}}_k^{surf}]_{ij} + [\underline{\mathbf{L}}_k]_{ij} \\ = \sum_{l=1}^{L_k} \mathbf{n}_{kl} \int_{\partial V_{kl}} d^2 r w_{ki}(\mathbf{r}) b_{kj}(\mathbf{r}) - \int_{V_k} d^3 r b_{kj}(\mathbf{r}) \nabla w_{ki}(\mathbf{r}) \\ = \int_{V_k} d^3 r w_{ki}(\mathbf{r}) \nabla b_{kj}(\mathbf{r}). \end{aligned} \quad (53)$$

We define the lumped sum as follows:

$$[\underline{\mathbf{L}}_k^{surf, lump}]_{ij} + [\underline{\mathbf{L}}_k^{lump}]_{ij} \equiv \nabla b_{kj}(\mathbf{r}_{ki}) \int_{V_k} d^3 r w_{ki}(\mathbf{r}). \quad (54)$$

The lumped within-cell gradient matrix is therefore

$$[\underline{\mathbf{L}}_k^{lump}]_{ij} \equiv \nabla b_{kj}(\mathbf{r}_{ki}) \int_{\mathbb{V}_k} d^3r w_{ki}(\mathbf{r}) - [\underline{\mathbf{L}}_k^{surf, lump}]_{ij} . \quad (55)$$

We illustrate this with the fully lumped BLD (FLBLD) equations:

$$\begin{aligned} & \frac{\mu\Delta y}{2} \begin{bmatrix} -\psi_{1L} \\ \psi_{2R} \\ \psi_{3R} \\ -\psi_{4L} \end{bmatrix} + \frac{\mu\Delta y}{4} \begin{bmatrix} 1 & 1 & 0 & 0 \\ -1 & -1 & 0 & 0 \\ 0 & 0 & -1 & -1 \\ 0 & 0 & 1 & 1 \end{bmatrix} \begin{bmatrix} \psi_1 \\ \psi_2 \\ \psi_3 \\ \psi_4 \end{bmatrix} \\ & + \frac{\eta\Delta x}{4} \begin{bmatrix} 1 & 0 & 0 & 1 \\ 0 & 1 & 1 & 0 \\ 0 & -1 & -1 & 0 \\ -1 & 0 & 0 & -1 \end{bmatrix} \begin{bmatrix} \psi_1 \\ \psi_2 \\ \psi_3 \\ \psi_4 \end{bmatrix} \\ & + \frac{\eta\Delta x}{2} \begin{bmatrix} -\psi_{1B} \\ -\psi_{2B} \\ \psi_{3T} \\ \psi_{4T} \end{bmatrix} + \frac{\sigma\Delta x\Delta y}{4} \begin{bmatrix} \psi_1 \\ \psi_2 \\ \psi_3 \\ \psi_4 \end{bmatrix} \\ & = \frac{(\sigma - \sigma_a)\Delta x\Delta y}{(4\pi)4} \begin{bmatrix} \phi_1 \\ \phi_2 \\ \phi_3 \\ \phi_4 \end{bmatrix} + \frac{\Delta x\Delta y}{(4\pi)4} \begin{bmatrix} q_1 \\ q_2 \\ q_3 \\ q_4 \end{bmatrix} . \quad (56) \end{aligned}$$

The FLBLD equations can also be cast in the form of Eqs. (42) through (45), with the following intriguingly simple definitions of parameters:

$$\theta_x = \theta_y = \gamma_x = \gamma_y = \delta_x = \delta_y = 1 , \quad \text{FLBLD} . \quad (57)$$

It is also interesting to note that the FLBLD equations have a very simple physical interpretation, namely, that they enforce particle conservation (or balance) on each of four “corner” subcells. The first row of Eq. (56), for example, is

$$\begin{aligned} & \frac{\mu\Delta y}{2} \left(\frac{\psi_1 + \psi_2}{2} - \psi_{1L} \right) + \frac{\eta\Delta x}{2} \left(\frac{\psi_1 + \psi_4}{2} - \psi_{1B} \right) \\ & + \frac{\sigma\Delta x\Delta y}{4} \psi_1 = \frac{\Delta x\Delta y}{4} \frac{Q_{tot,1}}{4\pi} . \quad (58) \end{aligned}$$

Here ψ_1 plays the role of the volume-averaged solution over the lower left quarter of the cell, $\mu(\psi_1 + \psi_2)/2$ is the net outleakage rate density on the right surface of that subcell, $-\mu\psi_{1L}$ is the net outleakage rate density on the left surface of that subcell, etc. With these and other similar interpretations, Eq. (58) is simply a statement of particle conservation on the lower left rectangular quarter of the cell.

This observation led to the creation of a new but related family of methods based on enforcing particle balance on corner subcells.¹¹ The methods are called corner-balance methods, and they are applicable to arbitrary grids. We will refer to these occasionally during our analysis of DFEMs in thick diffusive problems.

II.D. Summary of DFEMs

The DFEMs that we analyze here are given by Eqs. (10) through (17). These equations are very general; they hold for an infinite variety of DFEMs in one, two, or three dimensions, and for arbitrary spatial grids. We have given two specific examples of standard DFEMs—the BLD and LD methods on rectangular cells in XY geometry. We have discussed mass-matrix lumping and introduced other forms of lumping, and in each case we have illustrated with BLD on two-dimensional rectangles.

III. ASYMPTOTIC ANALYSIS

III.A. Exact Transport

We begin with a brief review of the behavior of the exact transport solution in a diffusive region. This review is taken from Ref. 19 and references therein. We begin by considering a scaled version of the exact transport equation:

$$\begin{aligned} \boldsymbol{\Omega} \cdot \nabla \Psi + \frac{\sigma(\mathbf{r})}{\epsilon} \Psi(\mathbf{r}, \boldsymbol{\Omega}) &= \frac{1}{4\pi} \left(\frac{\sigma(\mathbf{r})}{\epsilon} - \epsilon\sigma_a(\mathbf{r}) \right) \Phi(\mathbf{r}) \\ &+ \epsilon \frac{q_{ext}(\mathbf{r})}{4\pi} , \quad \mathbf{r} \in \mathbb{V} , \quad (59) \end{aligned}$$

$$\Phi(\mathbf{r}) = \int_{4\pi} d\Omega \Psi(\mathbf{r}, \boldsymbol{\Omega}) , \quad (60)$$

and

$$\begin{aligned} \Psi(\mathbf{r}, \boldsymbol{\Omega}) &= \psi_{inc}(\mathbf{r}, \boldsymbol{\Omega}) , \\ \mathbf{r} \in \partial\mathbb{V} , \quad \mathbf{n}(\mathbf{r}) \cdot \boldsymbol{\Omega} &< 0 . \quad (61) \end{aligned}$$

Here ϵ is a small parameter that determines the extent to which the problem is diffusive: The smaller ϵ becomes, the more optically thick and highly scattering the problem becomes. We guess that the solution is a power series in ϵ .

$$\text{Postulate: } \Psi = \Psi^{(0)} + \epsilon\Psi^{(1)} + \epsilon^2\Psi^{(2)} + \dots . \quad (62)$$

We then find that in the interior of the domain \mathbb{V} (i.e., away from boundaries), the leading-order angular intensity is isotropic and satisfies a diffusion equation:

$$\Psi^{(0)}(\mathbf{r}, \boldsymbol{\Omega}) = \frac{1}{4\pi} \Phi^{(0)}(\mathbf{r}) \quad (63)$$

and

$$-\nabla \cdot \frac{1}{3\sigma(\mathbf{r})} \nabla \Phi^{(0)} + \sigma_a(\mathbf{r}) \Phi^{(0)}(\mathbf{r}) = q_{ext}(\mathbf{r}) . \quad (64)$$

This does not fully describe the leading-order interior solution, for the solution of the diffusion equation is not unique until it is subjected to appropriate boundary conditions. One finds after considerable analysis that the boundary condition that gives the correct leading-order interior solution is

$$\Phi^{(0)}(\mathbf{r}) = 2 \int_{\mathbf{n} \cdot \boldsymbol{\Omega} < 0} d\Omega W(|\mathbf{n} \cdot \boldsymbol{\Omega}|) \psi_{inc}(\mathbf{r}, \boldsymbol{\Omega}) , \quad \mathbf{r} \in \partial \mathbb{V} . \quad (65)$$

Here, W is defined in terms of Chandrasekhar's H -function²⁰ for a purely scattering medium; it is reasonably well approximated by a simple polynomial:

$$W(\mu) \equiv \frac{\sqrt{3}}{2} \mu H(\mu) = 0.91\mu + 1.635\mu^2 \pm \text{a few } \% \\ \approx \mu + \frac{3}{2} \mu^2 . \quad (66)$$

We note two things about the boundary condition satisfied by the leading-order interior solution:

1. It is a Dirichlet condition, specifying the scalar intensity on the boundary.
2. It retains no memory of azimuthal variations (about the surface normal) in the incident angular intensity.

III.B. Discontinuous Finite Element Methods

III.B.1. First Stage of Analysis

We now apply a similar analysis to our family of DFEMs. We begin with scaled versions of the DFEM equations, written in the matrix form of Eq. (11):

$$\boldsymbol{\Omega} \cdot [\underline{\mathbf{L}}_k^{surf} \underline{\psi}_k^{surf} + \underline{\mathbf{L}}_k \underline{\psi}_k] + \frac{1}{\epsilon} \underline{\mathbf{T}}_k \underline{\Psi}_k \\ = \frac{1}{4\pi} \left[\frac{1}{\epsilon} \underline{\mathbf{T}}_k - \epsilon \underline{\mathbf{A}}_k \right] \underline{\phi}_k + \frac{\epsilon}{4\pi} \underline{q}_k . \quad (67)$$

We postulate a power-series expansion for the unknowns:

$$u = u^{(0)} + \epsilon u^{(1)} + \epsilon^2 u^{(2)} + \dots , \quad (68)$$

where $u = \phi_{kj}$ or $\psi_{kj}(\boldsymbol{\Omega})$. [A proof by Börger, described in Ref. 7, shows that this postulate is rigorously correct. This basically follows from the fact that the matrices in Eq. (67) are independent of ϵ .]

Given the reasonable provision that the mass matrix is invertible in each cell, the coefficients of ϵ^{-1} in Eq. (67) immediately tell us that all leading-order cell-interior unknowns are isotropic:

$$\psi_{kj}^{(0)}(\boldsymbol{\Omega}) = \frac{1}{4\pi} \phi_{kj}^{(0)} , \quad j = 1 \dots I_k , \quad k = 1 \dots K . \quad (69)$$

The coefficients of ϵ^0 in the same equation, with $\boldsymbol{\Omega}$ taken to be a quadrature direction $\boldsymbol{\Omega}_m$, satisfy

$$\boldsymbol{\Omega}_m \cdot [\underline{\mathbf{L}}_k^{surf} \underline{\psi}_k^{surf(0)} + \underline{\mathbf{L}}_k \underline{\psi}_k^{(0)}] + \underline{\mathbf{T}}_k \underline{\psi}_k^{(1)} = \frac{1}{4\pi} \underline{\mathbf{T}}_k \underline{\phi}_k^{(1)} . \quad (70)$$

If we multiply by the quadrature weight Δ_m and sum over all quadrature directions $m = 1 \dots M$, we find that most of the terms vanish or cancel, leaving

$$\sum_{m=1}^M \Delta_m \boldsymbol{\Omega}_m \cdot \underline{\mathbf{L}}_k^{surf} \underline{\psi}_k^{surf(0)} = 0 . \quad (71)$$

Here, we have made two mild assumptions about the discrete ordinates quadrature set:

$$\sum_{m=1}^M \Delta_m = 4\pi , \quad \sum_{m=1}^M \Delta_m \boldsymbol{\Omega}_m = 0 . \quad (72)$$

Equations (71) contain a great deal of information. They will tell us the resolution of each DFEM, which is the number of degrees of freedom in the leading-order solution that are devoted to satisfying the correct diffusion equation. For example, they will identify DFEMs that have zero resolution and thus fail miserably in thick diffusive regions. They will also allow us to define DFEM properties that guarantee full resolution. To unlock this wealth of information, however, we must perform some manipulations. We first rewrite the ki 'th of Eqs. (71) using the definition, Eq. (15), of the surface term:

$$\sum_{l=1}^{L_k} \mathbf{n}_{kl} \cdot \sum_{m=1}^M \Delta_m \boldsymbol{\Omega}_m \int_{\partial \mathbb{V}_{kl}} d^2 r w_{ki}(\mathbf{r}) \psi^{(0)}(\mathbf{r}_{kl}, \boldsymbol{\Omega}_m) = 0 . \quad (73)$$

(For now we assume no surface lumping. We discuss the effects of lumping later.) We then employ the upstream definition, Eq. (10):

$$\sum_{l=1}^{L_k} \int_{\partial \mathbb{V}_{kl}} d^2 r w_{ki}(\mathbf{r}) \left\{ \sum_{m: \mathbf{n}_{kl} \cdot \boldsymbol{\Omega}_m > 0} \Delta_m \mathbf{n}_{kl} \cdot \boldsymbol{\Omega}_m \psi^{(0)}(\mathbf{r}_{kl}^-, \boldsymbol{\Omega}_m) \right. \\ \left. + \sum_{m: \mathbf{n}_{kl} \cdot \boldsymbol{\Omega}_m < 0} \Delta_m \mathbf{n}_{kl} \cdot \boldsymbol{\Omega}_m \psi^{(0)}(\mathbf{r}_{kl}^+, \boldsymbol{\Omega}_m) \right\} = 0 , \quad (74)$$

where the $+$ and $-$ superscripts refer to a point just outside or inside of cell k . If the surface kl is in the problem interior, then the point \mathbf{r}_{kl}^+ is just inside an adjacent cell. Otherwise, the point is just outside the problem

boundary, and the incident angular intensity at that point is given by the boundary condition shown in Eq. (3).

Consider first a cell k in the problem interior. Then by Eq. (69) we know that each angular intensity in Eq. (74) is isotropic, and we obtain

$$\sum_{l=1}^{L_k} \int_{\partial V_{kl}} d^2 r w_{ki}(\mathbf{r}) \sum_{m: \mathbf{n}_{kl} \cdot \mathbf{\Omega}_m > 0} \Delta_m \mathbf{n}_{kl} \times \mathbf{\Omega}_m [\phi^{(0)}(\mathbf{r}_{kl}^-) - \phi^{(0)}(\mathbf{r}_{kl}^+)] = 0 ,$$

k in interior . (75)

Here, we have used the second of the quadrature assumptions in Eqs. (72) and multiplied through by 4π . It is convenient to define

$$\rho_{kl} \equiv \frac{2 \sum_{m: \mathbf{n}_{kl} \cdot \mathbf{\Omega}_m > 0} \Delta_m \mathbf{n}_{kl} \cdot \mathbf{\Omega}_m}{\sum_{m: \mathbf{n}_{kl} \cdot \mathbf{\Omega}_m > 0} \Delta_m}$$

$$= \frac{2 \sum_{m: \mathbf{n}_{kl} \cdot \mathbf{\Omega}_m < 0} \Delta_m |\mathbf{n}_{kl} \cdot \mathbf{\Omega}_m|}{\sum_{m: \mathbf{n}_{kl} \cdot \mathbf{\Omega}_m < 0} \Delta_m} \approx 1 . \quad (76)$$

Equations (75) hold for all cells, even those on the boundary, if we define

$$\phi^{(0)}(\mathbf{r}_{kl}^+) \equiv \phi_{bdy}(\mathbf{r}_{kl})$$

$$\equiv 2 \sum_{m: \mathbf{n}_{kl} \cdot \mathbf{\Omega}_m < 0} \Delta_m \frac{2 \mathbf{n}_{kl} \cdot \mathbf{\Omega}_m}{\rho_{kl}} \psi_{inc}(\mathbf{r}_{kl}^+, \mathbf{\Omega}_m) ,$$

$\mathbf{r}_{kl} \in \partial V$. (77)

This defines a boundary scalar intensity such that if the incident angular intensity were $1/4\pi$ times that value, the incident particle flow rate would be the same as the actual rate. We can now rewrite Eqs. (75) as follows:

$$\sum_{l=1}^{L_k} \rho_{kl} \int_{\partial V_{kl}} d^2 r w_{ki}(\mathbf{r}) [\phi^{(0)}(\mathbf{r}_{kl}^-) - \phi^{(0)}(\mathbf{r}_{kl}^+)] = 0 ,$$

all k and i . (78)

In words, this result says that the leading-order DFEM scalar intensity is *continuous in a weighted-residual sense* but not necessarily continuous pointwise.

Equations (78) are simply manipulations of Eqs. (71), which as we mentioned contain a great deal of information. They relate leading-order scalar-intensity unknowns to each other and to certain weighted integrals of the incident angular intensities on the problem boundary. This is a very important observation. As we shall see, it means that for some DFEMs the leading-order cell-interior scalar intensities are determined solely by the incident an-

gular intensities, *with no regard for interior sources or cross sections*.

To show this and to learn more about the leading-order scalar intensities, we shall manipulate Eqs. (78) into matrix form. For a problem-interior cell surface kl , we denote by $\langle kl \rangle'$ the cell that shares surface kl with cell k . Then we can rewrite Eqs. (78) as follows:

$$\sum_{l=1}^{L_k} \rho_{kl} \int_{\partial V_{kl} \notin \partial V} d^2 r w_{ki}(\mathbf{r}) \times \left[\sum_{j=1}^{J_k} \phi_{kj}^{(0)} b_{kj}(\mathbf{r}_{kl}^-) - \sum_{j=1}^{J_{\langle kl \rangle'}} \phi_{\langle kl \rangle' j}^{(0)} b_{\langle kl \rangle' j}(\mathbf{r}_{kl}^+) \right]$$

$$+ \sum_{l=1}^{L_k} \rho_{kl} \int_{\partial V_{kl} \in \partial V} d^2 r w_{ki}(\mathbf{r}) \sum_{j=1}^{J_k} \phi_{kj}^{(0)} b_{kj}(\mathbf{r}_{kl}^-)$$

$$= \sum_{l=1}^{L_k} \rho_{kl} \int_{\partial V_{kl} \in \partial V} d^2 r w_{ki}(\mathbf{r}) \phi_{bdy}(\mathbf{r})$$

$$\equiv \beta_{bdy}^{ki} = \text{known} , \quad \text{all } k \text{ and } i . \quad (79)$$

The left side of each equation is simply a linear combination of the DFEM's leading-order scalar-intensity unknowns. Thus, when all k and i are considered, the left side is a square matrix multiplying the vector of leading-order unknowns. The right side of each equation is known in terms of the boundary condition; thus, when all k and i are considered, the right side is a known vector. We therefore have

$$\underline{\underline{B}} \underline{\phi}_{int} = \underline{\beta}_{bdy} . \quad (80)$$

III.B.2. Consequences of Eq. (80)

The matrix $\underline{\underline{B}}$ depends only on the grid, the values of ρ as defined in Eq. (76), the DFEM weight functions, and the DFEM basis functions. That is, this matrix contains nothing about the physical problem being solved. Note that the matrix $\underline{\underline{B}}$ is square. We emphasize the following:

1. The matrix equation (80) is I_{tot} equations for the I_{tot} leading-order scalar-intensity unknowns $\{\phi_{kj}^{(0)}\}$, where $I_{tot} = \sum_k J_k$.

2. If all I_{tot} of these equations are independent (that is, if the matrix $\underline{\underline{B}}$ is invertible), then they completely determine the $\{\phi_{kj}^{(0)}\}$.

3. The leading-order scalar intensities $\{\phi_{kj}^{(0)}\}$ completely determine the leading-order DFEM solution. [See Eq. (69).]

4. Equations (80) contain no information about sources or cross sections; thus, if they determine the leading-order solution, the leading-order solution will be absurd.

For example, if all I_{tot} Eqs. (80) are independent and the problem has vacuum boundaries [which makes the right side of each equation vanish], the leading-order solution will be zero, regardless of what sources may be present. We note that equations very similar to Eqs. (80) also arise with characteristic methods, with exactly the same implications.⁶

The matrix $\underline{\underline{B}}$ is $I_{tot} \times I_{tot}$, where I_{tot} = total number of weight functions = total number of scalar-intensity unknowns in the problem. If this matrix is invertible, the DFEM will produce absurd solutions in thick diffusive regions, as detailed previously. If, on the other hand, it has one or more rows that are linear combinations of other rows, then some of Eqs. (80) are redundant, and thus they do not fully determine the leading-order solution. Only DFEMs with such redundancies have the potential to obtain reasonable solutions in thick diffusive domains. The number of redundant rows in Eqs. (80) determines the *resolution* of the DFEM in thick diffusive regions because, as we show later, each such redundancy corresponds to a discrete diffusion equation satisfied by the leading-order solution. If there is one redundancy per vertex (or face or edge), then we call the DFEM *full-resolution*.

In deriving Eq. (80), we assumed no lumping of the surface matrix. With lumping, Eq. (80) still holds, but it represents the following lumped version of Eq. (79):

$$\begin{aligned} & \sum_{l=1}^{L_k} \rho_{kl} [\phi_{ki}^{(0)} - \phi_{\langle kl \rangle' j'}^{(0)}] \int_{\partial \mathbb{V}_{kl} \notin \partial \mathbb{V}} d^2 r w_{ki}(\mathbf{r}) \\ & + \sum_{l=1}^{L_k} \rho_{kl} \phi_{ki}^{(0)} \int_{\partial \mathbb{V}_{kl} \in \partial \mathbb{V}} d^2 r w_{ki}(\mathbf{r}) \\ & = \sum_{l=1}^{L_k} \rho_{kl} \phi_{bdy}(\mathbf{r}_{ki}) \int_{\partial \mathbb{V}_{kl} \in \partial \mathbb{V}} d^2 r w_{ki}(\mathbf{r}) \\ & \equiv \beta_{bdy}^{ki} = \text{known} \quad , \quad \text{all } k \text{ and } i \quad . \end{aligned} \quad (81)$$

(Here j' is defined such that the support point for basis function $b_{\langle kl \rangle' j'}$ is the same as the support point for weight function w_{ki} and basis function b_{ki} .) Lumping will generally make the matrix $\underline{\underline{B}}$ of Eq. (80) sparser. All of the previous comments still apply; for example, $\underline{\underline{B}}$ must have one redundant row per vertex (or face or edge) for the DFEM to attain full resolution.

III.B.3. Litmus Test for Full-Resolution Discontinuous Finite Element Method Behavior

In the conference paper that led to the present work, we presented properties of the weight functions $\{w_{ki}\}$ that are sufficient to guarantee redundant Eqs. (80) (Ref. 3). We refer to these as the *locality* and *surface-matching* properties. In the terminology of this paper, we shall show that these two properties are sufficient to guarantee full resolution.

“Locality” of weight functions means that in Eq. (79), only tightly clustered faces l of cell k will produce non-zero surface integrals. “Tightly clustered” faces can mean a single face or it can mean a set of faces that touch a single edge or vertex. See Fig. 2 for a two-dimensional example. (In two dimensions, edges and faces are the same objects.)

The BLD cardinal weight functions on rectangular cells in two dimensions have the locality property: Each is zero on all surfaces except for the two adjacent to its support-point vertex. However, these same BLD weight functions, which have the same span as $\{1, x, y, xy\}$, do not have the locality property on general quadrilaterals; in fact, no polynomial functions do.²¹ The LD weight functions on rectangles do not have the locality property: Each function (and each linear combination of functions) is a plane, which cannot be zero on more than one surface of a rectangle unless it is zero everywhere. However, the LD weight functions on triangles do have the locality property. Figure 3a shows an example of a weight function that is local to the edges that touch one vertex of a rectangle.

Figure 4 gives examples of tightly clustered faces in three dimensions. In three dimensions, the analog of BLD is trilinear DFEM (TLD), whose weight and basis functions have the same span as $\{1, x, y, z, xy, xz, yz, xyz\}$. The TLD cardinal functions on orthogonal hexahedral (brick-shaped) cells have the locality property: Each is nonzero only on the three faces that touch a single vertex. In three dimensions, the LD method’s weight and basis functions span the space of $\{1, x, y, z\}$. Thus, LD has the locality property on tetrahedral cells in three dimensions, but not on cells with more than four vertices. Similarly, TLD does not have the locality property on nonorthogonal hexahedral cells (i.e., those whose surfaces do not meet at right angles), nor does it have this property on other polyhedral cells in general.

When combined with the locality property, the surface-matching property guarantees redundancies in Eqs. (80). Surface matching means that for each face kl in the local cluster for the i ’th weight function in cell k , a weight function that exactly matches w_{ki} on the surface kl exists in the adjacent cell $\langle kl \rangle'$. The BLD and LD weight functions have this property on rectangles and triangles, respectively, in two dimensions: Each is

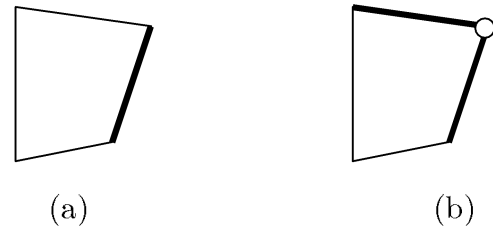


Fig. 2. Graphic representation of tightly clustered faces in two dimensions: (a) single edge and (b) two edges touching a single vertex.

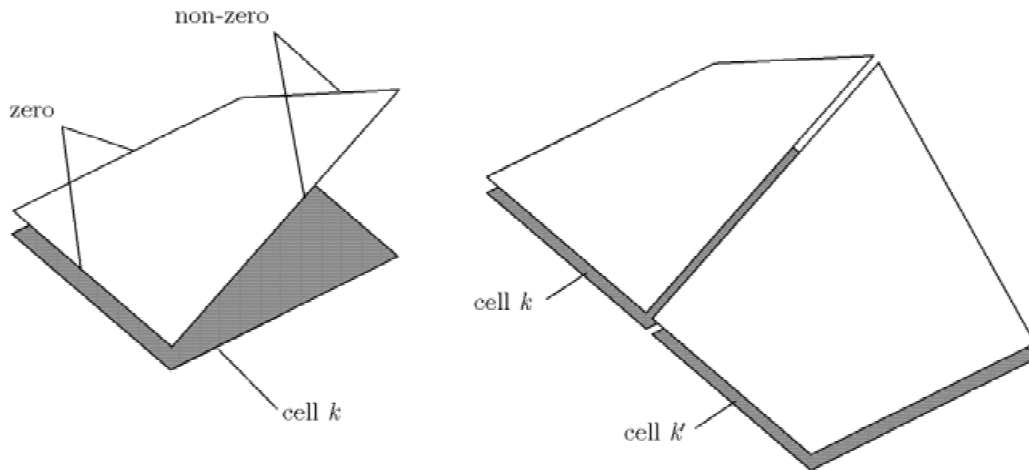


Fig. 3. (a) A weight function that is local to a vertex. (b) Two surface-matching weight functions.

simply a straight line on any given cell edge. The TLD weight functions have this property on orthogonal hexahedra (brick shapes) in three dimensions: Each is a cardinal bilinear function on any given cell face. Also, the LD functions have this property on tetrahedral cells in three dimensions. Figure 3b shows an example of two weight functions in neighboring two-dimensional rectangular cells that have the surface-matching property on the surface between the cells.

If a DFEM's weight functions have the locality and surface-matching properties, then each local cluster of faces in the interior of the problem will yield a redundant row in the matrix $\underline{\underline{B}}$. We shall show later that each redundancy arising from these properties results in a discrete diffusion equation that is satisfied by the leading-order solution. A full-resolution DFEM will have such a redundancy at each interior local cluster (which could mean each face, each edge, or each vertex) in the problem. On a rectangular grid in two dimensions, BLD has such a redundancy at each interior vertex. On the same grid, LD has no such redundancies at all and is thus a zero-resolution method in our terminology. TLD has such a redundancy at each interior vertex in a three-dimensional grid of brick-shaped cells, as does LD on grids of tetrahedral (three-dimensional) or triangular (two-dimensional) cells.

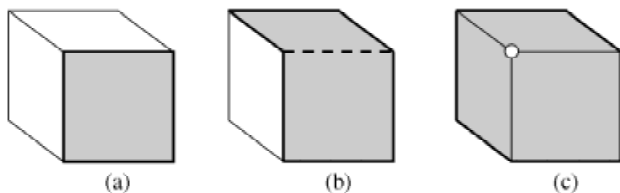


Fig. 4. Graphic representation of tightly clustered faces in three dimensions: (a) single face, (b) two faces touching a single edge, and (c) three faces touching a single vertex.

The locality and surface-matching properties are *sufficient* to cause redundant rows in $\underline{\underline{B}}$ and in fact are sufficient to ensure that the DFEM is full-resolution. These properties are not *necessary* for redundant rows—it is possible to have redundant rows for other reasons—but we suspect that they are necessary for a full-resolution leading-order solution. That is, we have been unable to imagine a DFEM that has full resolution without the locality and surface-matching properties.

One way for $\underline{\underline{B}}$ to be singular without the locality and surface-matching properties is for some weight functions to be zero on all cell boundaries. Some DFEMs can have cardinal weight sets with support points in cell interiors as well as on cell surfaces. A weight function whose support point is in a cell interior can easily be zero on all cell surfaces, in which case Eq. (78) produces a row of zeros in the matrix $\underline{\underline{B}}$. If for each such cell-interior weight function there is a cell-interior basis function, then the matrix will have a column of zeros for every row of zeros. These trivial rows and columns should be eliminated from the matrix, and the vector ϕ_{int} should be similarly reduced by removing the unknowns that are coefficients of the cell-interior basis functions. After this reduction, we obtain a reduced version of Eq. (80) to which the locality and surface-matching tests can be applied. For example, if this reduced system is nonsingular, the method will have zero resolution, and its leading-order scalar intensities will be absurd, by the arguments given previously.

We have already mentioned that on rectangular cells in two dimensions, BLD has the locality and surface-matching properties while LD does not. Thus, our theory predicts that LD will fail in thick diffusive regions given rectangular grids in two dimensions. (Our numerical results illustrate this rather dramatic failure.) However, given triangular cells in two dimensions, LD does have the locality and surface-matching properties. We therefore predict that LD on triangles (or on

tetrahedra in three dimensions) will be full-resolution. This is consistent with computational experience reported by others.¹⁶

We summarize some of what this means in two dimensions in Table I. The first column illustrates a cell shape, the second describes the function space spanned by the method's weight functions, and the third describes the resolution of the method. Table II contains similar information for three dimensions.

III.B.4. Remainder of Analysis

We now continue the analysis. We assume that the DFEM in question has the locality and surface-matching properties previously described and thus is a full-resolution method. Let us suppose for the moment that the DFEM has cardinal weight functions that are local to each vertex of each cell, which means each weight function produces nonzero surface moments only on cell surfaces that touch its vertex. [The BLD method on rectangles (two dimensions), the LD method on triangles (two dimensions) and tetrahedra (three dimensions), and the TLD method on orthogonal hexahedra (three dimensions) are examples of such DFEMs.] We shall show that the leading-order solution satisfies a set of discretized diffusion equations, with one equation per vertex.

If we consider the i 'th weight function of cell k , Eq. (78) becomes

$$\sum_{\substack{\text{surfaces } l \text{ of cell } k \\ \text{touching point } p}} \rho_{kl} \int_{\partial \mathbb{V}_{kl}} d^2 r w_{ki}(\mathbf{r}) [\phi^{(0)}(\mathbf{r}_{kl}^-) - \phi^{(0)}(\mathbf{r}_{kl}^+)] = 0 . \quad (82)$$

(We have used the assumption of locality to restrict the limits on the summation.) It is convenient to define cell-surface spatial moments:

$$F_{kli}^{(0)} \equiv \frac{1}{A_{kl}} \int_{\partial \mathbb{V}_{kl}} d^2 r w_{ki}(\mathbf{r}) \phi^{(0)}(\mathbf{r}_{kl}^-) ,$$

$$A_{kl} \equiv \int_{\partial \mathbb{V}_{kl}} d^2 r . \quad (83)$$

In this notation, Eq. (82) becomes

$$\sum_{\substack{\text{surfaces } l \text{ of cell } k \\ \text{touching point } p}} \rho_{kl} A_{kl} [F_{kli}^{(0)} - F_{\langle k l i \rangle}^{(0)}] = 0 ,$$

$$p \equiv \text{index of } i\text{'th vertex of cell } k . \quad (84)$$

Here, we have used $\langle k l i \rangle$ to denote the indices k' , l' , and i' , where

TABLE I
Performance of Selected DFEMs on Selected Cell Shapes in Two Dimensions

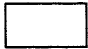
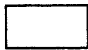

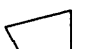

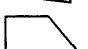
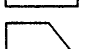
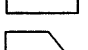
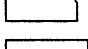
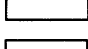









Cell Shape	Weight-Function Space	Resolution
	$\{1, x, y\}$ (LD)	Zero (Absurd solution)
	$\{1, x, y, xy\}$ (BLD)	Full
	$\{1, x, y\}$ (LD)	Full
	$\{1, x, y, xy\}$ (BLD)	Zero (Absurd solution)
	$\{1, a, b, ab\}$ (BLD in mapped coordinates with cell mapped to square)	Full
	{Any four functions}	Zero (Absurd solution)
	{Any set of polynomials}	Zero (Absurd solution)
	{Five rational polynomials a la Wachpress ²¹ }	Full
	$\{1, x, y, xy\}$ (Mass-lumped BLD)	Full
	$\{1, x, y, xy\}$ (Fully lumped BLD)	Full

TABLE II

Performance of Selected DFEMs on Selected Cell Shapes in Three Dimensions

Cell Shape	Weight-Function Space	Resolution
	$\{1, x, y, z\}$ (LD)	Zero (Absurd solution)
	$\{1, x, y, z, xy, xz, yz, xyz\}$ (TLD)	Full
	$\{1, x, y, z\}$ (LD)	Full
	$\{1, x, y, z, xy, xz, yz, xyz\}$ (TLD)	Zero (Absurd solution)
	$\{1, a, b, c, ab, ac, bc, abc\}$ (TLD in mapped coordinates with cell mapped to cube)	Full
	{Any eight functions}	Zero (Absurd solution)
	{Any set of polynomials}	Zero (Absurd solution)
	$\{1, x, y, z, xy, xz, yz, xyz\}$ (Mass-lumped TLD)	Full
	$\{1, x, y, z, xy, xz, yz, xyz\}$ (Fully lumped TLD)	Full

k' = cell that shares surface l with cell k

l' = cell (k')'s index of the shared surface

i' = weight function in cell k' that mirrors w_{ki} on the surface l' .

If the surface l is on the problem boundary, then $F_{kli}^{(0)}$ is defined in terms of ϕ_{bdy} [see Eq. (77)]. If the surface matrix is lumped, then the only change is that Eq. (83) is replaced by

$$F_{kli}^{(0)} \equiv \frac{1}{A_{kl}} \phi^{(0)}(\mathbf{r}_{ki}) \int_{\partial \mathbb{V}_{kl}} d^2 r w_{ki}(\mathbf{r}_{kl}) \text{ (if surface lumping)} . \quad (85)$$

This does not change the manipulations that follow.

Suppose p is not on the problem boundary. Then there is an equation similar to Eq. (84) for each cell k' that touches the interior point p . In each such equation, the cell-surface spatial moments of that cell appear with positive coefficients, while those of neighboring cells appear with negative coefficients of the same magnitude. If we add all of these equations, we find that each surface moment appears once with a positive coefficient and once with a negative coefficient:

$$\sum_{\substack{kli: w_{ki} \text{ is} \\ \text{local at } p \text{ and} \\ l \text{ touches } p}} (A_{kl} \rho_{kl} - A_{kl} \rho_{kl}) F_{kli}^{(0)} = 0 , \quad \text{or } 0 = 0 . \quad (86)$$

This means that one Eq. (80) is redundant for each interior vertex. Thus, we have shown that if a DFEM has weight functions that are local to cell vertices and have the surface-matching property, then there are many redundant Eqs. (80)—one per interior vertex. It follows that Eqs. (80) do not completely determine the leading-order scalar intensity and in fact that there remains one degree of freedom in the leading-order scalar intensity for each interior vertex. These remaining degrees of freedom are determined by a discretized diffusion equation, as we show later. This is what we call *full resolution*.

The preceding argument considered weight functions that were local to vertices. Similar arguments hold for weight functions that are local to cell edges or cell surfaces. We conclude that if a DFEM has the local and surface-matching properties, there exists a linear combination of Eqs. (80) that is the trivial equation $0 = 0$ for each interior local cluster of surfaces (which means each interior vertex or edge or surface). This means there exist N sets of multipliers $\{\alpha_{ki}^p\}$, $p = 1, \dots, N$, where N is the number of interior local clusters, such that

$$\sum_{\text{all } k, i} \alpha_{ki}^p \sum_{l=1}^{L_k} A_{kl} \rho_{kl} (F_{kli}^{(0)} - F_{\langle k|l \rangle}^{(0)}) = \sum_{\text{some local set of } k, l, i} (0) F_{kli}^{(0)} . \quad (87)$$

Let us investigate what this implies about the leading-order solution. We consider first the coefficients of ϵ^1 in Eqs. (67). If we multiply by Δ_m , sum over all quadrature directions $m = 1 \dots M$, and rearrange, we obtain

$$\sum_{m=1}^M \Delta_m \Omega_m \cdot [\underline{\mathbf{L}}_k^{surf} \underline{\psi}_k^{surf(1)} + \underline{\mathbf{L}}_k \underline{\psi}_k^{(1)}] + \underline{\mathbf{A}}_k \underline{\phi}_k^{(0)} = \underline{q}_k . \quad (88)$$

We consider the i 'th row of this matrix equation and rewrite the cell-surface term using Eqs. (10) and (15) (which assumes no lumping of the surface matrix):

$$\begin{aligned} \sum_{m=1}^M \Delta_m \Omega_m \cdot [\underline{\mathbf{L}}_k^{surf} \underline{\psi}_k^{surf(1)}]_i &= \sum_{l=1}^{L_k} \mathbf{n}_{kl} \cdot \sum_{m=1}^M \Delta_m \Omega_m \int_{\partial V_{kl}} d^2 r w_{ki}(\mathbf{r}) \psi^{(1)}(\mathbf{r}_{kl}, \Omega_m) \\ &= \sum_{l=1}^{L_k} \int_{\partial V_{kl}} d^2 r w_{ki}(\mathbf{r}) \\ &\quad \times \left\{ \sum_{m: \mathbf{n}_{kl} \cdot \Omega_m > 0} \Omega_m \mathbf{n}_{kl} \cdot \Omega_m \psi^{(1)}(\mathbf{r}_{kl}^-, \Omega_m) \right. \\ &\quad \left. + \sum_{m: \mathbf{n}_{kl} \cdot \Omega_m < 0} \Omega_m \mathbf{n}_{kl} \cdot \Omega_m \psi^{(1)}(\mathbf{r}_{kl}^+, \Omega_m) \right\} \\ &= \sum_{l=1}^{L_k} \int_{\partial V_{kl}} d^2 r w_{ki}(\mathbf{r}) \{ J_k^{out(1)}(\mathbf{r}_{kl}) - J_{\langle k|l \rangle}^{out(1)}(\mathbf{r}_{kl}) \} , \end{aligned} \quad (89)$$

where we have defined $J_k^{out(1)}(\mathbf{r}_{kl})$ to be the order- ϵ one-way flow rate out of cell k at position \mathbf{r}_{kl} and again used $\langle kl \rangle'$ to denote the cell that shares surface kl with cell k . We again define surface spatial moments:

$$\begin{aligned} J_{kli}^{out(1)} &\equiv \frac{1}{A_{kl}} \int_{\partial V_{kl}} d^2 r w_{ki}(\mathbf{r}_{kl}) J_k^{out(1)}(\mathbf{r}_{kl}) , \\ A_{kl} &\equiv \int_{\partial V_{kl}} d^2 r . \end{aligned} \quad (90)$$

This allows us to write the surface term from the ki 'th Eq. (88) as follows:

$$\begin{aligned} \sum_{m=1}^M \Delta_m \Omega_m \cdot [\underline{\mathbf{L}}_k^{surf} \underline{\psi}_k^{surf(1)}]_i &= \sum_{l=1}^{L_k} A_{kl} \{ J_{kli}^{out(1)} - J_{\langle k|l \rangle}^{out(1)} \} \\ &= \sum_{l=1}^{L_k} A_{kl} \rho_{kl} \{ J_{kli}^{out(1)} / \rho_{kl} - J_{\langle k|l \rangle}^{out(1)} / \rho_{kl} \} . \end{aligned} \quad (91)$$

If the surface matrix is lumped, then the only thing that changes in this equation is the definition of the surface spatial moments of the outgoing one-way flow rates:

$$J_{kli}^{out(1)} \equiv \frac{1}{A_{kl}} J_k^{out(1)}(\mathbf{r}_{kl}) \int_{\partial V_{kl}} d^2 r w_{ki}(\mathbf{r}_{kl}) \quad (\text{if surface lumping}) . \quad (92)$$

Note that the surface term in Eq. (88) has exactly the same form as Eq. (84). This means that if there is a linear combination of Eqs. (84) that produces the trivial equation $0 = 0$, as in Eq. (86), then the same linear combination will make the cell-surface terms of Eqs. (88) vanish. Thus, the p 'th set of multipliers $\{\alpha_{ki}^p\}$ applied to the rows of Eqs. (88) yields

$$0 + \sum_{\text{all } k, i} \alpha_{ki}^p \{ [\underline{\mathbf{L}}_k \cdot \underline{\mathbf{J}}_k^{(1)}]_i + [\underline{\mathbf{A}}_k \underline{\phi}_k^{(0)}]_i \} = \sum_{\text{all } k, i} \alpha_{ki}^p q_{ki} , \quad (93)$$

where we have defined the $O(\epsilon)$ net current densities:

$$\underline{\mathbf{J}}_k^{(1)} \equiv \sum_{m=1}^M \Delta_m \Omega_m \underline{\psi}_k^{(1)} . \quad (94)$$

We shall now show that Eq. (93) is simply a weighted spatial integral of the particle-balance equation (which is itself an angle-integrated transport equation). We first insert the definitions, Eqs. (16) and (17), of the matrices in Eq. (93):

$$\begin{aligned} \sum_{\text{all } k, i} \alpha_{ki}^p \sum_{j=1}^{J_k} \left\{ - \int_{V_k} d^3 r b_{kj}(\mathbf{r}) \nabla w_{ki} \cdot \underline{\mathbf{J}}_{kj}^{(1)} \right. \\ \left. + \int_{V_k} d^3 r w_{ki}(\mathbf{r}) \sigma_a(\mathbf{r}) b_{kj}(\mathbf{r}) \phi_{kj}^{(0)} \right\} \\ = \sum_{\text{all } k, i} \alpha_{ki}^p \int_{V_k} d^3 r w_{ki}(\mathbf{r}) q_{cxi}(\mathbf{r}) . \end{aligned} \quad (95)$$

(This assumes no lumping; we explain the effects of lumping later.) We shall continue to use a short-hand notation for basis-function expansions:

$$\begin{aligned} \phi^{(0)}(\mathbf{r}) &\equiv \sum_{j=1}^{J_k} \phi_{kj}^{(0)} b_{kj}(\mathbf{r}) , \\ \underline{\mathbf{J}}^{(1)}(\mathbf{r}) &\equiv \sum_{j=1}^{J_k} \underline{\mathbf{J}}_{kj}^{(1)} b_{kj}(\mathbf{r}) , \quad \mathbf{r} \in V_k . \end{aligned} \quad (96)$$

We now define a new weight function that is a linear combination of the $\{w_{ki}\}$:

$$v_p(\underline{r}) \equiv \sum_{k=1}^K \sum_{i=1}^{I_k} \alpha_{ki}^p w_{ki}(\mathbf{r}) . \quad (97)$$

With this notation and definition, we can rewrite Eq. (95) or as follows:

$$\begin{aligned} & - \int_{\mathbb{V}} d^3r \nabla v_p \cdot \mathbf{J}^{(1)}(\mathbf{r}) + \int_{\mathbb{V}} d^3r v_p(\mathbf{r}) \sigma_a(\mathbf{r}) \phi^{(0)}(\mathbf{r}) \\ & = \int_{\mathbb{V}} d^3r v_p(\mathbf{r}) q_{ext}(\mathbf{r}) . \end{aligned} \quad (98)$$

The integration is over the entire problem domain \mathbb{V} , because the summation in Eq. (95) is over all cells k . Note that the locality property guarantees that $v_p(\mathbf{r})$ vanishes on the boundary of \mathbb{V} . It follows that Eq. (98) is just a particle conservation equation, multiplied by $v_p(\mathbf{r})$ and integrated over the problem domain, with basis-function expansions used as approximations for $\phi^{(0)}$ and $\mathbf{J}^{(1)}$:

$$\begin{aligned} & \int_{\mathbb{V}} d^3r v_p \{ \nabla \cdot \mathbf{J}^{(1)} + \sigma_a \phi^{(0)} - q_{ext} \} \\ & = \int_{\partial\mathbb{V}} d^2r v_p \mathbf{n} \cdot \mathbf{J}^{(1)} \\ & + \int_{\mathbb{V}} d^3r \{ -(\nabla v_p) \cdot \mathbf{J}^{(1)} + v_p \sigma_a \phi^{(0)} - v_p q_{ext} \} . \end{aligned} \quad (99)$$

Equation (98) is completely equivalent to Eq. (93); we have simply manipulated it into a form that shows that it is a weighted integral of the conservation equation.

The next step in the analysis is to find the relationship between $\phi^{(0)}$ and $\mathbf{J}^{(1)}$. Toward this end, we consider the coefficients of ϵ^0 in Eqs. (67). If we multiply by $\mathbf{\Omega}_m \Delta_m$, sum over all quadrature directions $m = 1 \dots M$, and rearrange, we obtain

$$\sum_{m=1}^M \Delta_m \mathbf{\Omega}_m \mathbf{\Omega}_m \cdot [\underline{\mathbf{L}}_k^{surf} \psi_k^{surf(0)} + \underline{\mathbf{L}}_k \psi_k^{(0)}] + \underline{\mathbf{T}}_k \mathbf{J}_k^{(1)} = 0 . \quad (100)$$

If we examine the i 'th row of this matrix equation and use our definitions [such as Eq. (96)] of DFEM approximate functions, we find

$$\begin{aligned} & \sum_{l=1}^{L_k} \mathbf{n}_{kl} \cdot \sum_{m=1}^M \Delta_m \mathbf{\Omega}_m \mathbf{\Omega}_m \int_{\partial\mathbb{V}_{kl}} d^2r w_{ki}(\mathbf{r}) \psi^{(0)}(\mathbf{r}_{kl}, \mathbf{\Omega}_m) \\ & - \sum_{m=1}^M \Delta_m \mathbf{\Omega}_m \mathbf{\Omega}_m \int_{\mathbb{V}_k} d^3r \frac{\phi^{(0)}(\mathbf{r})}{4\pi} \nabla w_{ki}(\mathbf{r}) \\ & + \int_{\mathbb{V}_k} d^3r w_{ki}(\mathbf{r}) \sigma(\mathbf{r}) \mathbf{J}^{(1)}(\mathbf{r}) = 0 , \end{aligned} \quad (101)$$

$$\begin{aligned} & \sum_{l=1}^{L_k} \mathbf{n}_{kl} \cdot \sum_{m=1}^M \Delta_m \mathbf{\Omega}_m \mathbf{\Omega}_m \int_{\partial\mathbb{V}_{kl}} d^2r w_{ki}(\mathbf{r}) \psi^{(0)}(\mathbf{r}_{kl}, \mathbf{\Omega}_m) \\ & - \frac{1}{3} \int_{\mathbb{V}_k} d^3r \phi^{(0)}(\mathbf{r}) \nabla w_{ki}(\mathbf{r}) \\ & + \int_{\mathbb{V}_k} d^3r w_{ki}(\mathbf{r}) \sigma(\mathbf{r}) \mathbf{J}^{(1)}(\mathbf{r}) = 0 . \end{aligned} \quad (102)$$

Here, we have assumed that the quadrature set properly integrates the second-order polynomials in the direction cosines:

$$\sum_{m=1}^M \Delta_m \mathbf{\Omega}_m \mathbf{\Omega}_m = \frac{4\pi}{3} \underline{\mathbf{I}} , \quad (103)$$

where $\underline{\mathbf{I}}$ is the identity tensor.

The angular intensity in the surface term of Eq. (102) is the upstream value defined by Eq. (10). Let us consider for the moment a cell k that is in the problem interior so that no surface kl in Eq. (102) is on the problem boundary. Then it follows from Eq. (10) and our earlier result, Eq. (69), (i.e., the result that each DFEM unknown is isotropic) that the surface angular intensity is half-range isotropic at each surface point. We extend our assumption of Eq. (103) to half-range integrals, so that

$$\mathbf{n} \cdot \sum_{m: \mathbf{n} \cdot \mathbf{\Omega}_m > 0} \Delta_m \mathbf{\Omega}_m \mathbf{\Omega}_m = \frac{2\pi}{3} \mathbf{n} , \quad \mathbf{n} \text{ any vector} . \quad (104)$$

[We show in Appendix A that this is true, for example, for any symmetric quadrature set that satisfies Eq. (103).] It follows that for interior cells k Eq. (102) becomes

$$\begin{aligned} & \frac{1}{3} \sum_{l=1}^{L_k} \int_{\partial\mathbb{V}_{kl}} d^2r w_{ki}(\mathbf{r}) \mathbf{n}_{kl} \frac{\phi^{(0)}(\mathbf{r}_{kl}^-) + \phi^{(0)}(\mathbf{r}_{kl}^+)}{2} \\ & - \frac{1}{3} \int_{\mathbb{V}_k} d^3r \phi^{(0)}(\mathbf{r}) \nabla w_{ki}(\mathbf{r}) \\ & + \int_{\mathbb{V}_k} d^3r w_{ki}(\mathbf{r}) \sigma(\mathbf{r}) \mathbf{J}^{(1)}(\mathbf{r}) = 0 . \end{aligned} \quad (105)$$

This is simply the w_{ki} -moment of an equation satisfied by the exact transport solution in our asymptotic limit, namely, $\frac{1}{3} \nabla \phi^{(0)}(\mathbf{r}) + \sigma(\mathbf{r}) \mathbf{J}^{(1)}(\mathbf{r}) = 0$, with one difference: The scalar intensity on the surface of the cell in Eq. (105) is the average of the scalar intensities on either side of the surface. [Note that the scalar intensity is potentially discontinuous at cell surfaces—thus far, the only continuity result we have obtained is the weighted-integral continuity of Eq. (78).]

Equation (105) holds only for interior cells; the more general expression that holds also for cells on the problem boundary is

$$\begin{aligned} & \frac{1}{3} \sum_{l: \partial V_{kl} \in \partial \mathbb{V}} \int_{\partial V_{kl}} d^2 r w_{kl}(\mathbf{r}) \\ & \times \frac{1}{2} \left[\mathbf{n}_{kl} \phi^{(0)}(\mathbf{r}_{kl}^-) + \sum_{m: \mathbf{n}_{kl} \cdot \mathbf{n}_m < 0} \Delta_m 3 \mathbf{n}_{kl} \cdot \mathbf{n}_m \psi_{inc}(\mathbf{r}_{kl}, \mathbf{n}_m) \right] \\ & + \frac{1}{3} \sum_{l: \partial V_{kl} \notin \partial \mathbb{V}} \int_{\partial V_{kl}} d^2 r w_{kl}(\mathbf{r}) \mathbf{n}_{kl} \frac{1}{2} [\phi^{(0)}(\mathbf{r}_{kl}^+) + \phi^{(0)}(\mathbf{r}_{kl}^-)] \\ & - \frac{1}{3} \int_{V_k} d^3 r \phi^{(0)}(\mathbf{r}) \nabla w_{kl}(\mathbf{r}) + \int_{V_k} d^3 r w_{kl}(\mathbf{r}) \sigma(\mathbf{r}) \mathbf{J}^{(1)}(\mathbf{r}) = 0 . \end{aligned} \quad (106)$$

This completes the asymptotic analysis of DFEMs in thick, diffusive regions; i.e., we have now found a complete set of equations that fully describe the leading-order DFEM solution in such regions. These are Eqs. (69), (78), (98), and (106), along with various definitions made along the way. We recognize that it is difficult to glean much meaning from this set of rather abstract and general equations without further guidance. Thus, in the following subsections we discuss these results in detail and provide examples in an attempt to clarify what the analysis has uncovered about DFEMs.

III.C. Results with Lumping

We now show how Eqs. (69), (78), (98), and (106) are affected by lumping. We assume that the weight and basis functions are cardinal at vertices and that the weight functions have the locality and surface-matching properties.

Lumping does not change Eq. (69), which simply says that the leading-order DFEM angular intensity is isotropic. Lumping of the mass matrix and/or the within-cell gradient matrix has no effect on Eq. (78), which is the weighted continuity equation. However, if surface-matrix lumping is employed, then Eq. (78) tells us that the leading-order DFEM solution will be *continuous* in the interior of a thick diffusive region—a very important property. Recall that with surface lumping, given weight functions that are cardinal with vertex support points, Eq. (78) becomes

$$\sum_{\substack{l: \partial V_{kl} \\ \text{touches} \\ \text{vertex } \mathbf{r}_{kl}}} \rho_{kl} [\phi^{(0)}(\mathbf{r}_{kl}^-) - \phi^{(0)}(\mathbf{r}_{kl}^+)] \int_{\partial V_{kl}} d^2 r w_{kl}(\mathbf{r}) = 0 , \quad \text{all } k \text{ and } i . \quad (107)$$

Continuing to assume cardinal basis functions, we observe that this equation involves only one unknown from cell k :

$$\phi^{(0)}(\mathbf{r}_{ki}^-) = \sum_{j=1}^{J_k} \phi_{kj}^{(0)} b_{kj}(\mathbf{r}_{ki}) = \phi_{ki}^{(0)} , \quad \text{all } k \text{ and } i . \quad (108)$$

Likewise, the equation involves only one unknown from each cell that shares a face with cell k at the ki vertex. There is one such equation for each cell that touches the vertex; together they can be cast in the following form:

$$\underline{\underline{\mathbf{M}}} \underline{\underline{\phi}}_{ki}^{(0)} = 0 . \quad (109)$$

Here, $\underline{\underline{\phi}}_{ki}^{(0)}$ is a vector of the leading-order scalar intensities at the vertex in question for all of the cells that meet at the vertex. Matrix $\underline{\underline{\mathbf{M}}}$ has the following properties:

1. $\tilde{M}_{ii} = -\sum_{j \neq i} \tilde{M}_{ij} = -\sum_{j \neq i} \tilde{M}_{ji}$.
2. $\underline{\underline{\mathbf{M}}}$ is symmetric.
3. $\underline{\underline{\mathbf{M}}}$ is singular (each row sums to zero, as does each column).

It is not difficult to show that the only way to satisfy Eqs. (109) [which just restate Eqs. (107)] is for all of the leading-order scalar intensities at the vertex to be equal. [We illustrate this in Appendix C, specifically for the BLD method on rectangles.] This means that *if surface lumping is used, then in the interior of a thick diffusive region the leading-order DFEM solution is continuous*. As we show in Appendix B and in our numerical results, if surface lumping is not used, DFEMs will in general have discontinuous solutions even in the interior of a thick diffusive region.

The remaining two equations are Eqs. (98) and (106), which we obtained by manipulating Eqs. (93) and (100), respectively. Equations (93) and (100) are correct with or without lumping, but some of the manipulations leading to Eqs. (98) and (106) assumed unlumped matrices. If the mass matrix is lumped, then the absorption matrix $[\underline{\underline{A}}_k$ in Eq. (93)] is diagonal. This adds to the diagonal element of the coefficient matrix in the diffusion discretization satisfied by the leading-order solution, and it removes positive terms from the off-diagonal elements. Both of these changes add robustness to the solution. Similarly, mass lumping makes the matrix $\underline{\underline{T}}_k$ in Eq. (100) diagonal and thus simplifies the relation between the order- ϵ current unknowns $\{\mathbf{J}_{kj}^{(1)}\}$ and the leading-order scalar intensities.

Lumping of the surface matrix has no effect on Eq. (98) because the surface matrix is not present in that equation or in its predecessor, Eq. (93). However, surface lumping has two significant effects on Eq. (106). The direct effect is that the functions $\phi^{(0)}$ and ψ_{inc} in Eq. (106) are replaced by their values at the vertex \mathbf{r}_{ki} . The indirect effect is that, as we noted earlier, surface lumping causes $\phi^{(0)}$ to be continuous across interior surfaces. As a result, the surface-lumped version of Eq. (106) is

$$\begin{aligned}
& \frac{1}{3} \sum_{l: \partial V_{kl} \in \partial V} \frac{1}{2} \left[\mathbf{n}_{kl} \phi_{ki}^{(0)} \right. \\
& \quad \left. + \sum_{m: \mathbf{n}_{kl} \cdot \mathbf{n}_m < 0} \Delta_m 3 \mathbf{n}_{kl} \cdot \mathbf{n}_m \mathbf{n}_m \psi_{inc}(\mathbf{r}_{ki}, \mathbf{n}_m) \right] \\
& \quad \times \int_{\partial V_{kl}} d^2 r w_{ki}(\mathbf{r}) \\
& \quad + \frac{1}{3} \sum_{l: \partial V_{kl} \notin \partial V} \mathbf{n}_{kl} \phi_{ki}^{(0)} \int_{\partial V_{kl}} d^2 r w_{ki}(\mathbf{r}) \\
& \quad - \frac{1}{3} \int_{V_k} d^3 r \phi^{(0)}(\mathbf{r}) \nabla w_{ki}(\mathbf{r}) \\
& \quad + \int_{V_k} d^3 r w_{ki}(\mathbf{r}) \sigma(\mathbf{r}) \mathbf{J}^{(1)}(\mathbf{r}) = 0 . \quad (110)
\end{aligned}$$

Lumping the within-cell gradient term changes both Eqs. (98) and (106). This change is easiest to describe by example; we do so later using BLD, but we offer a few comments here. It is simple to formally eliminate the $\{\mathbf{J}_{kj}^{(1)}\}$ from Eqs. (93) and (100); the result is a discretization of a diffusion equation. Given unlumped BLD on rectangles in two dimensions, this discretization has a nine-point stencil for the leakage term and also for the absorption term. Mass lumping alone causes the absorption term to be diagonal (a one-point stencil). Lumping the surface and gradient matrices changes the leakage stencil from nine to five points, the result being the standard vertex-centered finite difference approximation. As is well known, both of these changes increase the robustness (but not the accuracy, in the sense described in earlier sections) of the discretization.

III.D. Discussion of Analysis Results: General

Equations (69), (78), (98), and (106) (or their lumped versions) completely characterize the leading-order scalar intensity obtained by a DFEM in a thick, diffusive region. The crucial question is whether this system of equations is an accurate discretization of the correct diffusion equation (64) and boundary condition (65). We decompose this question into three parts:

1. Do Eqs. (78), (98), and (106) comprise a discretization of the correct diffusion equation?
2. If so, is this discretization accurate? Is it robust?
3. Is the boundary condition, implicit in Eq. (106), an accurate representation of the correct condition (65)?

If each of these is answered affirmatively, then the leading-order DFEM solution is accurate and robust in thick diffusive problems.

As we have already stressed, if for a given DFEM all of Eqs. (78) are independent, then the answer to the first

question is no. If, on the other hand, there is a redundant Eq. (78) for each interior “local cluster” of surfaces, the answer is yes, as we can see from the following exercise:

1. Write the diffusion equation as coupled first-order equations:

$$\nabla \cdot \mathbf{J} + \sigma_a \Phi = q_{ext} ; \quad \frac{1}{3} \nabla \Phi + \sigma \mathbf{J} = 0 .$$

2. Require that the weighted integral of the first equation be satisfied, with weight functions $\{v_p(\mathbf{r})\}$.
3. Require that the weighted integral of the second equation be satisfied, with weight functions $\{w_{ki}(\mathbf{r})\}$.
4. Impose weak continuity conditions at cell interfaces—Eqs. (78).

5. Expand the unknown scalar intensity $\Phi(\mathbf{r})$ and each component of the unknown current $\mathbf{J}(\mathbf{r})$ in terms of the basis functions $\{b_{ki}\}$ in each cell.

This produces Eqs. (78), (98), and (106) in the problem interior. That is, we can begin with the diffusion equation, discretize it, and obtain the same system of equations that the leading-order DFEM solution satisfies in the problem interior. Thus, Eqs. (78), (98), and (106) do indeed comprise a discretization of Eq. (64).

The answer to the second part—accuracy and robustness of this discretization—depends on many details, including the spatial grid, the weight and basis functions, the cross sections and sources, the boundary conditions, etc. To definitively answer this we must individually examine each DFEM and application of interest. We do this for the linear and bilinear DFEMs on rectangular cells in the following subsections. However, we can make some general observations. First, the discretization satisfied by the leading-order DFEM solution is a mixed finite element method (MFEM) discretization of the diffusion equation. (A mixed method uses the coupled first-order equations, allows different weight functions for each equation, and allows different basis functions for the scalar and vector unknowns.) It is an unusual MFEM discretization in at least two ways. First, the same basis functions are used for the scalar unknown and each component of the vector unknown—usually MFEMs use different basis functions. Second, the basis functions are discontinuous, whereas usually either the MFEM vector or scalar functions are chosen to be continuous. We will discuss this further in the subsections devoted to specific DFEMs.

The answer to the third part—accuracy of the boundary condition that is implicit in Eq. (106)—is more complicated. We recall that this boundary condition should be an accurate approximation of the Dirichlet condition shown in Eq. (65). To explore this further, we recall that the function $\phi^{(0)}$ in Eqs. (105) and (106) is defined as a basis-function expansion. Thus, we can rewrite Eq. (105) as

$$\begin{aligned}
& \frac{1}{3} \sum_{l=1}^{L_k} \int_{\partial V_{kl}} d^2 r w_{ki}(\mathbf{r}) \mathbf{n}_{kl} \\
& \times \frac{1}{2} \left[\sum_{j=1}^{J_k} \phi_{kj}^{(0)} b_{kj}(\mathbf{r}_{kl}^-) + \sum_{j=1}^{J_{(kl)'}} \phi_{(kl)j'}^{(0)} b_{(kl)j'}(\mathbf{r}_{kl}^+) \right] \\
& - \sum_{j=1}^{J_k} \phi_{kj}^{(0)} \frac{1}{3} \int_{\mathbb{V}_k} d^3 r b_{kj}(\mathbf{r}) \nabla w_{ki}(\mathbf{r}) \\
& + \int_{\mathbb{V}_k} d^3 r w_{ki}(\mathbf{r}) \sigma(\mathbf{r}) \mathbf{J}^{(1)}(\mathbf{r}) = 0 . \quad (111)
\end{aligned}$$

We define

$$\Phi_{kj} \equiv \begin{cases} \phi_{kj}^{(0)} , & \text{if support point } kj \notin \partial \mathbb{V} , \\ \phi_{kj}^{bc} , & \text{if support point } kj \in \partial \mathbb{V} , \end{cases} \quad (112)$$

where ϕ_{kj}^{bc} is the (thus-far-unknown) Dirichlet boundary condition satisfied by the leading-order DFEM solution. If such a boundary condition exists for a given DFEM, then it must be possible to manipulate Eq. (106) into the following form:

$$\begin{aligned}
& \frac{1}{3} \sum_{l=1}^{L_k} \int_{\partial V_{kl}} d^2 r w_{ki}(\mathbf{r}) \mathbf{n}_{kl} \\
& \times \frac{1}{2} \left[\sum_{j=1}^{J_k} \Phi_{kj} b_{kj}(\mathbf{r}_{kl}^-) + \sum_{j=1}^{J_{(kl)'}} \Phi_{(kl)j'} b_{(kl)j'}(\mathbf{r}_{kl}^+) \right] \\
& - \sum_{j=1}^{J_k} \Phi_{kj}^{(0)} \frac{1}{3} \int_{\mathbb{V}_k} d^3 r b_{kj}(\mathbf{r}) \nabla w_{ki}(\mathbf{r}) \\
& + \int_{\mathbb{V}_k} d^3 r w_{ki}(\mathbf{r}) \sigma(\mathbf{r}) \mathbf{J}^{(1)}(\mathbf{r}) = 0 . \quad (113)
\end{aligned}$$

In other words, if a set $\{\phi_{kj}^{bc}\}$ can be found such that Eq. (113) is equivalent to Eq. (106), then $\{\phi_{kj}^{bc}\}$ is the set of Dirichlet boundary conditions satisfied by the DFEM.

An ideal DFEM would have such a set, and its members would satisfy

$$\begin{aligned}
\phi_{bc}(\mathbf{r}) & \approx 2 \sum_{\mu_m < 0} \Delta \Omega_m W(|\mu_m|) \psi_{inc}(\mathbf{r}, \mathbf{\Omega}_m) , \\
\mu_m & \equiv \mathbf{n} \cdot \mathbf{\Omega}_m . \quad (114)
\end{aligned}$$

[See Eq. (65).] Furthermore, any absorption terms in Eq. (98) that involve boundary scalar intensities should, ideally, use the boundary scalar intensity of Eq. (114). This is a lot to ask, but fortunately not all of it is important from a practical point of view. In particular, it rarely makes much practical difference if the absorption terms in Eq. (98) contain the influence of nonideal boundary scalar intensities. [If leakage dominates absorption this is obvious. If absorption dominates leakage, the boundary conditions have little influence on the interior solution, and thus a nonideal boundary scalar intensity has little influence (at least if its relative error is not unreasonably large in magnitude). Besides, it is easy to eliminate any erroneous influence in the absorption term simply by lumping the mass matrix.] Further, we see from Eq. (98) that the only component of $\mathbf{J}^{(1)}$ that affects the solution is the component parallel to the gradient of v_p . The other components can contain inaccurate boundary information with no adverse effects. We will keep this in mind as we proceed.

The boundary term in Eq. (106) does not appear to have the same form as the ideal term in Eq. (113). In Eq. (113) the term on the kl 'th boundary surface points along the normal, \mathbf{n}_{kl} :

$$\text{ideal term} = \mathbf{n}_{kl} 2 \sum_{\mu_m < 0} \Delta \Omega_m W(|\mu_m|) \int_{\partial V_{kl}} d^2 r w_{ki}(\mathbf{r}) \psi_{inc}(\mathbf{r}, \mathbf{\Omega}_m) , \quad \mu_m \equiv \mathbf{n}_{kl} \cdot \mathbf{\Omega}_m . \quad (115)$$

The corresponding term in Eq. (106) points partly along \mathbf{n}_{kl} and partly along a direction that is a weighted sum of incident directions $\mathbf{\Omega}_m$:

$$\text{actual term} = \frac{1}{2} \int_{\partial V_{kl}} d^2 r w_{ki}(\mathbf{r}) \left[\mathbf{n}_{kl} \phi^{(0)}(\mathbf{r}_{kl}^-) + \sum_{m: \mathbf{n}_{kl} \cdot \mathbf{\Omega}_m < 0} \Delta \Omega_m 3 \mathbf{n}_{kl} \cdot \mathbf{\Omega}_m \mathbf{\Omega}_m \psi_{inc}(\mathbf{r}_{kl}, \mathbf{\Omega}_m) \right] . \quad (116)$$

(Lumping does not change this observation.) If we adopt a shorthand notation similar to that defined in Eq. (83), we can rewrite these equations as follows:

$$\text{ideal term} = A_{kl} \mathbf{n}_{kl} 2 \sum_{\mu_m < 0} \Delta \Omega_m W(|\mu_m|) \psi_{inc, kl}(\mathbf{\Omega}_m) , \quad \mu_m \equiv \mathbf{n}_{kl} \cdot \mathbf{\Omega}_m , \quad (117)$$

and

$$\text{actual term} = A_{kl} \frac{1}{2} \left[\mathbf{n}_{kl} \phi_{kli}^{(0)} + \sum_{m: \mathbf{n}_{kl} \cdot \mathbf{\Omega}_m < 0} \Delta \Omega_m 3 \mathbf{n}_{kl} \cdot \mathbf{\Omega}_m \mathbf{\Omega}_m \psi_{inc, kli}(\mathbf{\Omega}_m) \right] . \quad (118)$$

To keep things as simple as possible for a moment, let us consider a DFEM such that each weight function is local to one surface (as opposed to vertex or edge) of a polyhedral cell (or, in two dimensions, local to one edge of a polygonal cell). Then Eqs. (78) and (77) tell us that $\phi_{kli}^{(0)}$ in Eq. (116) is a weighted integral of the incident angular intensity:

$$\phi_{kli}^{(0)} = 2 \sum_{m: \mathbf{n}_{kl} \cdot \boldsymbol{\Omega}_m < 0} \Delta \Omega_m \frac{2 \mathbf{n}_{kl} \cdot \boldsymbol{\Omega}_m}{\rho_{kl}} \psi_{inc, kli}(\boldsymbol{\Omega}_m), \quad \mathbf{r}_{kl} \in \partial \mathbb{V}. \quad (119)$$

If we continue to let μ_m be $\mathbf{n}_{kl} \cdot \boldsymbol{\Omega}_m$, the normal component of $\boldsymbol{\Omega}_m$, then Eq. (118) becomes

$$\text{actual term} = A_{kl} \left[\sum_{m: \mathbf{n}_{kl} \cdot \boldsymbol{\Omega}_m < 0} \Delta \Omega_m \left[\mathbf{n}_{kl} \frac{2|\mu_m|}{\rho_{kl}} + 3 \mathbf{n}_{kl} \cdot \boldsymbol{\Omega}_m \boldsymbol{\Omega}_m \right] \psi_{inc, kli}(\boldsymbol{\Omega}_m) \right]. \quad (120)$$

We separate the incident direction $\boldsymbol{\Omega}_m$ into its normal and tangential components:

$$\boldsymbol{\Omega}_m = \mu_m \mathbf{n}_{kl} + \boldsymbol{\omega}_m, \quad \text{where } \boldsymbol{\omega}_m \equiv \boldsymbol{\Omega}_m - \mu_m \mathbf{n}_{kl} = \text{tangential component}. \quad (121)$$

Then we can rewrite Eq. (120):

$$\text{actual term} = A_{kl} \left[\mathbf{n}_{kl} \Phi_{bc, kli} + \sum_{m: \mathbf{n}_{kl} \cdot \boldsymbol{\Omega}_m < 0} \Delta \Omega_m [3 \mu_m \boldsymbol{\omega}_m] \psi_{inc, kli}(\boldsymbol{\Omega}_m) \right], \quad (122)$$

where

$$\Phi_{bc, kli} \equiv \sum_{m: \mathbf{n}_{kl} \cdot \boldsymbol{\Omega}_m < 0} \Delta \Omega_m \left[\frac{2|\mu_m|}{\rho_{kl}} + 3 \mu_m^2 \right] \psi_{inc, kli}(\boldsymbol{\Omega}_m) \approx \text{“ideal” quantity}. \quad (123)$$

[The term in brackets is a reasonably good approximation of the exact weight function $W(\mu_m)$ as shown in Eq. (66).] Thus, the actual DFEM term contains a boundary term that is very close to the ideal but also an additional term that is not present in the ideal equation. We note the following about this additional term:

1. It vanishes if the incident angular intensity is azimuthally symmetric about the surface normal. Thus it is not present, for example, in typical one-dimensional problems. This is not hard to see given a quadrature set with 180-deg rotational symmetry about the surface normal, for in that case there are pairs of incident directions (m, m') such that $\mu_m = \mu_{m'}$ and $\boldsymbol{\omega}_m = -\boldsymbol{\omega}_{m'}$. Thus, if the incident intensities are the same in these two opposite directions, they will cancel each other. For arbitrarily oriented surfaces, however, it is unlikely that the quadrature set will have 180-deg rotational symmetry about the surface normal. In such cases, the definition of *azimuthally symmetric* must be altered to account for this asymmetry in the quadrature set relative to the surface. Basically, in such cases we shall define an azimuthally symmetric incident angular intensity as one that causes the second term in Eq. (122) to vanish. This implies that the additional term may not vanish even with an incident angular intensity that is physically azimuthally symmetric if the boundary surface is not oriented along a coordinate axis. We can show that it does vanish, given an isotropic incident intensity, provided that the quadrature set satisfies Eq. (104), which we have already assumed. However, this is probably not true for incident distributions with a more complicated physical asymmetry.

2. The additional term affects the net current density directly but the leading-order scalar intensity indirectly through the spatial moments of the net current density in boundary cells, as shown in Eq. (98).

3. If we separate $\mathbf{J}^{(1)}(\mathbf{r})$ in Eq. (113) into an ideal part and a part containing the additional term, we see that the additional term has the effect of adding an artificial source (which can be positive, negative, or zero) to cells near the boundary.

4. It is possible that only the normal component of $\mathbf{J}^{(1)}(\mathbf{r})$ enters into Eq. (98). In this case, the artificial source term in Eq. (122) does not contaminate the interior solution.

The foregoing detailed discussion of the boundary term assumed the special case of weight functions that are local to cell surfaces, an admittedly unusual case for DFEMs. Given the more common case of weight functions that are local to vertices, we cannot write Eqs. (119) or (120); however, we find very similar equations that involve averages of incident intensities over neighboring boundary surfaces. The comments regarding the additional term still apply. (We will illustrate this in our detailed examination of specific DFEMs in the next few subsections.) Also, the foregoing discussion of the boundary term did not go into detail on how the absorption term affects the boundary condition seen by the leading-order interior scalar intensity. We will illustrate this complication when we discuss the BLD method later.

In summary, the asymptotic analysis allows us to say a great deal about the behavior of DFEMs in thick diffusive regions. It allows us to find the resolution of most DFEMs by simply checking the locality and surface-matching properties of their weight functions. This exposes a set of DFEMs that have zero resolution and thus produce absurd solutions in thick diffusive regions; it also provides a sufficient condition that guarantees full resolution. The diffusion discretizations associated with full-resolution DFEMs are mixed finite element discretizations of the correct diffusion equation. The theory shows that if a method employs surface-matrix lumping, then its leading-order solution is continuous in the interior

of a thick diffusive region, a good property. The theory also suggests that in general, the various lumping techniques improve the robustness of DFEMs in such regions. The accuracy of broad groups of DFEMs in diffusive regions is not spelled out by the theory; this must be evaluated by examining what the theory says about each individual DFEM for each kind of problem. Finally, given an azimuthally asymmetric incident angular intensity (in the sense defined previously), leading-order DFEM solutions can be contaminated by boundary terms that in effect add fictitious sources to cells adjacent to the boundary.

III.E. Discussion of Analysis Results: Linear Discontinuous Finite Element Method on Rectangles

Given the LD method on rectangles, the matrix $\underline{\underline{B}}$ in Eq. (80) is invertible. Thus, the leading-order solution in a thick diffusive problem will depend only on the spatial grid and the boundary conditions—neither volumetric sources nor variations in cross sections will affect it. This is an example of a zero-resolution method. In particular, if there are vacuum boundary conditions around the entire problem, the leading-order solution is zero. This is obviously unphysical. We illustrate this behavior later with numerical results.

As we discussed earlier, the matrix $\underline{\underline{B}}$ will be singular only if there exist linear combinations of Eqs. (78) such that all coefficients multiplying scalar-intensity moments are zero. We argued that if the weight functions are not local, this will not happen. With the LD method, each weight function is a plane (of the form $a + bx + cy$). Each such plane must be nonzero on at least three edges of a rectangle, which means each Eq. (78) must include scalar-

intensity moments on each side of at least three cell edges. To cancel out the coefficients in front of these moments, then, we would have to add linear combinations of Eqs. (78) from at least three other cells. To cancel the new coefficients introduced by this procedure, we would have to add linear combinations from more cells. A bit of thought convinces us that there is no way to cancel all the coefficients, which is equivalent to saying there are no redundant Eqs. (78). Thus, the analysis says that LD on rectangles will fail in thick diffusive problems.

We remark that the theory predicts that LD on triangles will yield a full-resolution solution, much like BLD does on rectangles (as we discuss in Sec. III.F). In three dimensions, the theory predicts that LD will fail on any cell that has more than four sides but that it will have full resolution on tetrahedral cells.

III.F. Discussion of Analysis Results: Standard (Unlumped) Bilinear Discontinuous Finite Element Method on Rectangles

With bilinear weight functions, we find that the $\underline{\underline{B}}$ matrix of Eq. (80) is singular, for each cardinal bilinear weight function is local (nonzero on only two adjacent edges of a rectangle), and each has a surface-matching counterpart in the neighboring cell along each edge (because every cell has the same kind of weight functions). From the discussion following Table I, we see that the leading-order BLD solution therefore satisfies Eqs. (78), (98), and (106). The weight function v_p in Eq. (98) is simply the bilinear “tent” function that is unity at the p ’th interior vertex and zero at each of the surrounding eight vertices.

To interpret the equations satisfied by the leading-order BLD solution, it helps to define some notation. We shall refer to cells by the double index ij and define

$\phi_{ij}^{NE}, \phi_{ij}^{NW}, \phi_{ij}^{SW}, \phi_{ij}^{SE} \equiv$ intensity in northeast, northwest, southwest, and southeast corners, respectively, of cell ij .

We employ a similar notation for the net current density. Further, we define

$$J_{x,ij}^N \equiv \hat{\mathbf{x}} \cdot \frac{\mathbf{J}_{ij}^{NE(1)} + \mathbf{J}_{ij}^{NW(1)}}{2}, \quad J_{y,ij}^E \equiv \hat{\mathbf{y}} \cdot \frac{\mathbf{J}_{ij}^{NE(1)} + \mathbf{J}_{ij}^{SE(1)}}{2}, \quad \text{etc.} \quad (124)$$

(Here, $\hat{\mathbf{u}}$ is a unit vector along the u axis.) In this notation, Eq. (98) for the standard BLD method is

$$\begin{aligned} & \frac{\Delta y_{j+1}}{2} \left\{ \left[\frac{2}{3} J_{x,i+1,j+1}^S + \frac{1}{3} J_{x,i+1,j+1}^N \right] - \left[\frac{2}{3} J_{x,i,j+1}^S + \frac{1}{3} J_{x,i,j+1}^N \right] \right\} + \frac{\Delta y_j}{2} \left\{ \left[\frac{2}{3} J_{x,i+1,j}^N + \frac{1}{3} J_{x,i+1,j}^S \right] - \left[\frac{2}{3} J_{x,ij}^N + \frac{1}{3} J_{x,ij}^S \right] \right\} \\ & + \frac{\Delta x_{i+1}}{2} \left\{ \left[\frac{2}{3} J_{y,i+1,j+1}^W + \frac{1}{3} J_{y,i+1,j+1}^E \right] - \left[\frac{2}{3} J_{y,i+1,j}^W + \frac{1}{3} J_{y,i+1,j}^E \right] \right\} + \frac{\Delta x_i}{2} \left\{ \left[\frac{2}{3} J_{y,i,j+1}^E + \frac{1}{3} J_{y,i,j+1}^W \right] - \left[\frac{2}{3} J_{y,ij}^E + \frac{1}{3} J_{y,ij}^W \right] \right\} \\ & + (\sigma_a \Delta x \Delta y)_{ij} \left[\frac{4}{36} \phi_{ij}^{NE} + \frac{2}{36} \phi_{ij}^{NW} + \frac{2}{36} \phi_{ij}^{SE} + \frac{1}{36} \phi_{ij}^{SW} \right] + (\sigma_a \Delta x \Delta y)_{i+1,j} \left[\frac{4}{36} \phi_{i+1,j}^{NW} + \frac{2}{36} \phi_{i+1,j}^{NE} + \frac{2}{36} \phi_{i+1,j}^{SW} + \frac{1}{36} \phi_{i+1,j}^{SE} \right] \\ & + (\sigma_a \Delta x \Delta y)_{i+1,j+1} \left[\frac{4}{36} \phi_{i+1,j+1}^{SW} + \frac{2}{36} \phi_{i+1,j+1}^{NW} + \frac{2}{36} \phi_{i+1,j+1}^{SE} + \frac{1}{36} \phi_{i+1,j+1}^{NE} \right] \\ & + (\sigma_a \Delta x \Delta y)_{i,j+1} \left[\frac{4}{36} \phi_{i,j+1}^{SE} + \frac{2}{36} \phi_{i,j+1}^{SW} + \frac{2}{36} \phi_{i,j+1}^{NE} + \frac{1}{36} \phi_{i,j+1}^{NW} \right] \\ & = \int_{\text{cells around } i+1/2, j+1/2} dx dy v_{i+1/2, j+1/2}(x, y) q_{\text{ext}}(x, y), \quad (x_{i+1/2}, y_{j+1/2}) \text{ in interior.} \end{aligned} \quad (125)$$

From Eqs. (105) we obtain (after some manipulation) a relation between these net current densities and the leading-order scalar intensities for cells ij in the problem interior:

$$J_{x,ij}^N = -\frac{\phi_{ij}^{NE} - \phi_{ij}^{NW}}{3\sigma_{ij}\Delta x_i}, \quad J_{x,ij}^S = -\frac{\phi_{ij}^{SE} - \phi_{ij}^{SW}}{3\sigma_{ij}\Delta x_i} \quad (126)$$

and

$$J_{y,ij}^E = -\frac{\phi_{ij}^{NE} - \phi_{ij}^{SE}}{3\sigma_{ij}\Delta y_j}, \quad J_{y,ij}^W = -\frac{\phi_{ij}^{NW} - \phi_{ij}^{SW}}{3\sigma_{ij}\Delta y_j},$$

cell ij in interior . (127)

The leading-order BLD solution is easier to describe if the incident particle flow rates are spatially continuous around the boundary of the problem. As we show in Ap-

pendix B, this causes the leading-order intensity to be continuous throughout the interior of the problem. We consider this case first.

III.F.1. Continuous Incident Partial Currents

In Appendix B we show that given incident particle flow rates (partial currents) that are spatially continuous around the problem boundary (including around corners), the leading-order BLD scalar intensity is pointwise continuous:

$$\phi_{ij}^{NE} = \phi_{i+1,j}^{NW} = \phi_{i+1,j+1}^{SW} = \phi_{i,j+1}^{SE} \equiv \phi_{i+1/2,j+1/2} . \quad (128)$$

In this case (which includes the special case of vacuum boundaries), Eq. (98) for the standard BLD method becomes

$$\begin{aligned} & \frac{\Delta y_{j+1}}{2} \left\{ \left[\frac{2}{3} J_{x,i+1,j+1}^S + \frac{1}{3} J_{x,i+1,j+1}^N \right] - \left[\frac{2}{3} J_{x,i,j+1}^S + \frac{1}{3} J_{x,i,j+1}^N \right] \right\} + \frac{\Delta y_j}{2} \left\{ \left[\frac{2}{3} J_{x,i+1,j}^N + \frac{1}{3} J_{x,i+1,j}^S \right] - \left[\frac{2}{3} J_{x,ij}^N + \frac{1}{3} J_{x,ij}^S \right] \right\} \\ & + \frac{\Delta x_{i+1}}{2} \left\{ \left[\frac{2}{3} J_{y,i+1,j+1}^W + \frac{1}{3} J_{y,i+1,j+1}^E \right] - \left[\frac{2}{3} J_{y,i,j+1}^W + \frac{1}{3} J_{y,i,j+1}^E \right] \right\} + \frac{\Delta x_i}{2} \left\{ \left[\frac{2}{3} J_{y,i,j+1}^E + \frac{1}{3} J_{y,i,j+1}^W \right] - \left[\frac{2}{3} J_{y,ij}^E + \frac{1}{3} J_{y,ij}^W \right] \right\} \\ & + (\sigma_a \Delta x \Delta y)_{ij} \left[\frac{4}{36} \phi_{i+1/2,j+1/2} + \frac{2}{36} \phi_{i-1/2,j+1/2} + \frac{2}{36} \phi_{i+1/2,j-1/2} + \frac{1}{36} \phi_{i-1/2,j-1/2} \right] \\ & + (\sigma_a \Delta x \Delta y)_{i+1,j} \left[\frac{4}{36} \phi_{i+1/2,j+1/2} + \frac{2}{36} \phi_{i+3/2,j+1/2} + \frac{2}{36} \phi_{i+1/2,j-1/2} + \frac{1}{36} \phi_{i+3/2,j-1/2} \right] \\ & + (\sigma_a \Delta x \Delta y)_{i+1,j+1} \left[\frac{4}{36} \phi_{i+1/2,j+1/2} + \frac{2}{36} \phi_{i+3/2,j+1/2} + \frac{2}{36} \phi_{i+1/2,j+3/2} + \frac{1}{36} \phi_{i+3/2,j+3/2} \right] \\ & + (\sigma_a \Delta x \Delta y)_{i,j+1} \left[\frac{4}{36} \phi_{i+1/2,j+1/2} + \frac{2}{36} \phi_{i-1/2,j+1/2} + \frac{2}{36} \phi_{i+1/2,j+3/2} + \frac{1}{36} \phi_{i-1/2,j+3/2} \right] \\ & = \int_{\text{cells around } i+1/2,j+1/2} dx dy v_{i+1/2,j+1/2}(x,y) q_{\text{ext}}(x,y), \quad (x_{i+1/2}, y_{j+1/2}) \text{ in interior} . \end{aligned} \quad (129)$$

Upon substitution of Eqs. (126) and (127) into Eq. (129), we see that the leading-order BLD solution satisfies a standard bilinear continuous finite element discretization of the diffusion equation. To avoid rewriting a lengthy and complicated equation, we shall write it only for the simple case of uniform mesh spacing, constant material properties, and constant extraneous source in each cell:

$$\begin{aligned} & -\frac{\Delta y}{3\sigma\Delta x} \frac{1}{6} [\phi_{i-1/2,j+3/2} - 2\phi_{i+1/2,j+3/2} + \phi_{i+3/2,j+3/2} \\ & \quad + 4\phi_{i-1/2,j+1/2} - 8\phi_{i+1/2,j+1/2} + 4\phi_{i+3/2,j+1/2} \\ & \quad + \phi_{i-1/2,j-1/2} - 2\phi_{i+1/2,j-1/2} + \phi_{i+3/2,j-1/2}] \\ & -\frac{\Delta x}{3\sigma\Delta y} \frac{1}{6} [\phi_{i-1/2,j+3/2} + 4\phi_{i+1/2,j+3/2} + \phi_{i+3/2,j+3/2} \\ & \quad - 2\phi_{i-1/2,j+1/2} - 8\phi_{i+1/2,j+1/2} - 2\phi_{i+3/2,j+1/2} \\ & \quad + \phi_{i-1/2,j-1/2} + 4\phi_{i+1/2,j-1/2} + \phi_{i+3/2,j-1/2}] \\ & + \sigma_a \Delta x \Delta y \frac{1}{36} [\phi_{i-1/2,j+3/2} + 4\phi_{i+1/2,j+3/2} + \phi_{i+3/2,j+3/2} \\ & \quad + 4\phi_{i-1/2,j+1/2} + 16\phi_{i+1/2,j+1/2} + 4\phi_{i+3/2,j+1/2} \\ & \quad + \phi_{i-1/2,j-1/2} + 4\phi_{i+1/2,j-1/2} + \phi_{i+3/2,j-1/2}] \\ & = \frac{\Delta x \Delta y}{4} [q_{ij} + q_{i+1,j} + q_{i+1,j+1} + q_{i,j+1}], \\ & \text{for } i \text{ and } j \text{ such that cells } (ij), (i+1,j), (i+1,j+1), \text{ and } (i,j+1) \text{ are in interior} . \end{aligned} \quad (130)$$

This nine-point vertex-centered discretization will be accurate in many problems; however, given $\Delta x/\Delta y$ away from unity or cells that are coarse compared to a diffusion length ($L = 1/\sqrt{3\sigma\sigma_a}$), it can produce unphysical oscillations and even negative solutions.

We turn next to boundary cells, for which we must use Eq. (106) to express the currents \underline{J} in terms of incident angular intensities and leading-order scalar intensities. We consider first a cell on the bottom boundary ($j = 1$) but not in a corner ($i \neq 1, i \neq i_{\max}$). After simple manipulations, we find

$$J_{y,i,1}^E = -\frac{1}{3\sigma_{i,1}\Delta y_1} \left[\phi_{i+1/2,3/2} - \sum_{\hat{\mathbf{y}} \cdot \underline{\Omega}_m > 0} \Delta\Omega_m \left(2 \frac{\hat{\mathbf{y}} \cdot \underline{\Omega}_m}{\rho_y} + 3(\hat{\mathbf{y}} \cdot \underline{\Omega}_m)^2 \right) \psi_{inc,i,1/2}^E(\underline{\Omega}_m) \right], \quad (131)$$

$$J_{y,i,1}^W = -\frac{1}{3\sigma_{i,1}\Delta y_1} \left[\phi_{i-1/2,3/2} - \sum_{\hat{\mathbf{y}} \cdot \underline{\Omega}_m > 0} \Delta\Omega_m \left(2 \frac{\hat{\mathbf{y}} \cdot \underline{\Omega}_m}{\rho_y} + 3(\hat{\mathbf{y}} \cdot \underline{\Omega}_m)^2 \right) \psi_{inc,i,1/2}^W(\underline{\Omega}_m) \right], \quad (132)$$

$$J_{x,i,1}^N = -\frac{1}{3\sigma_{i,1}\Delta x_i} \left[\phi_{i+1/2,3/2} - \phi_{i-1/2,3/2} - \sum_{\hat{\mathbf{y}} \cdot \underline{\Omega}_m > 0} \Delta\Omega_m 3\hat{\mathbf{y}} \cdot \underline{\Omega}_m \hat{\mathbf{x}} \cdot \underline{\Omega}_m \left(\frac{\psi_{inc,i,1}^E(\underline{\Omega}_m) + \psi_{inc,i,1}^W(\underline{\Omega}_m)}{2} \right) \right], \quad (133)$$

and

$$J_{x,i,1}^S = -\frac{1}{3\sigma_{i,1}\Delta x_i} \left[\phi_{i+1/2,1/2} - \phi_{i-1/2,1/2} + 2 \sum_{\hat{\mathbf{y}} \cdot \underline{\Omega}_m > 0} \Delta\Omega_m 3\hat{\mathbf{y}} \cdot \underline{\Omega}_m \hat{\mathbf{x}} \cdot \underline{\Omega}_m \left(\frac{\psi_{inc,i,1}^E(\underline{\Omega}_m) + \psi_{inc,i,1}^W(\underline{\Omega}_m)}{2} \right) \right]. \quad (134)$$

Note that a fictitious source term, discussed in Sec. III.E, has appeared in each of Eqs. (133) and (134). However, this term vanishes when combining $2J_{x,ij}^N + J_{x,ij}^S$, which is the only combination that appears in the equation for the leading-order scalar intensity, Eq. (129). Thus, with BLD on rectangles, the fictitious source will not contaminate the solution. Note further that the terms that function as boundary scalar intensities in Eqs. (131) and (132) are exactly the approximately ideal quantities described in Eq. (123).

We would like to find scalar intensities at all boundary vertices that would make Eq. (130) valid for interior vertices of boundary cells. These scalar intensities would be the boundary conditions satisfied by the leading-order BLD intensity in the interior of the problem. [This is seeking, specifically for the BLD method, a set of $\{\phi_{kj}^{bc}\}$ that makes Eq. (113) equivalent to Eq. (106).] For noncorner vertices ($i + 1/2, 1/2$) on the bottom boundary, for example, this means we seek boundary-condition scalar intensities $\phi_{i-1/2,1/2}^{bc}$, $\phi_{i+1/2,1/2}^{bc}$, and $\phi_{i+3/2,1/2}^{bc}$ such that

$$\begin{aligned} & \frac{(\sigma_a \Delta x \Delta y)_{i,1}}{36} [2\phi_{i+1/2,1/2} + \phi_{i-1/2,1/2}] + \frac{(\sigma_a \Delta x \Delta y)_{i+1,1}}{36} [2\phi_{i+1/2,1/2} + \phi_{i+3/2,1/2}] \\ & - \frac{\Delta y_1}{6} [2J_{x,i,1}^N + J_{x,i,1}^S - 2J_{x,i+1,1}^N - J_{x,i+1,1}^S] - \frac{\Delta x_i}{6} [2J_{y,i,1}^E + J_{y,i,1}^W] - \frac{\Delta x_{i+1}}{6} [2J_{y,i+1,1}^W + J_{y,i+1,1}^E] \\ & = \frac{(\sigma_a \Delta x \Delta y)_{i,1}}{36} [2\phi_{i+1/2,1/2}^{bc} + \phi_{i-1/2,1/2}^{bc}] + \frac{(\sigma_a \Delta x \Delta y)_{i+1,1}}{36} [2\phi_{i+1/2,1/2}^{bc} + \phi_{i+3/2,1/2}^{bc}] \\ & + \frac{\Delta y_1}{6} \left[2 \frac{\phi_{i+1/2,3/2} - \phi_{i-1/2,3/2}}{3\sigma_{i,1}\Delta x_i} + \frac{\phi_{i+1/2,1/2}^{bc} - \phi_{i-1/2,1/2}^{bc}}{3\sigma_{i,1}\Delta x_i} \right] - \frac{\Delta y_1}{6} \left[2 \frac{\phi_{i+3/2,3/2} - \phi_{i+1/2,3/2}}{3\sigma_{i+1,1}\Delta x_{i+1}} + \frac{\phi_{i+3/2,1/2}^{bc} - \phi_{i+1/2,1/2}^{bc}}{3\sigma_{i+1,1}\Delta x_{i+1}} \right] \\ & + \frac{\Delta x_i}{6} \left[2 \frac{\phi_{i+1/2,3/2} - \phi_{i+1/2,1/2}^{bc}}{3\sigma_{i,1}\Delta y_1} + \frac{\phi_{i-1/2,3/2} - \phi_{i-1/2,1/2}^{bc}}{3\sigma_{i,1}\Delta y_1} \right] + \frac{\Delta x_{i+1}}{6} \left[2 \frac{\phi_{i+1/2,3/2} - \phi_{i+1/2,1/2}^{bc}}{3\sigma_{i+1,1}\Delta y_1} + \frac{\phi_{i+3/2,3/2} - \phi_{i+3/2,1/2}^{bc}}{3\sigma_{i+1,1}\Delta y_1} \right], \end{aligned} \quad (135)$$

where the J terms are given by Eqs. (131) through (134), and we use upper-case ϕ^{bc} to denote the unknown quantities that function as boundary conditions. There are $2(i_{\max} - 2 + j_{\max} - 2) = 2(i_{\max} + j_{\max}) - 8$ equations of this form, and there are $2(i_{\max} + j_{\max})$ unknown boundary-condition scalar intensities. This yields an underdetermined system, which simply means that there are many different boundary conditions that will give the same leading-order interior solution. A calculation to determine a set of boundary-condition scalar intensities that satisfy Eqs. (135) appears to be more trouble than it is worth. However, we have studied this system enough to say the following:

1. In general the ideal boundary-condition scalar intensity of Eq. (123) does not satisfy Eqs. (135).

2. Given the trivial case of all incident intensities isotropic, the simple solution $\phi_{i+1/2,1/2}^{bc} = \phi_{i+1/2,1/2}$ satisfies Eqs. (135). (In this trivial case, this also equals the ideal boundary-condition scalar intensity.)

3. The boundary-condition scalar intensity at a given boundary vertex will depend in general on things that the ideal boundary-condition scalar intensity does not depend on, such as absorption cross sections and boundary conditions at other points. [Equations (135) are the two-dimensional analog of the one-dimensional equations discussed in the corrigendum of Ref. 2. This corrigendum gives a good example of how numerical methods can bring nonphysical terms into the boundary-condition intensity.]

In summary, given incident partial currents that are spatially continuous around the problem boundary, the standard BLD method on rectangular cells yields a leading-order solution that satisfies a bilinear continuous finite element discretization of the correct diffusion equation. This is a reasonably good result, but this discretization is not robust: It can produce nonmonotonic and even negative solutions. Also, the boundary condition satisfied by the leading-order interior BLD solution will not usually equal the ideal boundary condition. It will differ most for sharply varying incident currents and for boundary cells that are not thin compared to a diffusion length ($L = 1/\sqrt{3\sigma\sigma_a}$).

III.F.2. Discontinuous Incident Partial Currents

Section III.F.1 addressed the special case of continuous incident partial currents. Given incident intensities that are not spatially continuous around the boundary, the leading-order solution will be discontinuous in the interior, as we show in Appendix B. In this case, we cannot simplify Eq. (125) to Eq. (129). Equations (125), (126), and (127) do not combine to give a simple bilinear finite element discretization of the diffusion equation (unless the interior solution is continuous, as in Sec. III.F.1). In fact, these equations alone do not fully

describe the leading-order solution—they must be supplemented by Eqs. (B.6) and (B.15) of Appendix B, which describe the discontinuities in the leading-order BLD solution at each vertex. [These equations are a restatement of the weighted-integral continuity equations, Eqs. (78).]

In practice, we observe that the leading-order BLD solution in thick diffusive regions is noticeably discontinuous near boundaries that have discontinuous incident flow rates but that the solution discontinuities appear to damp out quickly away from such boundary points. Thus, deep in the interior of a thick diffusive problem, even with discontinuous incident partial currents, the leading-order BLD almost satisfies the bilinear continuous finite element diffusion discretization discussed in Sec. III.F.1. Also, the same comments apply to the boundary-condition scalar intensities as in that subsection.

In summary, given incident partial currents that are not spatially continuous around the problem boundary, the standard BLD method on rectangular cells yields a leading-order solution that satisfies an unusual discretization of the correct diffusion equation. Away from boundary points at which the incident partial current is discontinuous, the leading-order solution very nearly satisfies a bilinear continuous diffusion discretization. This is a reasonably good result, but this discretization is even less robust than that obtained with continuous incident partial currents. The boundary condition satisfied by the leading-order interior BLD solution will not usually equal the ideal boundary condition. It differs most for sharply varying incident currents and for boundary cells that are not thin compared to a diffusion length ($L = 1/\sqrt{3\sigma\sigma_a}$).

III.G. Discussion of Analysis Results: Lumped Bilinear Discontinuous Finite Element Method on Rectangles

III.G.1. Mass-Matrix Lumping

The mass-lumped BLD method produces slightly different results from the standard BLD method. For example, instead of Eq. (125), at interior vertices the mass-lumped method produces

$$\begin{aligned}
 & \frac{\Delta y_{j+1}}{2} \left\{ \left[\frac{2}{3} J_{x,i+1,j+1}^S + \frac{1}{3} J_{x,i+1,j+1}^N \right] - \left[\frac{2}{3} J_{x,i,j+1}^S + \frac{1}{3} J_{x,i,j+1}^N \right] \right\} + \frac{\Delta y_j}{2} \left\{ \left[\frac{2}{3} J_{x,i+1,j}^N + \frac{1}{3} J_{x,i+1,j}^S \right] - \left[\frac{2}{3} J_{x,ij}^N + \frac{1}{3} J_{x,ij}^S \right] \right\} \\
 & + \frac{\Delta x_{i+1}}{2} \left\{ \left[\frac{2}{3} J_{y,i+1,j+1}^W + \frac{1}{3} J_{y,i+1,j+1}^E \right] - \left[\frac{2}{3} J_{y,i+1,j}^W + \frac{1}{3} J_{y,i+1,j}^E \right] \right\} \\
 & + \frac{\Delta x_i}{2} \left\{ \left[\frac{2}{3} J_{y,i,j+1}^E + \frac{1}{3} J_{y,i,j+1}^W \right] - \left[\frac{2}{3} J_{y,ij}^E + \frac{1}{3} J_{y,ij}^W \right] \right\} \\
 & + \frac{(\sigma_a \Delta x \Delta y)_{ij}}{4} \phi_{ij}^{NE} + \frac{(\sigma_a \Delta x \Delta y)_{i+1,j}}{4} \phi_{i+1,j}^{NW} + \frac{(\sigma_a \Delta x \Delta y)_{i+1,j+1}}{4} \phi_{i+1,j+1}^{SW} + \frac{(\sigma_a \Delta x \Delta y)_{i,j+1}}{4} \phi_{i,j+1}^{SE} \\
 & = \frac{(\Delta x \Delta y)_{ij}}{4} q_{ij}^{NE} + \frac{(\Delta x \Delta y)_{i+1,j}}{4} q_{i+1,j}^{NW} + \frac{(\Delta x \Delta y)_{i+1,j+1}}{4} q_{i+1,j+1}^{SW} + \frac{(\Delta x \Delta y)_{i,j+1}}{4} q_{i,j+1}^{SE} .
 \end{aligned} \tag{136}$$

Given the simple case of continuous incident flow rates, uniform mesh spacing, constant material properties, and constant extraneous source in each cell, the leading-order mass-lumped BLD solution satisfies the following equation instead of Eq. (130):

$$\begin{aligned}
& -\frac{\Delta y}{3\sigma\Delta x} \frac{1}{6} [\phi_{i-1/2,j+3/2} - 2\phi_{i+1/2,j+3/2} + \phi_{i+3/2,j+3/2} \\
& \quad + 4\phi_{i-1/2,j+1/2} - 8\phi_{i+1/2,j+1/2} + 4\phi_{i+3/2,j+1/2} \\
& \quad + \phi_{i-1/2,j-1/2} - 2\phi_{i+1/2,j-1/2} + \phi_{i+3/2,j-1/2}] \\
& -\frac{\Delta x}{3\sigma\Delta y} \frac{1}{6} [\phi_{i-1/2,j+3/2} + 4\phi_{i+1/2,j+3/2} + \phi_{i+3/2,j+3/2} \\
& \quad - 2\phi_{i-1/2,j+1/2} - 8\phi_{i+1/2,j+1/2} - 2\phi_{i+3/2,j+1/2} \\
& \quad + \phi_{i-1/2,j-1/2} + 4\phi_{i+1/2,j-1/2} + \phi_{i+3/2,j-1/2}] + \sigma_a \Delta x \Delta y \phi_{i+1/2,j+1/2} \\
& = \frac{\Delta x \Delta y}{4} [q_{ij} + q_{i+1,j} + q_{i+1,j+1} + q_{i,j+1}] . \tag{137}
\end{aligned}$$

The equation for the boundary-condition scalar intensity becomes slightly simpler than Eq. (135), which was the equation for standard BLD:

$$\begin{aligned}
& -\frac{\Delta y_1}{6} [2J_{x,i,1}^N + J_{x,i,1}^S - 2J_{x,i+1,1}^N - J_{x,i+1,1}^S] - \frac{\Delta x_i}{6} [2J_{y,i,1}^E + J_{y,i,1}^W] - \frac{\Delta x_{i+1}}{6} [2J_{y,i+1,1}^W + J_{y,i+1,1}^E] \\
& = \frac{\Delta y_1}{6} \left[2 \frac{\phi_{i+1/2,3/2} - \phi_{i-1/2,3/2}}{3\sigma_{i,1} \Delta x_i} + \frac{\phi_{i+1/2,1/2}^{bc} - \phi_{i-1/2,1/2}^{bc}}{3\sigma_{i,1} \Delta x_i} \right] \\
& - \frac{\Delta y_1}{6} \left[2 \frac{\phi_{i+3/2,3/2} - \phi_{i+1/2,3/2}}{3\sigma_{i+1,1} \Delta x_{i+1}} + \frac{\phi_{i+3/2,1/2}^{bc} - \phi_{i+1/2,1/2}^{bc}}{3\sigma_{i+1,1} \Delta x_{i+1}} \right] \\
& + \frac{\Delta x_i}{6} \left[2 \frac{\phi_{i+1/2,3/2} - \phi_{i+1/2,1/2}^{bc}}{3\sigma_{i-1/2,1} \Delta y_1} + \frac{\phi_{i-1/2,3/2} - \phi_{i-1/2,1/2}^{bc}}{3\sigma_{i,1} \Delta y_1} \right] \\
& + \frac{\Delta x_{i+1}}{6} \left[2 \frac{\phi_{i+1/2,3/2} - \phi_{i+1/2,1/2}^{bc}}{3\sigma_{i+1,1} \Delta y_1} + \frac{\phi_{i+3/2,3/2} - \phi_{i+3/2,1/2}^{bc}}{3\sigma_{i+1,1} \Delta y_1} \right] . \tag{138}
\end{aligned}$$

Note that absorption cross sections do not appear in this equation. Thus, as is the case in one dimension, mass-matrix lumping removes one of the nonphysical characteristics of DFEMs in thick diffusive regions. However, the following remains true for the mass-lumped method. Given incident partial currents that are spatially continuous around the problem boundary, the mass-lumped BLD method on rectangular cells yields a leading-order solution that satisfies a mass-lumped bilinear continuous finite element discretization of the correct diffusion equation. This is a reasonably good result, but this discretization is not robust: It can produce nonmonotonic and even negative solutions. Also, the boundary condition satisfied by the leading-order interior BLD solution does not usually equal the ideal boundary condition. It differs most for sharply varying incident currents.

III.G.2. Fully Lumped Bilinear Discontinuous Finite Element Method (Simple Corner Balance)

The FLBLD method, which given rectangular cells in XY geometry is equivalent to the simple corner-balance (SCB) method, produces noticeably different results from the standard and mass-lumped BLD methods. For example, instead of Eq. (125) or (136), at interior vertices FLBLD/SCB produces

$$\begin{aligned}
& \frac{\Delta y_{j+1}}{2} \{J_{x,i+1,j+1}^S - J_{x,i,j+1}^S\} + \frac{\Delta y_j}{2} \{J_{x,i+1,j}^N - J_{x,ij}^N\} + \frac{\Delta x_{i+1}}{2} \{J_{y,i+1,j+1}^W - J_{y,i+1,j}^W\} + \frac{\Delta x_i}{2} \{J_{y,i,j+1}^E - J_{y,ij}^E\} \\
& + \frac{(\sigma_a \Delta x \Delta y)_{ij}}{4} \phi_{ij}^{NE} + \frac{(\sigma_a \Delta x \Delta y)_{i+1,j}}{4} \phi_{i+1,j}^{NW} + \frac{(\sigma_a \Delta x \Delta y)_{i+1,j+1}}{4} \phi_{i+1,j+1}^{SW} + \frac{(\sigma_a \Delta x \Delta y)_{i,j+1}}{4} \phi_{i,j+1}^{SE} \\
& = \frac{(\Delta x \Delta y)_{ij}}{4} q_{ij}^{NE} + \frac{(\Delta x \Delta y)_{i+1,j}}{4} q_{i+1,j}^{NW} + \frac{(\Delta x \Delta y)_{i+1,j+1}}{4} q_{i+1,j+1}^{SW} + \frac{(\Delta x \Delta y)_{i,j+1}}{4} q_{i,j+1}^{SE} . \tag{139}
\end{aligned}$$

More importantly, the FLBLD/SCB versions of the weighted-integral continuity equations, Eqs. (78), imply pointwise continuity of the solution, regardless of discontinuities in the incident particle flow rates. (We prove this in Appendix C.)

Given the simple case of continuous incident flow rates, uniform mesh spacing, constant material properties, and constant extraneous source in each cell, the leading-order FLBLD/SCB solution satisfies the following equation instead of Eq. (130) or (137):

$$\begin{aligned} & -\frac{\Delta y}{3\sigma\Delta x} [\phi_{i-1/2,j+1/2} - 2\phi_{i+1/2,j+1/2} + \phi_{i+3/2,j+1/2}] \\ & -\frac{\Delta x}{3\sigma\Delta y} [\phi_{i+1/2,j+3/2} - 2\phi_{i+1/2,j+1/2} \\ & \quad + \phi_{i+1/2,j-1/2}] + \sigma_a \Delta x \Delta y \phi_{i+1/2,j+1/2} \\ & = \frac{\Delta x \Delta y}{4} [q_{ij} + q_{i+1,j} + q_{i+1,j+1} + q_{i,j+1}]. \end{aligned} \quad (140)$$

This five-point finite-volume discretization of the diffusion equation is somewhat simpler and significantly more robust than the nine-point bilinear continuous discretizations satisfied by the standard and mass-lumped BLD methods. One desirable characteristic of this discretization is that its coefficient matrix is an M -matrix, which means that every element of its inverse is a nonnegative number. (See Appendix D.) Thus, the theory predicts that given nonnegative sources and boundary conditions, FLBLD/SCB will produce nonnegative solutions in thick diffusive regions. In addition, the solution of Eqs. (140) is known to be well-behaved in that it resists unphysical oscillations. This prediction is borne out by our numerical results.

In addition, it is easy to show that the SCB leading-order solution satisfies boundary conditions that are the approximately ideal values shown in Eq. (123). In contrast to Eq. (135) for BLD and Eq. (138) for mass-lumped BLD, the equation satisfied by the SCB boundary-condition scalar intensity on the $x = \frac{1}{2}$ surface is

$$\begin{aligned} & -\frac{\Delta x_i}{2} [J_{y,i,1}^E] - \frac{\Delta x_{i+1}}{2} [J_{y,i+1,1}^W] \\ & = \frac{\Delta x_i}{2} \left[\frac{\phi_{i+1/2,3/2} - \phi_{i+1/2,1/2}^{bc}}{3\sigma_{i,1}\Delta y_1} \right] \\ & \quad + \frac{\Delta x_{i+1}}{2} \left[\frac{\phi_{i+1/2,3/2} - \phi_{i+1/2,1/2}^{bc}}{3\sigma_{i+1,1}\Delta y_1} \right]. \end{aligned} \quad (141)$$

Note that unlike the standard or mass-lumped BLD case, here we have only one boundary-condition scalar intensity appearing in each such equation. Thus, using the definitions of the J_y terms, Eqs. (131) and (132), we can easily solve for this intensity:

$$\begin{aligned} \phi_{i+1/2,1/2}^{bc} &= \sum_{\hat{\mathbf{y}} \cdot \mathbf{\Omega}_m > 0} \Delta \Omega_m \left(2 \frac{\hat{\mathbf{y}} \cdot \mathbf{\Omega}_m}{\rho_y} + 3(\hat{\mathbf{y}} \cdot \mathbf{\Omega}_m)^2 \right) \\ & \times \frac{\Delta x_i \psi_{inc,i,1/2}^E(\mathbf{\Omega}_m) + \Delta x_{i+1} \psi_{inc,i+1,1/2}^W(\mathbf{\Omega}_m)}{\Delta x_i + \Delta x_{i+1}}. \end{aligned} \quad (142)$$

Note that this is identical to the approximately ideal boundary condition of Eq. (123), with incident intensity given by a weighted average of the two incident intensities just to the left and right of the point $(x_{i+1/2}, y_{1/2})$. (The weights are the lengths of the i and $i+1$ edges.) Thus, as far as boundary conditions are concerned, the FLBLD/SCB method on rectangular grids in XY geometry is as close to ideal as any DFEM is likely to be. It is precisely the two-dimensional analog of the mass-lumped LD method in slab geometry. The same is true of a fully lumped TLD (or SCB) method on orthogonal hexahedral cells in three dimensions.

The analysis thus tells us that the leading-order FLBLD/SCB solution in interior cells will behave as if that solution satisfied a Dirichlet condition given by Eq. (142) and similar equations on other surfaces. However, the analysis does not say that the leading-order solution in cells adjacent to the boundary will behave this way; in fact, Eqs. (77) and (78) tell us that in such cells, the solution satisfies the Marshak boundary condition described by Eq. (77). This is true of all DFEMs because all DFEMs satisfy Eqs. (77) and (78). We now take a moment to discuss this.

This interesting result was first obtained specifically for the LD method in slab geometry by Larsen and Morel.² In a cell that contains an unresolved boundary layer, every DFEM solution will vary from a Marshak value on the cell surface to an interior value that is consistent with, in general, a different boundary condition. We illustrate this general behavior in Fig. 5. In this figure, we show the exact transport solution, the solution of the diffusion

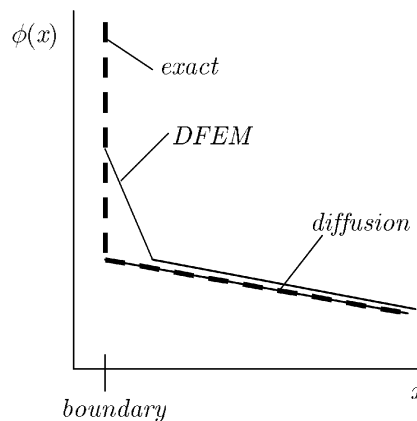


Fig. 5. Illustration of general DFEM behavior at unresolved boundary layer.

problem to which the exact transport solution limits in the interior, and a solution from a DFEM that has approximately ideal boundary-layer behavior. Several points are worth noting.

1. The transport and diffusion solutions are essentially identical except in a narrow boundary layer, which appears as a vertical line in the figure.

2. The DFEM solution almost matches the correct solution in the interior even though it is nowhere close in the boundary cell; i.e., DFEM errors in boundary cells do not propagate to the interior.

3. The reason the interior DFEM solution does not more closely match the exact solution in the interior is that the approximately ideal DFEM boundary condition [as in Eq. (142), for example] is not exactly equal to the exact boundary condition of Eq. (65); i.e., $\mu + 1.5\mu^2$ is not exactly equal to $W(\mu)$.

In Sec. IV, we will provide numerical results that exhibit the two-dimensional analog of this behavior.

III.H. Simple Corner Balance on Polyhedra

Thus far, we have not considered any specific DFEM examples except on rectangular grids. We shall now briefly discuss more general cell shapes, still using XY geometry for illustration.

First, let us consider arbitrary quadrilateral cells. Then, as Table I indicates, the BLD method will fail if it uses weight functions that span the same space as $\{1, x, y, xy\}$. This follows from the fact that such functions cannot have the locality property on general quadrilateral cells. In fact, this is true of any finite set of polynomial functions of x and y . However, a BLD method that maps each cell to a logical square with coordinate axes a and b will not fail if it uses weight functions spanning the same space as $\{1, a, b, ab\}$ because these weight functions do have the locality and surface-matching properties and thus pass the DFEM litmus test described previously. If we map these weight functions back to the (x, y) coordinate system we find that they are actually ratios of polynomials in x and y . A different set of rational functions, also possessing the locality and surface-matching properties, was devised in the early 1970s by Wachpress.²¹ Our theory predicts that a DFEM that uses Wachpress's functions will also produce a full-resolution solution.

If we consider cells with more than four edges, we find that any polynomial basis set, even in a mapped coordinate space, fails the locality and surface-matching test. However, Wachpress's rational functions once again pass the test, and thus we predict that a DFEM using his functions will attain full resolution. To our knowledge no one has yet tested this prediction. An alternative that also passes the test, although it is not strictly speaking a DFEM, is the SCB method. If the FLBLD/SCB method de-

scribed previously is viewed from the corner-balance point of view, it is easy to extend it to arbitrary polygonal cells, as has been reported before.¹¹ In this case, SCB has many of the same properties it had on rectangular grids: Its leading-order solution is pointwise continuous in the interior even when incident flow rates are discontinuous, and its boundary condition is a reasonably good approximation of the ideal. However, the diffusion discretization satisfied by its leading-order solution has some flaws. First, if the grid is skewed badly enough, the solution can exhibit unphysical oscillations and negativities. Second, if the grid remains skewed as it is refined, then the solution does not necessarily limit to the analytic solution of the diffusion equation. That is, the diffusion discretization has zeroth-order truncation error on skewed grids. (None of this is obvious from what we have presented in this paper; we are simply reporting results from Ref. 11 that are related to the present discussion.)

In summary, on arbitrary polygonal grids in two dimensions, much work remains to develop and demonstrate a truly robust and accurate DFEM (or corner-balance method) for thick diffusive problems. The same obviously is true for arbitrary polyhedral grids in three dimensions.

IV. NUMERICAL RESULTS

We consider several test problems in XY geometry. The first problem shows that given rectangular cells, the linear DFEM (LD) fails dramatically, while the bilinear DFEM (BLD) obtains the correct solution, exactly as predicted by the asymptotic analysis in Sec. III. The second problem shows that in some cases, the standard BLD method and even the mass-lumped BLD method can give unphysical solutions, while the fully lumped BLD method (equivalent to simple corner-balance) produces robust results.

The first problem is a homogeneous square, 1×1 cm, with a uniformly distributed isotropic source and vacuum boundaries. The cross sections and source are $\sigma = 1/\epsilon$, $\sigma_a = \epsilon$, and $q = \epsilon$; we vary the parameter ϵ from 0.1 to 0.00001. We solve the problem with an S_8 level-symmetric quadrature set²² and a uniform 20×20 spatial mesh,

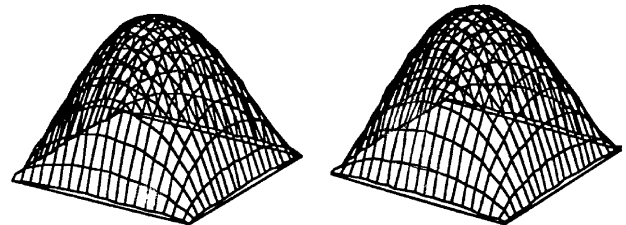


Fig. 6. The LD (left) and BLD solutions of test problem 1, $\epsilon = 10^{-2}$.

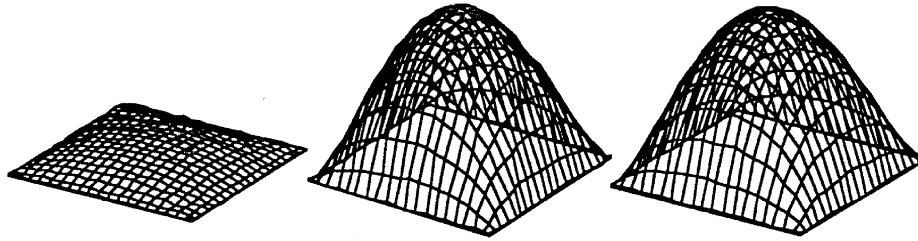


Fig. 7. The LD (left), BLD (middle), and diffusion solutions of test problem 1, $\epsilon = 10^{-5}$.

using both the LD and BLD methods. We also numerically solve (with a very fine mesh) the diffusion problem that is satisfied by the exact transport solution in the limit as ϵ approaches zero. In Figs. 6 and 7, we plot the LD and BLD scalar intensities, and in Fig. 7 we include the correct limiting diffusion solution that the exact transport solution should approach as ϵ approaches zero. We see that the LD solution approaches zero as ϵ approaches zero, while the BLD solution approaches the correct diffusion solution. This is precisely as predicted by the asymptotic analysis.

The second test problem is designed to illustrate several predictions made by the theory. The problem, depicted in Fig. 8, is a source-free square with a constant cross section and no absorption ($\sigma_a = q = 0$). The spatial grid is slightly nonuniform, containing some cells with a 5:3 aspect ratio. The boundary condition is designed to produce boundary layers. On part of the boundary, alternating cells are exposed to a monodirectional beam incident at the most grazing angles in the S_8 level-symmetric quadrature set that we use; remaining cells are exposed to a vacuum. The incident intensity is symmetric about the surface normal and thus does not generate the artificial source terms discussed earlier.

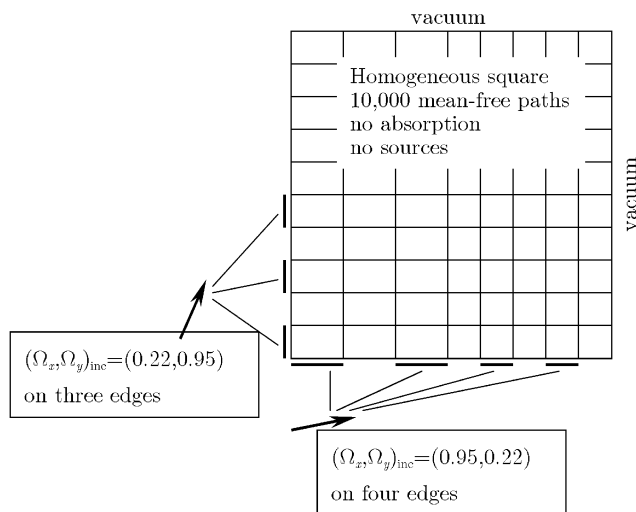


Fig. 8. Contrived difficult test problem.

In the figures that follow, we compare surface plots of various solutions of this problem. We begin with Figs. 9, which show the solution in the entire domain from the mass-lumped BLD (MLBLD) method and the FLBLD. Each figure was generated as follows. The finite element solution was evaluated using its basis function expansion at each point on a uniform 300×300 grid spread across the problem. Thus, despite having only 80 cells, we generated 90 000 data points to plot. The resulting surface shows the shape of the solution within each cell, and it allows us to see discontinuities at cell surfaces. (The plotted surface is not discontinuous, because the plotting software simply connects adjacent data points, but it is easy to see that very steep gradients at cell surfaces are the result of actual solution discontinuities.)

From these figures, we can see that the two methods (mass-lumped and fully-lumped BLD) have similar behavior in the boundary cells on which the grazing intensity is incident. If we ignore the oscillations caused by the incident intensity appearing only on alternate boundary cells, we can see the two-dimensional analog

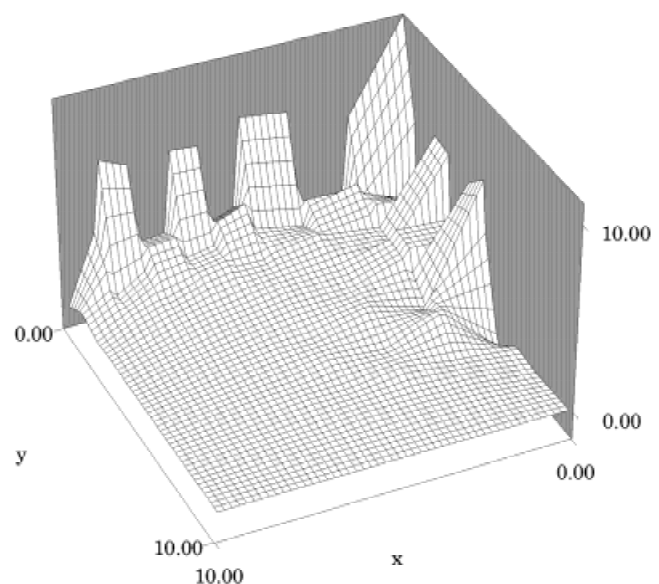


Fig. 9a. The MLBLD solution of problem shown in Fig. 8.

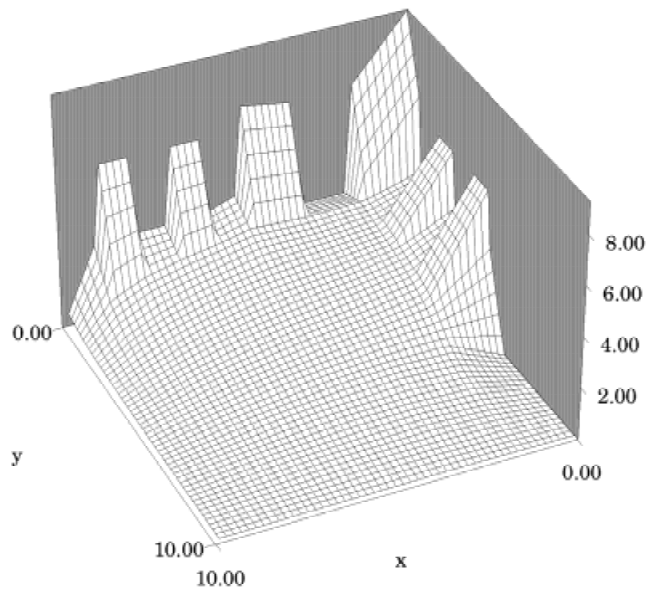


Fig. 9b. The FLBLD solution of problem shown in Fig. 8.

of the behavior illustrated in Fig. 5. That is, the interior solution satisfies a boundary condition that is markedly different from the solution in the boundary cells. In cells other than those illuminated by the incident intensity, the MLBLD and FLBLD solutions behave somewhat differently. The FLBLD solution remains positive at every point in the problem, whereas the MLBLD solution is negative in two regions near the boundary. This is one example of the robustness added by the new lumping procedures outlined in this paper.

We turn now to the question of how accurate and robust the DFEM solutions are in the problem interior. In

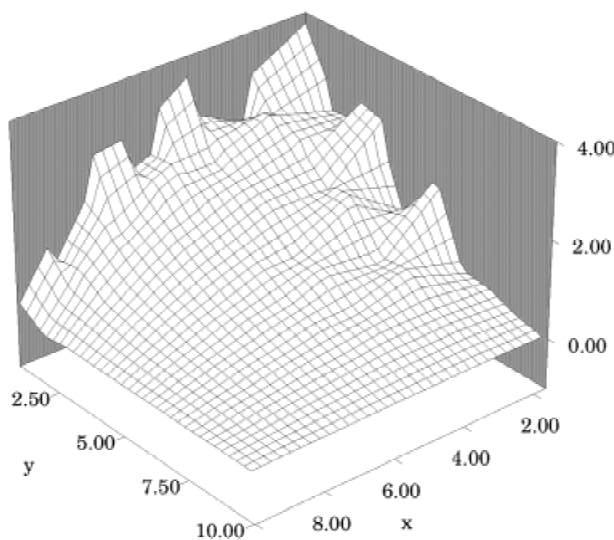


Fig. 10a. The MLBLD solution in interior ($x > 1.67$; $y > 1$) of problem shown in Fig. 8.

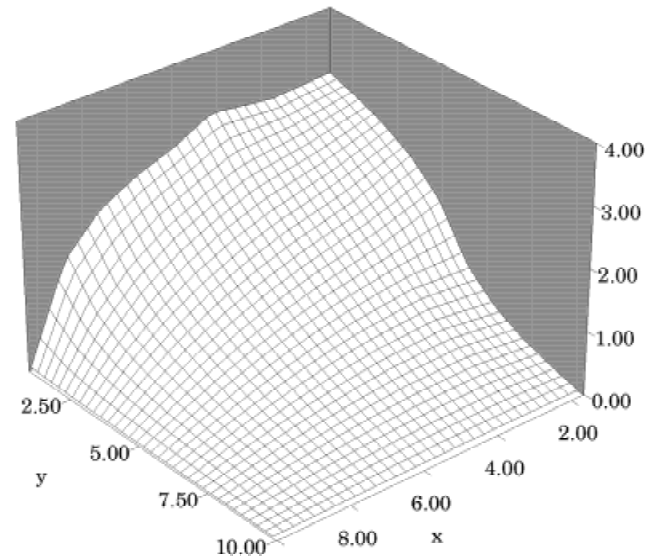


Fig. 10b. The FLBLD solution in interior ($x > 1.67$; $y > 1$) of problem shown in Fig. 8.

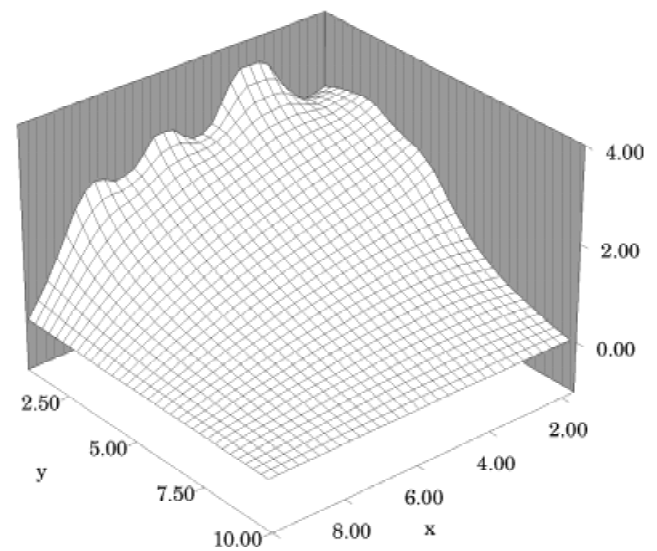


Fig. 10c. Diffusion solution in interior ($x > 1.67$; $y > 1$) of problem shown in Fig. 8.

Figs. 10 we provide close-ups of the interior solutions. These figures display significant differences between the MLBLD and FLBLD solutions in the interior of the diffusive test problem. The mass-matrix-lumped bilinear DFEM solution exhibits discontinuities and oscillations in the interior, just as the analysis predicts. In contrast, the fully lumped method is smooth and continuous. Again, this is an example of the robustness added by lumping.

We turn now to the question of the accuracy of the interior solutions. In Fig. 10c we show the interior solution as obtained by solving a diffusion problem with the

boundary conditions shown in Eq. (65). According to asymptotic theory, the exact transport solution will equal this diffusion solution to leading order in the problem interior; thus, this diffusion solution is a good reference to which to compare our DFEM transport solutions. Our diffusion result is not perfect; it was solved with a mesh considerably finer than that shown in Fig. 8, but still not extremely fine. Nevertheless, it provides a useful point of comparison.

A comparison of Figs. 10a, 10b, and 10c illustrates several of our theoretical results. The reference solution (the diffusion solution of Fig. 10c) is smooth and continuous in the problem interior, while the MLBLD solution is not. This is an example of the MLBLD scheme lacking robustness and continuity. The FLBLD solution is continuous and very smooth, but in fact it is *too* smooth. This is an example of the typical trade-off between robustness and accuracy: Highly robust methods tend to be less able to follow true oscillations in a solution. The MLBLD solution appears at first glance to be trying to follow the smooth oscillations in the reference solution; however, closer inspection reveals that its oscillations are completely out of phase. That is, the MLBLD solution in the interior is high where the reference solution is low and vice versa. This is an example of what can happen with methods that lack robustness. In this case, it is the result of at least two factors working together: The nine-point discretization satisfied by the leading-order solution permits oscillations, and the discontinuous boundary condition produces discontinuous interior solutions (because the method is not surface-lumped).

We remark that we could not obtain the results in this section without some form of iterative acceleration—standard source iteration for such thick and diffusive problems converges far too slowly to be of practical use. For acceleration in all of the transport calculations discussed here, we employed the modified four-step (M4S) diffusion-synthetic acceleration (DSA) method of Adams and Martin.¹⁷ We solved the M4S diffusion equations using brute-force LU decomposition. This is not the most efficient way to solve the equations, but it was simple to implement and sufficient for our purpose, which was simply to obtain the answers. We note that Morel et al.¹⁸ have developed a highly efficient solution procedure for solving the M4S DSA equations, and we recommend this algorithm for BLD applications in which computational efficiency is important.

V. SUMMARY AND CONCLUSIONS

We have performed an asymptotic analysis of a family of DFEMs for spatially discretizing the discrete ordinates transport equation. The analysis holds in one, two, and three dimensions for any spatial grid composed of arbitrarily connected polygonal or polyhedral cells. The

cell surfaces are permitted to have curvature. The main result of our work is a theory that describes how the numerical transport solution from any DFEM in the family will behave in thick diffusive regions. This theory can be used to rule out certain methods for certain kinds of problems, to explain previously unexpected results that are seen in some problems, and to guide development of new DFEMs that will perform well in diffusive problems.

We have used our theory to draw some rather general conclusions. We have found that some DFEMs, including the standard linear discontinuous method on rectangular XY grids, fail dramatically in thick diffusive regions. We call these zero-resolution methods. This subfamily's leading-order solutions are determined by equations that contain almost no physical information. Other DFEMs attain full resolution, meaning that they devote at least one degree of freedom per spatial vertex (or cell edge or cell surface) to satisfying a mixed finite element discretization of the correct diffusion equation. We have shown that two simple properties of the DFEM weight functions—locality and surface matching—are sufficient to guarantee full resolution. The mixed finite element discretization satisfied by the leading-order solution of full-resolution DFEMs can be unusual and possibly inaccurate; this question must be answered case by case. (This does not mean the analysis must be performed from scratch for each proposed DFEM; it simply means that each DFEM must submit to specific tests laid out by our theory.) Further, the boundary condition satisfied by the leading-order solution can be very complicated, and in general it is not an accurate representation of the correct condition. For most DFEMs, the boundary condition at a point depends on the incident intensity at other points far away, and for many DFEMs nonphysical source terms (both positive and negative) appear in the equations satisfied by the leading-order solution.

The theory predicts that certain kinds of lumping can make DFEM solutions much more robust (resistant to oscillations and negative solutions) in thick diffusive regions. We have illustrated this using the BLD method on rectangular cells in XY geometry. Whereas mass-matrix lumping provides robustness in slab-geometry DFEMs, it is far from sufficient in two and three dimensions. There, our theory says that new kinds of lumping, or localization, are required to produce robust solutions in thick diffusive regions. We illustrated this with the FLBLD method, which we have noted is equivalent to SCB.

We have noted that at this time there is no DFEM that has been shown to be as robust on arbitrary quadrilateral cells as is the FLBLD/SCB method on rectangular cells. The same statement also holds, obviously, for arbitrary polygonal cells in two dimensions and arbitrary polyhedral cells in three dimensions. Both the corner-balance approach and a DFEM using Wachpress's rational functions appear to have promise; however, neither approach has been shown to yield a method that extends

the rectangle-cell FLBLD/SCB robustness to less-regular cell shapes. This remains an area for further research.

In this paper, we have considered only the Cartesian coordinate system. The DFEM discretizations of the transport equation in curvilinear coordinates can behave somewhat differently in thick diffusive regions than their Cartesian-coordinate counterparts. Palmer and Adams^{23,24} have studied this and reported preliminary results, but a complete study (analogous to this Cartesian work) remains to be published.

In this paper, we have studied only DFEMs that are algebraically linear. There has been much recent interest in spatial discretization methods that are algebraically nonlinear, and diffusion-limit analyses have been reported for some of these in limited geometric settings.²⁵⁻²⁷ An interesting area for future study is the extension of our general-geometry linear theory, reported here, to nonlinear DFEMs. We have begun such an extension and hope to report results in the near future.

APPENDIX A

Half-Range Quadrature Integration of $\mathbf{\Omega}\mathbf{\Omega}$

Here, we show that Eq. (104), which is

$$\mathbf{n} \cdot \sum_{m: \mathbf{n} \cdot \mathbf{\Omega}_m > 0} \Delta_m \mathbf{\Omega}_m \mathbf{\Omega}_m = \frac{2\pi}{3} \mathbf{n} , \quad \mathbf{n} \text{ any vector} , \quad (\text{A.1})$$

follows directly from Eq. (103), which is

$$\sum_{m=1}^M \Delta_m \mathbf{\Omega}_m \mathbf{\Omega}_m = \frac{4\pi}{3} \mathbf{I} , \quad (\text{A.2})$$

for any quadrature set that has reflective symmetry. We define reflective symmetry as follows:

If for each m there exists an m' :

$$\Delta_{m'} = \Delta_m \quad \text{and} \quad \mathbf{\Omega}_{m'} = -\mathbf{\Omega}_m , \quad (\text{A.3})$$

then we say that the quadrature set has reflective symmetry. Most quadrature sets that are commonly used have this property.

We begin by dotting an arbitrary vector \mathbf{n} into Eq. (A.2):

$$\mathbf{n} \cdot \sum_{m=1}^M \Delta_m \mathbf{\Omega}_m \mathbf{\Omega}_m = \mathbf{n} \cdot \frac{4\pi}{3} \mathbf{I} = \frac{4\pi}{3} \mathbf{n} . \quad (\text{A.4})$$

We separate the sum on the left side into three separate sums:

$$\begin{aligned} & \mathbf{n} \cdot \sum_{m: \mathbf{n} \cdot \mathbf{\Omega}_m > 0} \Delta_m \mathbf{\Omega}_m \mathbf{\Omega}_m + \mathbf{n} \cdot \sum_{m: \mathbf{n} \cdot \mathbf{\Omega}_m = 0} \Delta_m \mathbf{\Omega}_m \mathbf{\Omega}_m \\ & + \mathbf{n} \cdot \sum_{m: \mathbf{n} \cdot \mathbf{\Omega}_m < 0} \Delta_m \mathbf{\Omega}_m \mathbf{\Omega}_m = \frac{4\pi}{3} \mathbf{n} . \end{aligned} \quad (\text{A.5})$$

The middle term is, of course, zero. By symmetry, the third term is exactly equal to the first, as can be seen by making the substitution $-\mathbf{\Omega}_{m'} = \mathbf{\Omega}_m$, $\Delta_{m'} = \Delta_m$ in the equation. Thus, we have

$$2\mathbf{n} \cdot \sum_{m: \mathbf{n} \cdot \mathbf{\Omega}_m > 0} \Delta_m \mathbf{\Omega}_m \mathbf{\Omega}_m = \frac{4\pi}{3} \mathbf{n} , \quad (\text{A.6})$$

from which the desired result follows immediately.

APPENDIX B

Discontinuity of Standard BLD Solution

We show here that the leading-order standard BLD solution in a thick diffusive XY -geometry problem with rectangular cells is continuous if and only if the incident partial current is continuous all the way around the problem boundary (including around corners). We begin by defining some notation:

$$\phi_{ij}^{NE}, \phi_{ij}^{NW}, \phi_{ij}^{SW}, \phi_{ij}^{SE} = \begin{pmatrix} \text{intensity in the northeast,} \\ \text{northwest, southwest, and} \\ \text{southeast corners of cell } ij \end{pmatrix} .$$

In this notation, the standard BLD solution has the following form:

$$\begin{aligned} \phi(x, y) = & \phi_{ij}^{NE} \frac{x - x_{i-1/2}}{\Delta x_i} \frac{y_{j+1/2} - y}{\Delta y_j} \\ & + \phi_{ij}^{NW} \frac{x_{i+1/2} - x}{\Delta x_i} \frac{y_{j+1/2} - y}{\Delta y_j} \\ & + \phi_{ij}^{SW} \frac{x_{i+1/2} - x}{\Delta x_i} \frac{y - y_{j-1/2}}{\Delta y_j} \\ & + \phi_{ij}^{SE} \frac{x - x_{i-1/2}}{\Delta x_i} \frac{y - y_{j-1/2}}{\Delta y_j} , \\ & (x, y) \in \text{cell } ij . \end{aligned} \quad (\text{B.1})$$

A typical row of Eq. (79) for an interior cell is

$$\begin{aligned} & \frac{\Delta x_i}{3} [2(\phi_{ij}^{NE} - \phi_{i,j+1}^{SE}) + (\phi_{ij}^{NW} - \phi_{i,j+1}^{SW})] \\ & + \frac{\Delta y_j}{3} [2(\phi_{ij}^{NE} - \phi_{i+1,j}^{NW}) + (\phi_{ij}^{SE} - \phi_{i,j+1}^{SW})] = 0 . \end{aligned} \quad (\text{B.2})$$

(We have assumed a quadrature set with 90-deg rotational symmetry, which means all the ρ values in Eqs. (79) are the same and thus divide out.) We will find it useful to define an average scalar intensity at each interior vertex,

$$\phi_{i+1/2,j+1/2} = \frac{1}{4}(\phi_{ij}^{NE} + \phi_{i+1,j}^{NW} + \phi_{i+1,j+1}^{SW} + \phi_{i,j+1}^{SE}) , \quad (\text{B.3})$$

and discontinuities between each corner value and the associated vertex value,

$$\begin{aligned} \Delta_{ij}^{NE} &\equiv \phi_{ij}^{NE} - \phi_{i+1/2,j+1/2} , \\ \Delta_{i+1,j+1}^{SW} &\equiv \phi_{i+1,j+1}^{SW} - \phi_{i+1/2,j+1/2} , \quad \text{etc.} \end{aligned} \quad (\text{B.4})$$

With this definition, the following identity holds at each interior vertex:

$$\Delta_{ij}^{NE} + \Delta_{i+1,j}^{NW} + \Delta_{i,j+1}^{SE} + \Delta_{i+1,j+1}^{SW} = 0 . \quad (\text{B.5})$$

Also, we have

$$\phi_{ij}^{NE} - \phi_{i+1,j}^{NW} = \Delta_{ij}^{NE} - \Delta_{i+1,j}^{NW} , \quad \text{etc.} \quad (\text{B.6})$$

Thus, we can rewrite Eqs. (B.2) for each corner about the interior vertex $i + \frac{1}{2}, j + \frac{1}{2}$ in terms of Δ 's:

$$\begin{aligned} \frac{\Delta x_i}{3} [2(\Delta_{ij}^{NE} - \Delta_{i,j+1}^{SE}) + (\Delta_{ij}^{NW} - \Delta_{i,j+1}^{SW})] \\ + \frac{\Delta y_j}{3} [2(\Delta_{ij}^{NE} - \Delta_{i+1,j}^{NW}) + (\Delta_{ij}^{SE} - \Delta_{i,j+1}^{SW})] = 0 , \end{aligned} \quad (\text{B.7a})$$

$$\begin{aligned} \frac{\Delta x_i}{3} [2(\Delta_{i,j+1}^{SE} - \Delta_{ij}^{NE}) + (\Delta_{i,j+1}^{SW} - \Delta_{ij}^{NW})] \\ + \frac{\Delta y_{j+1}}{3} [2(\Delta_{i,j+1}^{SE} - \Delta_{i+1,j+1}^{SW}) \\ + (\Delta_{i,j+1}^{NE} - \Delta_{i+1,j+1}^{NW})] = 0 , \end{aligned} \quad (\text{B.7b})$$

$$\begin{aligned} \frac{\Delta x_{i+1}}{3} [2(\Delta_{i+1,j+1}^{SW} - \Delta_{i+1,j}^{NW}) + (\Delta_{i+1,j+1}^{SE} - \Delta_{i+1,j}^{NE})] \\ + \frac{\Delta y_{j+1}}{3} [2(\Delta_{i+1,j+1}^{SW} - \Delta_{i,j+1}^{SE}) \\ + (\Delta_{i+1,j+1}^{NW} - \Delta_{i,j+1}^{NE})] = 0 , \end{aligned} \quad (\text{B.7c})$$

and

$$\begin{aligned} \frac{\Delta x_{i+1}}{3} [2(\Delta_{i+1,j}^{NW} - \Delta_{i+1,j+1}^{SW}) + (\Delta_{i+1,j}^{NE} - \Delta_{i+1,j+1}^{SE})] \\ + \frac{\Delta y_j}{3} [2(\Delta_{i+1,j}^{NW} - \Delta_{ij}^{NE}) + (\Delta_{i,j+1}^{SW} - \Delta_{ij}^{SE})] = 0 . \end{aligned} \quad (\text{B.7d})$$

[In Eqs. (B.7) there appear some Δ 's at neighboring vertices, which could be on the boundary. We will define these shortly.] It is easy to see that Eqs. (B.7) are linearly dependent: If we add them all, we find that the coefficient of each Δ is zero. This verifies the claim made in the body of the paper that with BLD on rectangles, there is a redundant Eq. (79) at each interior vertex. We can therefore drop any one of Eqs. (B.7) without losing in-

formation. It is also not difficult to see that there is only one redundancy in Eqs. (B.7)—three of the equations are in fact independent. When we consider also Eq. (B.5), we find that we have four independent equations at each interior vertex for our set of Δ 's, and we note that the right side of each equation is zero.

We turn next to boundary vertices. Beginning with a vertex on the bottom boundary ($y = y_{1/2}$) but not at the left or right corner of the problem, we define

$$\phi_{i+1/2,1/2} = \frac{1}{2}(\phi_{i,0}^E + \phi_{i+1,0}^W) , \quad (\text{B.8})$$

where we have defined Marshak scalar intensities:

$$\phi_{i,0}^E \equiv \frac{2}{\rho} \sum_{\mathbf{e}_y \cdot \mathbf{\Omega}_m < 0} \Delta \Omega_m 2 |\mathbf{e}_y \cdot \mathbf{\Omega}_m| \psi_{inc}(x_{i+1/2}^-, \mathbf{\Omega}_m) \quad (\text{B.9a})$$

and

$$\phi_{i,0}^W \equiv \frac{2}{\rho} \sum_{\mathbf{e}_y \cdot \mathbf{\Omega}_m < 0} \Delta \Omega_m 2 |\mathbf{e}_y \cdot \mathbf{\Omega}_m| \psi_{inc}(x_{i+1/2}^+, \mathbf{\Omega}_m) , \quad (\text{B.9b})$$

where $x_{i+1/2}^\pm$ is the point just to the right or left of $x_{i+1/2}$. As before in the interior, we define discontinuities:

$$\begin{aligned} \Delta_{i,1}^{SE} &\equiv \phi_{i,1}^{SE} - \phi_{i+1/2,1/2} , \\ \Delta_{i+1,1}^{SW} &\equiv \phi_{i+1,1}^{SW} - \phi_{i+1/2,1/2} , \end{aligned} \quad (\text{B.10a})$$

$$\begin{aligned} \Delta_{i,0}^E &\equiv \phi_{i,0}^E - \phi_{i+1/2,1/2} = \frac{1}{2}(\phi_{i,0}^E - \phi_{i+1,0}^W) , \\ \Delta_{i+1,0}^W &\equiv \phi_{i+1,0}^W - \phi_{i+1/2,1/2} = \frac{1}{2}(\phi_{i+1,0}^W - \phi_{i,0}^E) . \end{aligned} \quad (\text{B.10b})$$

Analogous to Eqs. (B.7) are the two independent equations

$$\begin{aligned} \frac{\Delta x_i}{3} [2\Delta_{i,1}^{SE} + \Delta_{i,1}^{SW}] \\ + \frac{\Delta y_1}{3} [2(\Delta_{i,1}^{SE} - \Delta_{i+1,1}^{SW}) + (\Delta_{i,1}^{NE} - \Delta_{i+1,1}^{NW})] \\ = \frac{\Delta x_i}{3} [2\Delta_{i,0}^E + \Delta_{i,0}^W] \end{aligned} \quad (\text{B.11a})$$

and

$$\begin{aligned} \frac{\Delta x_{i+1}}{3} [2\Delta_{i+1,1}^{SW} + \Delta_{i+1,1}^{SE}] \\ + \frac{\Delta y_1}{3} [2(\Delta_{i+1,1}^{SW} - \Delta_{i,1}^{SE}) + (\Delta_{i+1,1}^{NW} - \Delta_{i,1}^{NE})] \\ = \frac{\Delta x_{i+1}}{3} [2\Delta_{i+1,0}^W + \Delta_{i+1,0}^E] . \end{aligned} \quad (\text{B.11b})$$

Similar relations hold for vertices (not at problem corners) on the left, right, and top boundaries of the problem.

Turning finally to the problem corner vertices, for example, the one at $(x_{1/2}, y_{1/2})$, we define

$$\phi_{1/2,1/2} = \frac{1}{2}(\phi_{1,0}^W + \phi_{0,1}^S), \quad (\text{B.12})$$

where $\phi_{1,0}^W$ and $\phi_{0,1}^S$ are the Marshak scalar intensities at the left of the bottom edge and the bottom of the left edge, respectively. We define discontinuities as before:

$$\Delta_{1,1}^{SW} = \phi_{1,1}^{SW} - \phi_{1/2,1/2} \quad (\text{B.13a})$$

and

$$\begin{aligned} \Delta_{1,0}^W &\equiv \phi_{1,0}^W - \phi_{1/2,1/2} = \frac{1}{2}(\phi_{1,0}^W - \phi_{0,1}^S), \\ \Delta_{0,1}^S &\equiv \phi_{0,1}^S - \phi_{1/2,1/2} = \frac{1}{2}(\phi_{0,1}^S - \phi_{1,0}^W). \end{aligned} \quad (\text{B.13b})$$

Then analogous to Eqs. (B.11) is the equation

$$\begin{aligned} \frac{\Delta x_1}{3} [2\Delta_{1,1}^{SW} + \Delta_{1,1}^{SE}] + \frac{\Delta y_1}{3} [2\Delta_{1,1}^{SW} + \Delta_{1,1}^{NW}] \\ = \frac{\Delta x_1}{3} [2\Delta_{1,0}^W + \Delta_{1,0}^E] + \frac{\Delta y_1}{3} [2\Delta_{0,1}^S + \Delta_{0,1}^N]. \end{aligned} \quad (\text{B.14})$$

Similar relations hold for the other three corners of the problem.

Let us summarize the equations we have developed. First, we have defined a discontinuity for each scalar-intensity unknown in the problem, which totals four per cell. If i_{\max} and j_{\max} are the numbers of cells in the x and y directions, respectively, this gives us $4i_{\max}j_{\max}$ unknown discontinuities. Equations (B.7) and (B.5) are four independent equations per interior vertex [$4(i_{\max}j_{\max} - i_{\max} - j_{\max} + 1)$ equations]; Eqs. (B.10) and others like them are two independent equations per edge vertex [$4(i_{\max} + j_{\max} - 2)$ equations]; Eqs. (B.14) and others like them are one independent equation per problem corner (four equations). This sums to $4i_{\max}j_{\max}$ independent equations for the $4i_{\max}j_{\max}$ unknown discontinuities. The only nonzero terms on the right sides of these equations are discontinuities in what we have termed Marshak boundary scalar intensities; see Eqs. (B.11) and (B.10b) and Eqs. (B.14) and (B.13b). These Marshak intensities are simply proportional to incident particle flow rates. [See Eqs. (B.9).] That is, we have

$$\underline{\underline{D}}\underline{\underline{\Delta}} = \underline{\underline{\delta}}, \quad (\text{B.15})$$

where

$\underline{\underline{D}}$ = invertible matrix

$\underline{\underline{\Delta}}$ = vector containing all the leading-order scalar-intensity discontinuities

$\underline{\underline{\delta}}$ = vector composed solely of zeros and discontinuities in incident partial currents.

[This includes discontinuities around corners, as Eqs. (B.14) and (B.13b) indicate.] Thus, if the incident partial current is continuous (even around corners), all discontinuities in the leading-order BLD scalar intensity will be zero: The leading-order scalar intensity will be continuous. This is a good result. However, if there is any discontinuity in the incident partial current, the leading-order scalar intensity can in general be discontinuous at every vertex in the problem, which is not such a good result.

APPENDIX C

Continuity of Fully Lumped Bilinear Discontinuous Finite Element Method (Simple Corner Balance) Solution

Here, we prove that Eqs. (78) imply that the leading-order FLBD/SCB solution is continuous in the interior of a thick diffusive region. There are four such equations at each interior vertex, given rectangular cells in XY geometry. In matrix form they are

$$\begin{bmatrix} \alpha_1 + \alpha_2 & -\alpha_1 & 0 & -\alpha_2 \\ -\alpha_1 & \alpha_1 + \alpha_3 & -\alpha_3 & 0 \\ 0 & -\alpha_3 & \alpha_3 + \alpha_4 & -\alpha_4 \\ -\alpha_2 & 0 & -\alpha_4 & \alpha_2 + \alpha_4 \end{bmatrix} \begin{bmatrix} \phi_{ij}^{NE} \\ \phi_{i+1,j}^{NW} \\ \phi_{i+1,j+1}^{SW} \\ \phi_{i,j+1}^{SE} \end{bmatrix} = \begin{bmatrix} 0 \\ 0 \\ 0 \\ 0 \end{bmatrix}, \quad (\text{C.1})$$

The α parameters depend on Δx , Δy , and the quadrature set. Their precise values are irrelevant; we note only that they are real positive numbers. Note that the only scalar intensities in the equations are the four that are centered at the given vertex.

The matrix in Eq. (C.1) is singular: Its rows sum to zero, as do its columns. Thus, these equations do not determine the four scalar intensities, which, as we have emphasized, is a good property. However, they do tell us something about that continuity of these intensities, as we now show. The first three rows of Eq. (C.1) can be written as follows:

$$\begin{bmatrix} \alpha_1 + \alpha_2 & -\alpha_1 & 0 \\ -\alpha_1 & \alpha_1 + \alpha_3 & -\alpha_3 \\ 0 & -\alpha_3 & \alpha_3 + \alpha_4 \end{bmatrix} \begin{bmatrix} \phi_{ij}^{NE} \\ \phi_{i+1,j}^{NW} \\ \phi_{i+1,j+1}^{SW} \end{bmatrix} = \begin{bmatrix} \alpha_2 \\ 0 \\ \alpha_4 \end{bmatrix} \phi_{i,j+1}^{SE}. \quad (\text{C.2})$$

The matrix in this equation is a symmetric positive-definite M -matrix whose inverse exists and has only non-negative entries. It follows immediately that each of the three scalar intensities on the left side of the equation is determined uniquely to be a positive constant times the scalar intensity on the right side. Given that this solution is unique, if we guess a solution that satisfies Eqs. (C.2), then we have found the solution. It is clear that the guess

$$\phi_{ij}^{NE} = \phi_{i+1,j}^{NW} = \phi_{i+1,j+1}^{SW} = \phi_{i,j+1}^{SE} \quad (\text{C.3})$$

does satisfy these equations. Therefore, the leading-order FLBLD/SCB solution is continuous at interior vertices, regardless of discontinuities in incident flow rates around the boundary.

APPENDIX D

The M Matrices

Here, we show that the inverse of an M -matrix has purely nonnegative entries. We say that a matrix \mathbf{A} is an M -matrix if it meets the following criteria:

1. It is square.
2. Every off-diagonal entry is either zero or negative.
3. Every diagonal entry is positive.
4. It is strictly diagonally dominant: $A_{ii} > \sum_{j \neq i} |A_{ij}|$.

We decompose \mathbf{A} into its diagonal and off-diagonal parts:

$$\mathbf{A} = \mathbf{D} - \mathbf{O}, \quad (\text{D.1})$$

where \mathbf{D} is a diagonal matrix with positive entries on the diagonal and \mathbf{O} has zeroes on the diagonal and nonnegative entries elsewhere. The inverse of \mathbf{A} satisfies

$$\mathbf{A}^{-1} = (\mathbf{D} - \mathbf{O})^{-1} = (\mathbf{I} - \mathbf{D}^{-1}\mathbf{O})^{-1}\mathbf{D}^{-1}. \quad (\text{D.2})$$

Of course \mathbf{D}^{-1} is a diagonal matrix with positive entries on the diagonal, and $\mathbf{D}^{-1}\mathbf{O}$ has only nonnegative entries. We will now show that $(\mathbf{I} - \mathbf{D}^{-1}\mathbf{O})^{-1}$ has only nonnegative entries.

If a matrix \mathbf{B} has eigenvalues of magnitude strictly less than unity, then

$$(\mathbf{I} - \mathbf{B})^{-1} = \mathbf{I} + \mathbf{B} + \mathbf{B}^2 + \mathbf{B}^3 + \dots \quad (\text{D.3})$$

(To see this, multiply both sides by $\mathbf{I} - \mathbf{B}$.) Thus, if we can show that $\mathbf{D}^{-1}\mathbf{O}$ has eigenvalues less than unity, our desired result will follow. By the diagonal dominance of our M -matrix, we know that

$$\sum_j [\mathbf{D}^{-1}\mathbf{O}]_{ij} < 1 \text{ for all } i. \quad (\text{D.4})$$

A well-known theorem by Gerschgorin shows that all of the eigenvalues of a matrix lie in the union of certain circles in the complex plane, with one circle per row of

the matrix. The center of each circle is the diagonal element of the row and the radius is the sum of the absolute values of the off-diagonal elements. This means that all of the eigenvalues of $\mathbf{D}^{-1}\mathbf{O}$ lie in a circle centered at the origin, with radius strictly less than unity. Thus, the eigenvalues of $\mathbf{D}^{-1}\mathbf{O}$ all have magnitude less than unity. Putting this all together we finally have

$$\begin{aligned} \mathbf{A}^{-1} &= (\mathbf{I} - \mathbf{D}^{-1}\mathbf{O})^{-1}\mathbf{D}^{-1} \\ &= (\mathbf{I} + [\mathbf{D}^{-1}\mathbf{O}] + [\mathbf{D}^{-1}\mathbf{O}]^2 + [\mathbf{D}^{-1}\mathbf{O}]^3 \\ &\quad + \dots)\mathbf{D}^{-1}. \end{aligned} \quad (\text{D.5})$$

Every element of every matrix on the right side is non-negative; thus, every element of the inverse of an M -matrix is nonnegative.

ACKNOWLEDGMENTS

We thank many colleagues, including E. Larsen, G. Pomraning, J. Morel, T. Wareing, T. Palmer, and P. Nowak, for helpful discussions during the early stages of this work. We are indebted to an anonymous reviewer for many helpful suggestions and constructive criticisms that greatly improved the presentation of this work.

REFERENCES

1. E. W. LARSEN, J. E. MOREL, and W. F. MILLER, Jr., "Asymptotic Solutions of Numerical Transport Problems in Optically Thick, Diffusive Regimes," *J. Comput. Phys.*, **69**, 283 (1987).
2. E. W. LARSEN and J. E. MOREL, "Asymptotic Solutions of Numerical Transport Problems in Optically Thick, Diffusive Regimes II," *J. Comput. Phys.*, **83**, 212 (1989); see also "Corrigendum," *J. Comput. Phys.*, **91**, 246 (1990).
3. M. L. ADAMS, "Discontinuous Finite-Element Transport Solutions in the Thick Diffusion Limit in Cartesian Geometry," *Proc. Int. Topl. Mtg. Advances in Mathematics, Computations, and Reactor Physics*, Pittsburgh, Pennsylvania, April 28–May 1, 1991, Vol. 5, p. 21.1 3-1, American Nuclear Society (1991).
4. M. L. ADAMS, "Even-Parity Finite-Element Transport Methods in the Diffusion Limit," *Prog. Nucl. Energy*, **25**, 2–3, 159 (1991).
5. M. L. ADAMS, "Even- and Odd-Parity Finite-Element Transport Solutions in the Thick Diffusion Limit," *Proc. Int. Conf. Advances in Mathematics, Computation, and Reactor Physics*, Pittsburgh, Pennsylvania, April 28–May 1, 1991, Vol. 5, p. 21.1 2-1, American Nuclear Society (1991).
6. M. L. ADAMS, T. A. WAREING, and W. F. WALTERS, "Characteristic Methods in Thick Diffusive Problems," *Nucl. Sci. Eng.*, **130**, 18 (1998).

7. E. W. LARSEN, "The Asymptotic Diffusion Limit of Discretized Transport Problems," *Nucl. Sci. Eng.*, **112**, 336 (1992).
8. J. E. MOREL, T. A. WAREING, and K. SMITH, "A Linear-Discontinuous Spatial Differencing Scheme for Sn Radiative Transfer Calculations," *J. Comput. Phys.*, **128**, 445 (1996).
9. M. L. ADAMS and P. F. NOWAK, "Asymptotic Analysis of a Computational Method for Time- and Frequency-Dependent Radiative Transfer," *J. Comput. Phys.*, **146**, 366 (1998).
10. T. A. WAREING, E. W. LARSEN, and M. L. ADAMS, "Diffusion Accelerated Discontinuous Finite Element Schemes for the SN Equations in Slab and X,Y Geometries," *Proc. Int. Conf. Advances in Mathematics, Computation, and Reactor Physics*, Pittsburgh, Pennsylvania, April 28–May 1, 1991, Vol. 3, p. 11.1 2-1, American Nuclear Society (1991).
11. M. L. ADAMS, "A Subcell Balance Method for Radiative Transfer on Arbitrary Spatial Grids," *Transp. Theory Stat. Phys.*, **26**, 4 & 5, 385 (1997).
12. M. L. ADAMS, "A New Transport Discretization Scheme for Arbitrary Spatial Meshes in XY Geometry," *Proc. Int. Conf. Advances in Mathematics, Computation, and Reactor Physics*, Pittsburgh, Pennsylvania, April 28–May 1, 1991, Vol. 3, p. 13.22-1, American Nuclear Society (1991).
13. K. G. THOMPSON and M. L. ADAMS, "A Spatial Discretization for Solving the Transport Equation on Unstructured Grids of Polyhedra," *Proc. Int. Conf. Mathematics and Computation, Reactor Physics and Environmental Analysis in Nuclear Applications*, Madrid, Spain, September 27–30, 1999, Vol. 2, p. 1196, Senda Editorial (1999).
14. T. L. EATON and M. L. ADAMS, "A New Corner-Balance/Linear-Discontinuous Method for Transport in Slab Geometry," *Trans. Am. Nucl. Soc.*, **70**, 158 (1994).
15. G. C. POMRANING, *The Equations of Radiation Hydrodynamics*, Pergamon Press, Oxford (1973).
16. T. A. WAREING, J. M. MCGHEE, J. E. MOREL, and S. D. PAUTZ, "Discontinuous Finite Element SN Methods on 3-D Unstructured Grids," *Proc. Int. Conf. Mathematics and Computation, Reactor Physics and Environmental Analysis in Nuclear Applications*, Madrid, Spain, September 27–30, 1999, Vol. 2, p. 1185, Senda Editorial (1999).
17. M. L. ADAMS and W. R. MARTIN, "Diffusion-Synthetic Acceleration of Discontinuous Finite-Element Transport Iterations," *Nucl. Sci. Eng.*, **111**, 145 (1992).
18. J. E. MOREL, J. E. DENDY, Jr., and T. A. WAREING, "Diffusion-Accelerated Solution of the Two-Dimensional Sn Equations with Bilinear-Discontinuous Differencing," *Nucl. Sci. Eng.*, **115**, 304 (1993).
19. F. MALGAVI and G. C. POMRANING, "Initial and Boundary Conditions for Diffusive Linear Transport Problems," *J. Math. Phys.*, **32**, 805 (1990).
20. S. CHANDRASEKHAR, *Radiative Transfer*, Dover, New York (1960).
21. E. L. WACHPRESS, *A Rational Finite Element Basis, Mathematics in Science and Engineering*, Vol. 114, Academic Press, New York (1975).
22. E. E. LEWIS and W. F. MILLER, Jr., *Computational Methods of Neutron Transport*, John Wiley and Sons, New York (1984).
23. T. S. PALMER and M. L. ADAMS, "Analysis of Spherical Geometry Finite Element Transport Solutions in the Thick Diffusion Limit," *Proc. Int. Conf. Advances in Mathematics, Computation, and Reactor Physics*, Pittsburgh, Pennsylvania, April 28–May 1, 1991, Vol. 5, p. 21.1 4-1, American Nuclear Society (1991).
24. T. S. PALMER and M. L. ADAMS, "Curvilinear Geometry Transport Discretizations in the 'Thick' Diffusion Limit," *Proc. Int. Conf. Mathematical Methods and Supercomputing in Nuclear Applications*, Karlsruhe, Germany, April 19–23, 1993, Vol. I, p. 3, Kernforschungszentrum Karlsruhe (1993).
25. W. F. WALTERS and T. A. WAREING, "A Nonlinear Positive Method for Solving the Transport Equation on Coarse Meshes," *Proc. 8th Int. Conf. Radiation Shielding*, Arlington, Texas, April 24–28, 1994, p. 173, American Nuclear Society (1994).
26. K. MATHEWS, G. SJODEN, and B. MINOR, "Exponential Characteristic Spatial Quadrature for Discrete Ordinates Radiation Transport in Slab Geometry," *Nucl. Sci. Eng.*, **118**, 24 (1994).
27. C. L. CASTRIANNI and M. L. ADAMS, "A Nonlinear Corner-Balance Spatial Discretization for Transport on Arbitrary Grids," *Nucl. Sci. Eng.*, **128**, 278 (1998).